ABSTRACT

Title of Dissertation:	STRUCTURAL BASIS FOR ESCAPING NEGATIVE SELECTION BY T CELL RECEPTOR WITH HIGH AFFINITY FOR SELF ANTIGEN
	Yiyuan Yin, Doctor of Philosophy, 2010
Directed By:	Professor Roy A. Mariuzza Department of Cell Biology and Molecular Genetics

The failure to eliminate self-reactive T cells is a prerequisite for autoimmunity. To escape thymic deletion, autoreactive T cell receptors (TCRs) may form relatively unstable complexes with self-peptide–MHC. These TCRs adopt suboptimal docking topologies in striking contrast to the classical topology of anti-microbial TCRs. Alternatively, escape can occur by weak binding between self-peptides and MHC. We determined the structure of a human autoimmune TCR (MS2-3C8) bound to a self-peptide from myelin basic protein (MBP) and the multiple sclerosis-associated MHC molecule HLA-DR4. MS2-3C8 is encephalitogenic in humanized transgenic mice. The structure showed loose accommodation of MBP in the HLA-DR4 binding groove, accounting for its low affinity. By contrast, MS2-3C8 binds MBP–DR4 as tightly as the most avid anti-microbial TCRs. Structurally, MS2-3C8 engages self-antigen via a docking mode that closely resembles the optimal topology of anti-microbial TCRs,

but is distinct from that of other autoreactive TCRs. Combined with a unique CDR3β conformation, this docking mode compensates for the weak binding of MBP to HLA-DR4 by maximizing interactions between MS2-3C8 and MBP. Thus, the MS2-3C8–MBP–DR4 complex reveals the basis for an alternative strategy whereby autoreactive T cells escape negative selection, yet retain the ability to initiate autoimmunity.

STRUCTURAL BASIS FOR ESCAPING NEGATIVE SELECTION BY T CELL RECEPTOR WITH HIGH AFFINITY FOR SELF ANTIGEN

By

Yiyuan Yin

Dissertation submitted to the Faculty of the Graduate School of the
University of Maryland, College Park, in partial fulfillment
of the requirements for the degree of
Doctor of Philosophy
2010

Advisory Committee:
Professor Roy A. Mariuzza, Chair
Professor Philip N. Bryan
Professor David Fushman
Professor Nicole A. LaRonde-LeBlanc
Professor Ian Heywood Mather
Professor Wenxia Song

Dedication

I dedicate this dissertation to my parents,

Xinhua Yin and Jufang Chu,

for their complete love.

Acknowledgements

I want to express my gratitude to the people who were there during my graduate work for their continuous support that makes this thesis possible.

My deepest gratefulness goes to my respectable advisor, Roy Mariuzza, for his many years of support and guidance. First, I want to thank Roy for his willingness to take me into his laboratory, since I came to the lab only with some fancy imaginations about protein structures. To jump-start me, Roy assigned a senior scientist, Dr. Yili Li, to teach me all the technical skills that I used for structural studies. This setup promised me a smooth and efficient start. During the later years, Roy supervised me with great patience and freedom, supplied me with resources and ideas and taught me how to write and how to collaborate. Roy has influenced me in many ways. His wit and wisdom, his devotion to science, his generosity are all what I greatly appreciate and want to learn.

Drs. Phil Bryan, David Fushman, Nicole LaRonde-Lablanc, Ian Mather and Wenxia Song generously serve as my advisory committee members. All professors are very nice and knowledgeable. They gave me valuable advice. They care about my career after the graduation. I sincerely appreciate their support.

I want to thank Dr. Yili Li, who not only taught me the experimental skills, but also familiarized me with the big picture of how structural studies work. Yili trained me with her exceptional experimental skills, which balanced between details and productiveness.

Her instinct-like scientific judgments amazed me all the time and also deeply influenced me.

I am indebted to previous and current members of the Mariuzza lab with whom I could obtain help on a daily basis. Particularly, I would like to acknowledge Dr. Gang Xu, Dr. Min Mo, Melissa Kerzic for their contributions to this thesis in different ways. Dr. Gang Xu gave me the engineered version of another TCR based on which I designed an engineered version for my own protein. He is also the most helpful source for trouble-shooting the technical problems in my work. Dr. Min Mo helped me set up the baculovirus system for expressing my proteins. Melissa is the lab manager who orders products for everyone. She also helped me to produce more proteins for catching up the revision deadline.

Dr. Shunyuan Xiao has his laboratory on the other side of the hallway. I did my first lab rotation with him when he just started at the university. He gave me valuable advice and recommendations on choosing a lab for my thesis. The most inspiring part is that, as a diligent and smart scientist, Dr. Xiao is probably the best case I can find for achieving career goals with hard-working. Congratulations on your tenure promotion!

Dr. Leslie Pick was the director of our program when I started my graduate studies. Everyone in MOCB appreciated her true-hearted care for the students. She wrote grants to support future students, so that they did not have to teach and could immediately be involved in research. Her door was always open to me when I needed advice. Those conversations with her helped me a lot for better handling course works, teaching sessions and lab rotations at the same time in my first year.

Dr. Shuwei Li is a knowledgeable chemical biologist. He taught me to use the peptide synthesizer and purify the peptides. He also maintains the mass spectrometer for us. Although being busy with writing grant proposals, he often updates me with scientific news and discoveries.

I am grateful to our program secretary, Sarah Biancardi. She is very organized and patient. She knows every detail of our graduate life. I always have my questions answered by her.

Many friends of mine from College Park to Shady Grove and from China to USA shine my graduate life with cheerful memories. Their sincere friendship is one of the most valuable assets of mine.

Though we are an ocean apart, the love from my parents is here with me every single day. Their love keeps my courage and perseverance. With their unconditioned love, I am so blessed. Writing these words makes me miss them more. I wish you both good health always!

Table of Contents

List of Abbreviations

In alphabetical order

APC	Antigen-presenting cell
AUC	Analytical ultracentrifugation
BBB	Blood-brain barrier
CDR	Complimentarity-determining region
CNS	Central nervous system
EAE	Experimental allergic encephalomyelitis
ELISA	Enzyme-linked immunosorbent assay
FPLC	Fast protein liquid chromatography
HPLC	High-performance liquid chromatography
ITC	Isothermal titration calorimetry
LN	Liquid nitrogen
MBP	Myelin basic protein
MHC	Major histocompatibility complex
MOG	Myelin oligodendrocyte glycoprotein
MR	Molecular replacement
MS	Multiple sclerosis
PDB	Protein data bank
PEG	Polyethylene glycol
PLP	Proteolipid protein
pMHC	Peptide-MHC
SLE	Systemic lupus erythematosus
SPR	Surface plasmon resonance
T1D	Type 1 diabetes
TCC	T cell clone
TCL	T cell line
TCR	T cell receptor

List of Tables

List of Figures

Chapter 1

Introduction

Our immune system is specialized for defense against invading microorganisms. Defense is mediated by different types of white blood cells which intervene at different stages of the immune response. Cells of the innate immune system represent the first line of defense, quickly responding to infections. However, the limited variability of innate immune receptors leads to limited defenses that may be overwhelmed by pathogens. Adaptive immunity is conveyed by B and T lymphocytes. Through gene rearrangements, these lymphocytes are able to achieve virtually unlimited variations for recognizing almost all pathogens. Once triggered, the adaptive immune response is specific, robust, and determined to win the battle against invading microbes. Meanwhile, all immune defenses are tightly regulated and are underpinned by mechanisms to distinguish self and foreign. However, as seen in autoimmune diseases, such as type 1 diabetes (T1D), multiple sclerosis (MS), and systemic lupus erythematosus (SLE), the host immune system may lose its ability to discriminate self from foreign and begin to attack normal tissues. In most of these diseases, damages are mediated by self-targeting $CD4^+$ T cells.

1.1 T cell-mediated immunity

Adaptive immunity can be divided into B lymphocyte-mediated humoral immunity and T lymphocyte-mediated cellular immunity. Each T lymphocyte expresses one clonotypic antigen receptor, the T cell receptor (TCR), which recognizes peptide antigens that are processed and presented by antigen-presenting cells (APCs). A mature T lymphocyte also expresses either the CD8 or CD4 co-receptor molecule, which binds to major histocompatibility complex (MHC) class I or class II molecules, respectively, on the APC surface. $CD8^+$ T cells respond to peptides presented by MHC class I molecules, whereas $CD4^+$ T cells recognize peptides presented by class II molecules. T cell activation also requires the co-stimulatory molecules B7 and CD28, which are expressed on the APC and T cell, respectively. Upon encountering a specific antigen, the engaged TCR delivers an activation signal to the T cell, with help from co-receptor and co-stimulatory molecules. An activated T cell will then exert its immune functions, depending on what type of T cell it is: $CD8^+$ T cells are cytotoxic cells that directly terminate infected target cells by releasing cytotoxins; $CD4^+$ T cells usually become T helper cells that secret cytokines to assist the function of other immune cells, such as macrophages, B cells, and $CD8^+$ T cells.

1.2 How does a T cell recognize its ligand?

1.2.1 Structure of the ligands

Two classes of MHC molecules are associated with antigenic peptides from different sources due to different antigen-processing pathways. MHC class I molecules bind to

peptides derived from cytosolic antigens, whereas class II molecules bind to peptides derived from endocytosed extracellular proteins. The peptide-binding site of MHC is shaped like a groove, with six β-strands forming the floor and two α-helices forming the walls (Figure 1.1). Depending on the topology of the groove, the lengths of the bound peptides are different for MHC class I and class II molecules. Because the binding groove of MHC class I is closed at both ends (Figure 1.1-B), it is restricted to binding peptides 9 residues in length. By contrast, the open-ended groove of MHC class II (Figure 1.1-D) molecules can accommodate peptides of 12–25 residues (Stern and Wiley, 1994).

The compositions of MHC molecules are distinct for the two classes, although both are non-disulfide-linked heterodimers. Class I molecules are composed of a heavy chain and β_2-microglobulin. The extracellular part of the heavy chain has three immunoglobulin-like (Ig) domains, designated α1, α2 and α3. The peptide-binding groove is formed by the α1 and α2 domains. β_2-microglobulin is an invariant single Ig like domain (Figure 1.1-A). Therefore, the peptide specificity of a class I molecule is solely determined by the heavy chain. Class II molecules, by contrast, are composed of α and β chains, two polypeptides of approximately equal length. Each chain has two Ig-like domains: α1 and α2, or β1 and β2. Peptide binding is determined by both chains, since the groove is formed by the α1 and β1 domains (Figure 1.1-C).

In human, MHC proteins are known as human leukocyte antigens (HLA), including HLA-A, HLA-B and HLA-C for class I, and HLA-DP, HLA-DQ and HLA-DR for class II. There are multiple alleles at the gene loci encoding these proteins. Some of the loci, such as HLA-A, -B, -C and -DRB1, have hundreds of alleles in human populations (Lefranc et al., 2009). Such high degree of polymorphism makes it possible for MHC

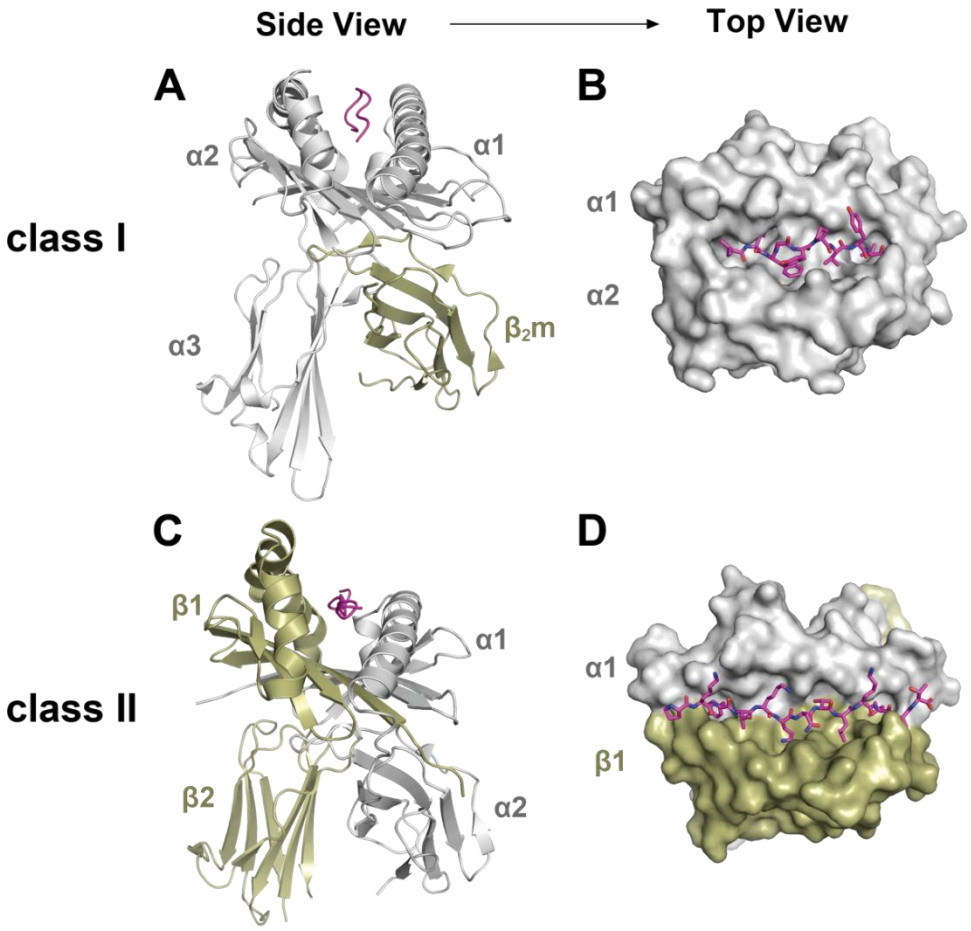

Figure 1.1: Structures of MHC class I and class II molecules.

(A) Ribbon diagram of a human MHC class I molecule, HLA-A2, bound to a 9-residue viral peptide, Tax (PDB code: 1DUZ) (Khan et al., 2000). The heavy chain of HLA-A2 (shown in gray) contains three domains. β_2-microglobulin is yellow and the peptide is magenta.

(B) Top view of the HLA-A2–Tax complex. The surface of HLA-A2 is gray, with the bound Tax peptide (magenta) shown as a stick model. The two ends of the peptide-binding groove are closed, which constrains the peptide length for MHC class I molecules.

(C) Ribbon diagram of a human MHC class II molecule, HLA-DR4, bound to a 13-residue hemaglutinin (HA) peptide (PDB code: 1J8H) (Hennecke and Wiley, 2002). Both the α (gray) and β (yellow) chains of HLA-DR4 contain two domains.

(D) Top view of the HLA-DR4–HA complex. Compared to MHC class I, both ends of the peptide-binding groove in MHC class II molecules are open, which allows peptides of varying length to bind.

molecules to present peptides of various sequences, which is critical for shaping diversified T cell repertoires to combat pathogens (Messaoudi et al., 2002).

1.2.2 Structure of T cell receptors

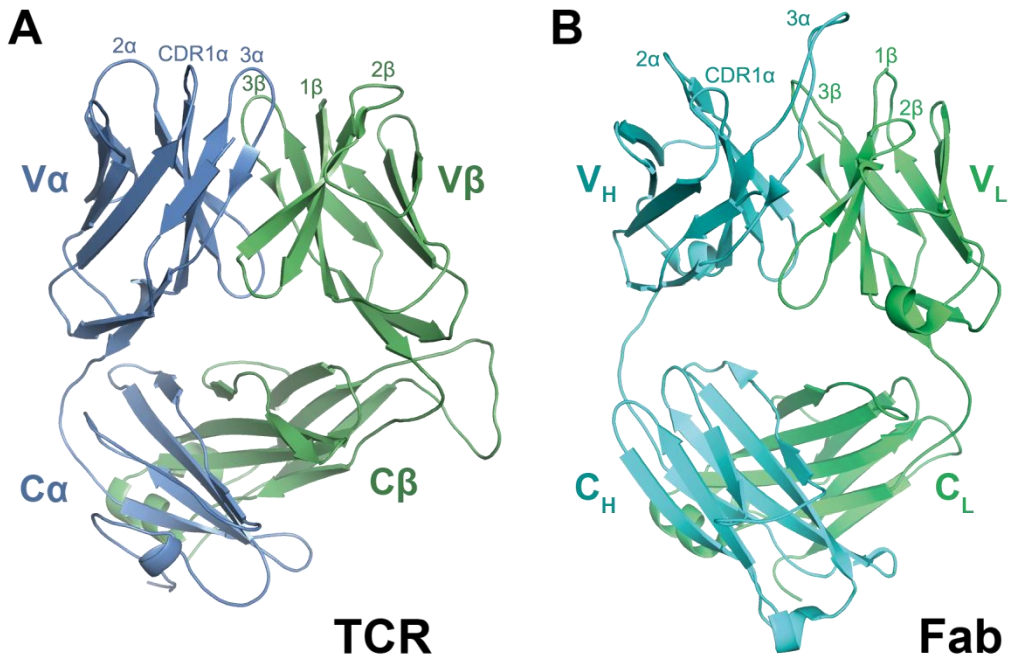

Figure 1.2 Structural resemblance between a TCR and the Fab fragment of an Ig.

(A) Ribbon diagram of the first TCR structure, mouse TCR 2C (PDB code: 1TCR) (Garcia et al., 1996). The α- and β-chains are blue and green, respectively. The individual domains and six CDR loops are labeled.

(B) Structure of the Fab fragment of an anti-HIV antibody, b12 (PDB code: 2NY7) (Zhou et al., 2007). The heavy chain is cyan and the light chain is green. The individual domains and six CDR loops are labeled.

T cell activation is initiated by the binding of a TCR to its cognate peptide–MHC (pMHC) ligand(s). Crystal structures of all TCRs in the Protein Data Bank (PDB) have revealed that the extracellular portion of a TCR is very similar to the Fab moiety of antibodies (Figure 1.2). The TCR molecule is composed of disulfide-linked α- and β-chains. Each chain has two Ig domains, a variable (V) domain and a constant (C) domain. During T cell development, genes encoding the full-length α- and β-chains are generated through somatic rearrangement of variable (V), diversity (D), joining (J) and C gene segments (Figure 1.3). For the human α-chain, the Vα domain is formed by one of 54 TRAV (Vα) genes and one of 61 TRAJ (Jα) genes (Lefranc et al., 2009). The Vβ domain of the human β-chain is formed by one of 67 TRBV (Vβ) genes, one of 2 TRBD (Dβ) segments, and one of 14 TRBJ (Jβ) segments (Lefranc et al., 2009). The C gene segments encode the constant domains, the connecting peptides and transmembrane polypeptides that follow the V domains. The ligand-binding site of a TCR consists of six complementarity-determining regions (CDRs), which are three hypervariable loops from each V domain corresponding to the CDRs of an antibody Fab fragment (Figure 1.2). The CDR1 and CDR2 loops are entirely encoded by the V segments, whereas the CDR3 loops are formed by connecting the V segments to either J (in Vα) or D and J (in Vβ) segments. V(D)J rearrangement is mediated by two lymphoid-specific proteins, RAG-1 and RAG-2, as well as several non-lymphoid-specific DNA repair enzymes (Swanson, 2004). Moreover, addition and deletion of nucleotides take place at the joining sites, which further increase the size of the TCR repertoire (Matthews and Oettinger, 2009; Tillman et al., 2004). The random pairing of α- and β-chains also contributes to repertoire diversity

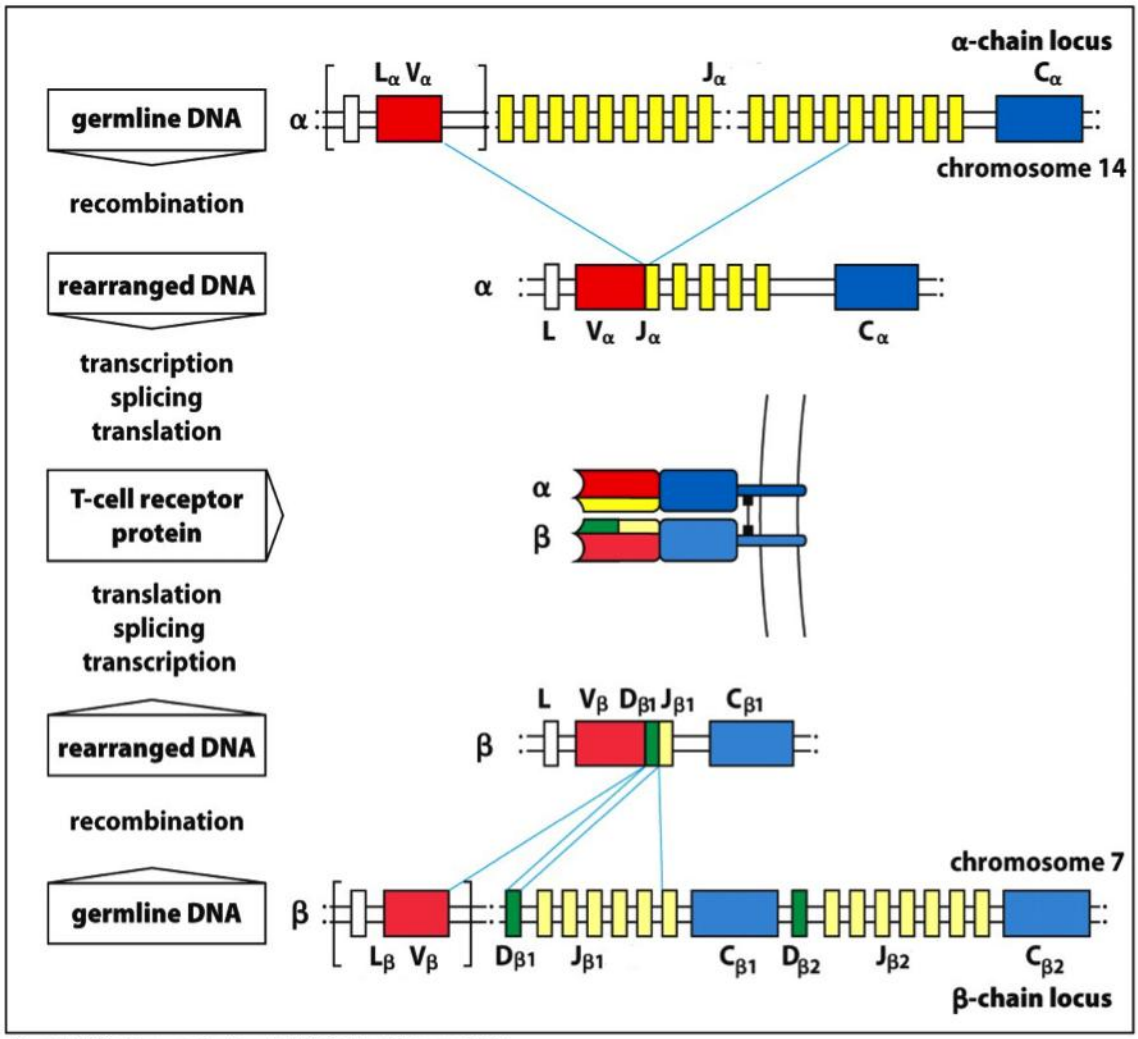

Figure 5.3 The Immune System, 3ed. (© Garland Science 2009)

Figure 1.3 Gene rearrangements of TCR α- and β-chains.

TCR gene rearrangements is DNA recombination events that in a clonotypic manner. After the V regions are formed by selected V(D)J segments, rearranged genes transcribe into mRNA followed by splicing to connect the C regions with the V regions. It is notable that α- and β-gene rearrangements take place at different stages of T cell development. TCR β-gene rearrangement occurs in the "double-negative" stage when each TCR β chain pairs with an invariant α-chain (pre-Tα). TCR α-gene rearrangement occurs in a later "double-positive" stage. Expressed α-chains then replace the pre-Tα to assemble functional αβTCR surface molecules.

(Krangel, 2009). Through these mechanisms, a mature TCR repertoire can ultimately achieve a diversity of 10^{14} receptors (Marrack and Kappler, 1988).

Collectively, the overall assembly process of TCR genes resembles that of antibody genes, and both can achieve highly diverse receptor repertoires. However, antigen recognition by TCRs differs from that by antibodies in a critical way: unlike antibodies, which recognize an unlimited variety of antigens, αβ TCRs have evolved to interact only with MHC molecules bearing peptide antigens. The mechanism for this inherent bias is yet not clear.

1.2.3 MHC Restriction

In the early 1970's, Rolf Zinkernagel and Peter Doherty discovered that the specific activities of cytotoxic T cells were associated with compatible MHC backgrounds of mouse strains (Doherty and Zinkernagel, 1975; Hafler et al., 1996; Steinman, 1996a; Steinman, 1996b). In other words, T cell recognition is MHC-restricted. Although MHC restriction appears quite obvious today when we have clearly understood the structural basis of T cell recognition (i.e. binding of a TCR to its peptide–MHC ligand), this was a remarkable finding at that time. The discovery gave important information for solving the puzzle of whether there were two types of TCRs, one for MHC and one for antigen, or one TCR for both (Janeway and Jason, 1980). When the crystal structure of the MHC class I molecule HLA-A2 was reported in 1987, the strong electron density between the α1 and α2 domains led to the conclusion that antigen was bound there as a processed peptide, immediately suggesting that MHC and antigen molecules are simultaneously

recognized by a single TCR (Bjorkman et al., 1987). This conclusion was validated in 1996 by the structure of TCR A6 bound to HLA-A2 and a viral peptide (Garboczi et al., 1996). It was in the same year that Zinkernagel and Doherty were awarded the Nobel Prize in Medicine for their discovery of MHC restriction.

1.3 Positive and negative selection

As the basis for T cell recognition, MHC restriction is essential for all aspects of cell-mediated immunity, including shaping the peripheral T cell repertoire during lymphocyte development, as well as specifically targeting pathogens in the periphery. At the end of the "double positive" stage of T cell development, each T cell expresses a fully-assembled surface TCR and is both $CD4^+$ and $CD8^+$ (Anderson and Jenkinson, 2001). However, the T cell repertoire is not prepared for properly exerting immune functions until all T cells in the thymus pass positive and negative selection. The main purpose of positive selection is to ensure that all T cells recognize antigens in a self-MHC-restricted fashion, while negative selection serves to establish central tolerance, which prevents autoreactive T cells from entering the periphery (Starr et al., 2003). In these selection processes, MHCs expressed on the medulla epithelial cells are bound to self-peptides. Thymic selection is primarily based on the affinities or avidities of TCRs for self-pMHC ligands. Whereas low-affinity ligands promote positive selection, strong interactions between TCR and self-pMHC induce negative selection. As a result, those T cells with no response to self-pMHCs, or with too strong responses, are eliminated, which generates a self-MHC-restricted and self-peptide-tolerant T cell repertoire that is prepared for

immune defense in the periphery (Huseby et al., 2008; Huseby et al., 2005).

However, the "quality control" process in the thymus is not perfect, as evidenced by the presence of T cells in the periphery reactive with autoantigens. Normally, these T cells are under the leash of peripheral regulatory machineries, but they may still evade peripheral surveillance and begin to attack self, resulting in autoimmune diseases, such as multiple sclerosis. Of the many factors that may initiate T cell-mediated autoimmunity, the existence of self-reactive T cells in the periphery is a prerequisite. Here, we are particularly interested in how autoimmune T cells escape negative selection. Through structural investigations, we hope to learn whether autoimmune TCRs share structural features that enable them to evade thymic deletion.

1.4 Multiple sclerosis and autoimmunity

Multiple sclerosis (MS) is a human autoimmune disease of the central nervous system (CNS). Approximately 400,000 people in the US and 2.5 million people worldwide are affected by MS (NMSS, 2010). Because most of the patients are between the ages of 20 and 50, MS is considered as socioeconomically important. Based on disease progression, MS can be generally divided into two categories: relapsing-remitting MS (85–90%) and primary progressive MS (10–15%) (Sospedra and Martin, 2005). More detailed examinations of patients' symptoms should give a more thorough classification of the disease, which highlights the complexity of MS pathology (Lucchinetti et al., 1996).

It is believed that the major player in MS are autoreactive CD4+ T lymphocytes that

attack and damage the myelin sheath around nerve axons (Figure 1.4) (Steinman, 1996b). The subsequent inflammation and destruction of myelin impairs the electrical conductivity of nerves and may eventually cause disability or even death. The myelin components that have been identified as autoantigens, including myelin basic protein (MBP), myelin oligodendrocyte glycoprotein (MOG) and myelin proteolipid protein (PLP), are present mostly in the CNS, except that MBP is also expressed in peripheral myelin tissues (Bruno et al., 2002; Seamons et al., 2003). To become pathogenic, an autoreactive T cell must first be activated under particular conditions. For example,

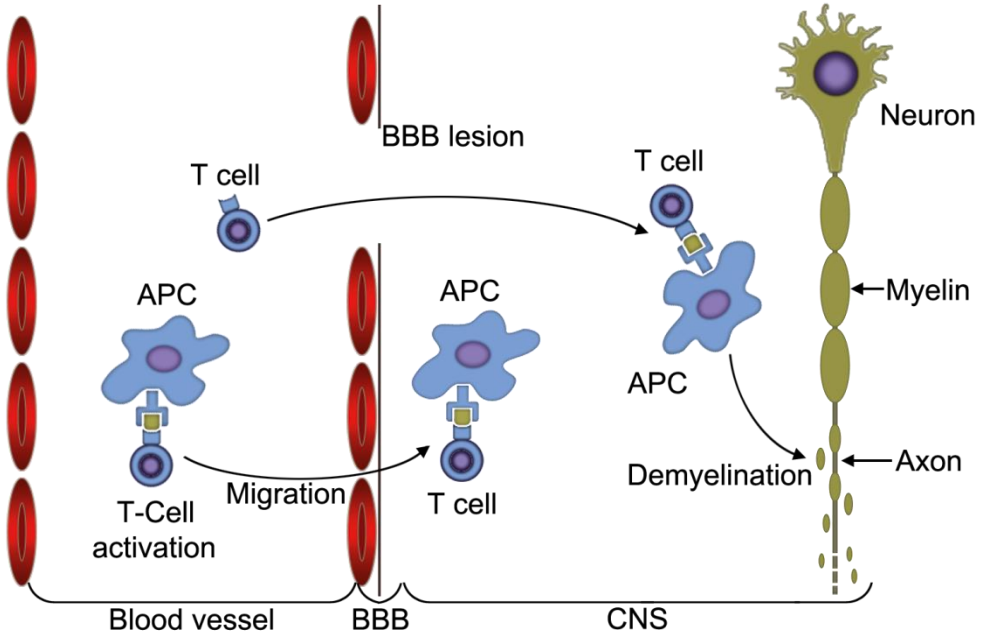

Figure 1.4 Multiple sclerosis is a $CD4^+$ T cell-mediated autoimmune disease of the CNS.

T cells that are activated in the periphery are able to migrate across the blood-brain barrier (BBB). In other cases, they may enter the CNS through breaches in the BBB. Autoreactive T cells can either be activated by myelin antigens or by cross-reactive microbial peptides. Activated T cells in the CNS then secrete cytokines that cause inflammation and disruption of myelin tissues.

altered cytokine production may break the immune balance by lowering the threshold for activating autoimmune cells (Banchereau et al., 2004). Alternatively, autoreactive T cells may accidentally cross-react with a foreign antigen, such as a microbial peptide, consequently triggering activation (Harkiolaki et al., 2009). Unlike other autoimmune diseases, autoantigens in MS, being sequestered behind the blood-brain barrier (BBB), are not accessible to the immune system under normal conditions (Williams and Hickey, 1995). However, activated T cells are found at inflammatory sites in the CNS, indicating that they are able to penetrate the BBB (Hickey, 1999). It is believed that the integrity of the BBB is compromised in the early development of MS, which exposes central nervous tissues to autoaggressive lymphocytes (Kermode et al., 1990).

Polymorphic MHC genes are known to be the greatest genetic risk factor for MS, as well as other autoimmune diseases (Sospedra and Martin, 2005). Certain MHC alleles have the ability to present particular self-antigens, which help promote positive selection, but avoid negative selection of autoreactive T cells. It is known that different ethnic populations have different genetic backgrounds that relate to predisposition to autoimmune diseases. For MS, the MHC haplotype HLA-DR2 confers susceptibility to the disease in Caucasians of nothern European descent (Barcellos et al., 2003), whereas HLA-DR4 confers susceptibility in those of southern Mediterranean populations (Marrosu et al., 1988). Most HLA-DR2-positive patients display the relapsing-remitting type of MS, whereas HLA-DR4 is more associated with primary progressive MS. How the MHC genotype contributes to the disease heterogeneity of MS is not understood. In addition to MS, HLA-DR4 is also a strong genetic risk factor for type 1 diabetes and

rheumatoid arthritis (Deighton et al., 1989; She, 1996).

To study the pathogenesis of MS, a mouse disease model for this disease, known as experimental autoimmune encephalomyelitis (EAE), has been extensively used. EAE can be induced by immunization with myelin-derived autoantigens or adoptive transfer of pre-activated autoimmune $CD4^+$ T cells (Constantinescu et al., 1998; Gold et al., 2006). Successful induction of EAE by adoptive transfer of $CD4^+$ T cells supports the idea that MS is a $CD4^+$ T cell-mediated autoimmune disease.

1.5 Biophysical and structural studies of MHC class II-restricted antigen recognition by TCRs

1.5.1 Peptide binding by MHC class II molecules

Naturally-processed MHC class II-bound peptides are 10–34 residues long, but the core binding sequences usually span nine residues (P1 to P9) (Appella et al., 1995). The peptide-binding groove of a class II molecule is formed by the two long helices of both chains and six β-strands (Figure 1.1-C). Peptide residues having side chains pointing towards the groove are called "anchor residues" (Figure 1.5, labeled residues), whereas other residues with side chains protruding out of the groove usually interact with the TCR. MHC molecules form pockets or cavities in the peptide-binding site to accommodate anchor residues. Peptide selectivity is achieved when a pocket is constructed with allele-specific polymorphic residues (Sinigaglia and Hammer, 1994). Among all human MHC class II gene loci, HLA-DRB1, encoding the β subunit of HLA-DR molecules, is the most polymorphic. By contrast, HLA-DRA, encoding the α subunit of HLA-DR, is

essentially invariable and can pair with any β-chain to form an HLA-DR heterodimer (Lefranc et al., 2009). A typical HLA-DR-binding peptide uses residues P1, P4, P6, P7 and P9 as anchors (Figure 1.5-A). A hydrophobic P1 residue can be shared by all HLA-DR molecules (Hammer et al., 1993). It is the most important anchor residue for binding. Previous studies showed that replacing hydrophobic P1 residues by residues with polar side chains results in complete loss of peptide binding to HLA-DR1, whereas a polyalanine analog with a tyrosine as the P1 anchor retained its binding ability (Hammer et al., 1994). The P1 and P4 pockets are less polymorphic than the P6, P7 and P9 pockets. The fine specificity of peptide binding is modulated mostly by the P6, P7 and P9 anchor residues, as high levels of polymorphism are observed at these pockets that define the sizes and chemical compositions of corresponding anchor residues (Chelvanayagam, 1997; Zavala-Ruiz et al., 2003). HLA-DR4 is highly homologous to HLA-DR1 and uses similar peptide selection criteria (Hammer et al., 1995).

Mouse MHC class II I-E molecules are homologous to HLA-DR, whereas I-A molecules are homologous to HLA-DQ (Figure 1.6). Thus, the peptide-binding motifs for I-E molecules are similar those of HLA-DR molecules, but different from the binding motifs of I-A or HLA-DQ molecules (Raddrizzani et al., 1997). Alignments of I-A-binding peptides indicated higher variability at P1, indicating that this position is not as conserved or critical as it is for binding to HLA-DR or I-E molecules. Instead, for HLA-DQ/I-A, residues P4 and P9 serve as primary anchors (Figure 1.5-B), while pockets P1, P6 and P7 contribute more to binding specificities (Reizis et al., 1998).

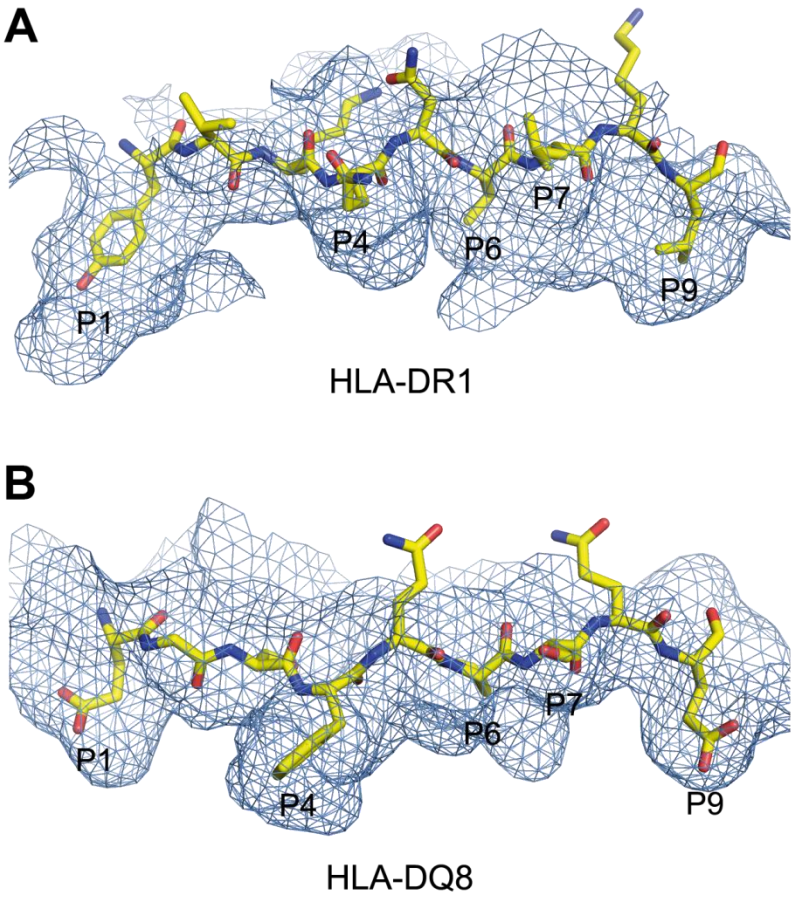

Figure 1.5 Peptide binding motifs of the class II molecules HLA-DR and HLA-DQ.

(A) Structure of HLA-DR1 bound to hemaglutinin peptide HA 308-316 (PDB code: 2G9H) (Fernandez et al., 2006). (B) Structure of HLA-DQ8 bound to a gluten peptide (PDB code: 2NNA) (Henderson et al., 2007). The peptide-binding sites of the two MHC molecules are represented by their blue meshed-surfaces. The peptides are shown in yellow sticks with labeled anchor residues.

Sequence alignment of α-chains

```
                  10        20        30        40        50        60
           ....|....|....|....|....|....|....|....|....|....|....|....|
HLA-DR-α   IKEEHVIIQAEFYLNPDQSGEFMFDFDGDEIFHVDMAKKETVWRLEEFGRFASFEAQGAL
I-E^k-α    .....T........L..KR.................IE.S..I......AK..........
HLA-DQ8-α  VADHVASYGVNL.QSYGP..QYSHE.....E.Y..LER.....Q.PL.R..RR.DP.F..
I-A^k-α    ---HVGSYGITV.QS.GDI.QYT.E.....L.Y..LD......M.P..AQLRR..P..G.

                  70        80        90       100       110       120
           ....|....|....|....|....|....|....|....|....|....|....|....|
HLA-DR-α   ANIAVDKANLEIMTKRSNYTPITNVPPEVTVLTNSPVELREPNVLICFIDKFTPPVVNVT
I-E^k-α    ..........DV.KE...N..DA..A......SR...N.G...I........S.......
HLA-DQ8-α  T....L.H..N.VI....S.AA..EV.....FSK...T.GQ..T...LV.NIF.....I.
I-A^k-α    Q...TG.H....L.....S..A..EA.QA..FPK...L.GQ..T....V.NIF...I.I.

                 130       140       150       160       170       180
           ....|....|....|....|....|....|....|....|....|....|....|....|
HLA-DR-α   WLRNGKPVTTGVSETVFLPREDHLFRKFHYLPFLPSTEDVYDCRVEHWGLDEPLLKQWEF
I-E^k-α    .....R...E..........D..........T.....D.F...E.D....E...R.T...
HLA-DQ8-α  ..S..HS..E.....S..SKS..S.F.IS..T....ADEI...K............H..P
I-A^k-α    ....S.S..D..Y..S.FVNR.YS.H.LS..T.I..DD.I...K......E..V..H..P
```

Sequence alignment of β-chains

```
                  10        20        30        40        50        60
           ....|....|....|....|....|....|....|....|....|....|....|....|
HLA-DR1-β  GDTRPRFLWQLKFECHFFNGTERVRLLERCIYNQEESVRFDSDVGEYRAVTELGRPDAEY
I-E^k-β    -GS..W..EYC.S....Y...Q.....V.YF..L..NL........F............N
HLA-DQ8-β  R.SPED.VY.F.GM.Y.T.........VT.Y...R..YA.......V.....P..P.A...
I-A^k-β    ----GS.VH.FQPF.Y.T...Q.I..VI.Y...R..Y.......................

                  70        80        90       100       110       120
           ....|....|....|....|....|....|....|....|....|....|....|....|
HLA-DR1-β  WNSQKDLLEQRRAAVDTYCRHNYG-VGESFTVQRRVEPKVTVYPSKTQPLQHHNLLVCSV
I-E^k-β    ....PEF...K..E...V.....E-IFDN.L.P.....T.....T.....E.........
HLA-DQ8-β  .....EV..RT..EL..V.....Q-LELRT.L......T..IS..R.EA.N.........
I-A^k-β    ..--.QY..RT..EL..V.....EKTETPTSLR.LEQ.S.VISL.R.EA.N...T.....

                 130       140       150       160       170       180
           ....|....|....|....|....|....|....|....|....|....|....|....|
HLA-DR1-β  SGFYPGSIEVRWFRNGQEEKAGVVSTGLIQNGDWTFQTLVMLETVPRSGEVYTCQVEHPS
I-E^k-β    .D....N.........K...T.I.....VR................Q.............
HLA-DQ8-β  TD...AQ.K......D...TT.....P..R.......I.....MT.QR.D....H.....
I-A^k-β    TD...AK.K..........TV..S..Q..R.......V.....MT..R......H.....

                  190
           ....|....|...
HLA-DR1-β  VTSPLTVEWRARS
I-E^k-β    L.D.V....K.Q.
HLA-DQ8-β  LQN.II.....Q.
I-A^k-β    L...I......--
```

Figure 1.6 Amino acid sequence alignment of human and mouse MHC alleles.

1.5.2 Structural properties of TCR reactive to foreign peptides

Since the first ternary structure of a TCR–pMHC complex was determined 14 years ago (Garboczi et al., 1996), structural studies have focused on TCRs specific for microbial and other foreign peptides. Collectively, these studies have revealed similar binding topologies for TCRs (Rudolph et al., 2002; Rudolph et al., 2006). For a typical class II-restricted TCR complex (Figure 1.7-A), with the peptide-binding groove facing up, the TCR molecule sits on top of the pMHC ligand, with its center over the central residue of the peptide at P5 (Figure 1.7-C). A typical interaction involves three CDRα loops contacting areas around the N-terminal half of the peptide and three CDRβ loops contacting areas around the C-terminal half. Thus, a "crossing angle" (see definition in legends of Figure 1.7) is defined to give a quantitative description of the TCR binding orientation (Reinherz et al., 1999). All anti-foreign TCRs bind with a crossing angle in the diagonal to orthogonal range (Figure 1.7-B). As a result, the MHC α-helices are mostly contacted by the CDR1 and CDR2 loops, while contacts to the peptide are largely mediated by CDR3 loops. With such a docking orientation, the TCR maximizes its contact surface with pMHC. It is also possible that the binding of co-receptors and other accessory molecules to form a signaling assembly may require such a docking orientation.

Such conserved binding topologies by anti-foreign TCRs are hardwired by the biased interaction between TCR and MHC. As discussed above, the antigen-binding sites of TCRs and antibodies are closely related in terms of their sequence and structural arrangements. However, unlike antibodies that can bind to virtually to antigen, αβTCRs

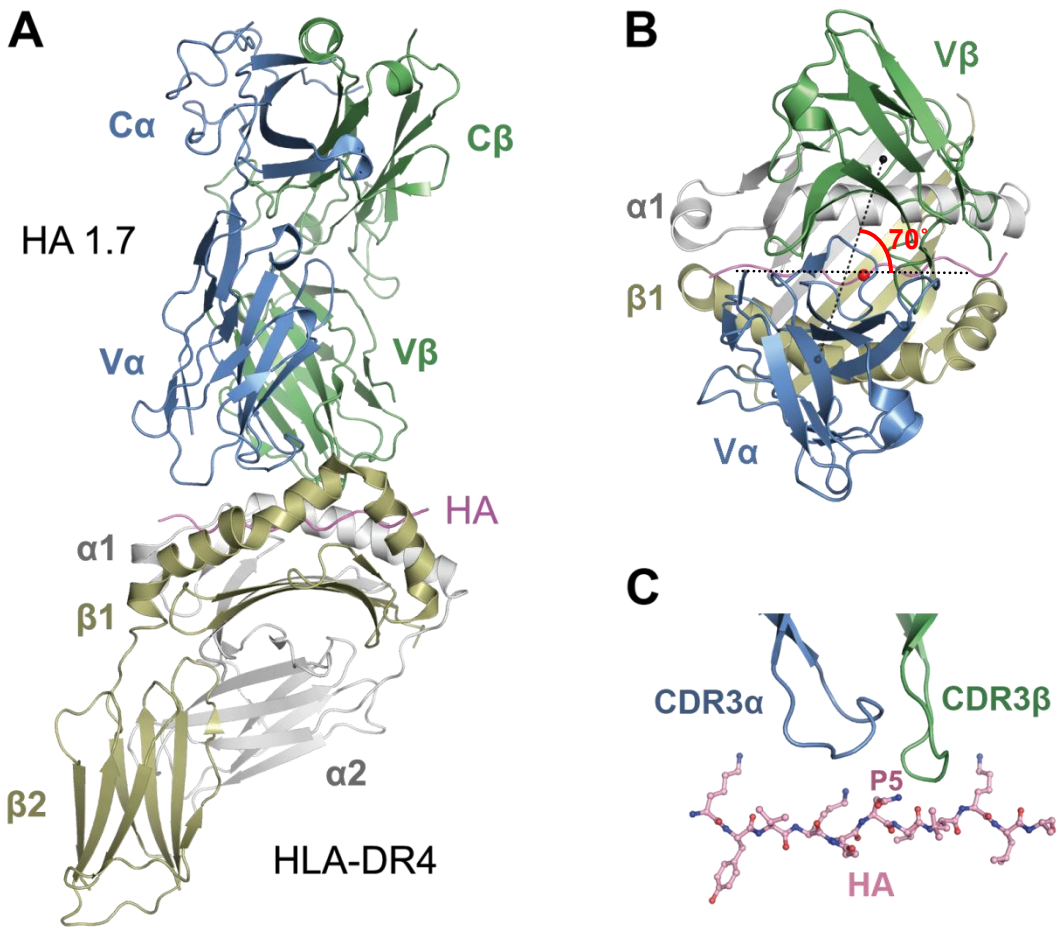

Figure 1.7 Structure of an anti-microbial TCR–pMHC complex.

(A) Overview of the complex of TCR HA1.7 and HLA-DR4 bound to a viral peptide, HA 306–318 (PDB code: 1J8H) (Hennecke and Wiley, 2002). (B) Top view of the structure. The Cα and Cβ domains of HA1.7, as well as the α2 and β2 domains of HLA-DR4, are removed for clarity. The P5 residue of HA is shown as a red sphere on the magenta backbone of HA. The two black spheres mark the centers of mass of the Vα and Vβ domains. A black dash line connecting the two dots forms an angle with a line drawn by linking the Cα atoms of the P1 and P9 residues of HA. This angle is defined as the "crossing angle" of TCR docking. (C) Side view of the interaction between the two CDR3 loops and the HA peptide. The center of the peptide, P5, is labeled.

are restricted to binding MHC molecules or the MHC-like molecule CD1. Conserved interactions between MHC and the germline-encoded CDR1 or CDR2 loops of TCR are found in almost all class I or class II complexes (Marrack et al., 2008). However, whether these phenomena are the result of co-evolution between MHC and TCR, or the consequence of positive selection during lymphocyte development, is still under considerable discussion (Collins and Riddle, 2008; Garcia et al., 2009; Marrack et al., 2008).

1.5.3 Biophysical characterizations of MHC class II-restricted recognition

As discussed previously, positive and negative selections are primarily based on TCR–pMHC affinities. In addition, affinities are a major determinant of T cell activation. Although TCRs share structural features with the Fab fragments of antibodies, TCRs have much weaker affinities for their peptide–MHC ligands. For instance, the affinity of an Fab for a protein antigen can exceed 10^{-9} M; by contrast, a typical TCR has an affinity in the range of 1–50 μM (Cole et al., 2007; Rudolph et al., 2006). In addition to affinity, the half-life or the dissociation rate constant, k_{off}, of an interaction may also play a role in T cell responses, which appears to be particularly important as it dictates how long a T cell "dwells" on a pMHC surface (Lyons et al., 1996; Stone et al., 2009). During thymic selection, the entire pre-mature T cell repertoire is scanned by self-peptide–MHC complexes to prevent further development of autoreactive clones. To make the process efficient, the time each T cell clone remains ligated to an individual pMHC should be relatively short, but still long enough for signal transductions to occur. As a result, the

half-lives of peripheral TCR–pMHC interactions also fall within a narrow window of 0.2–30 seconds (Cole et al., 2007; Rudolph et al., 2006).

Extensive measurements of TCR binding affinities and kinetics have been carried out to understand the biophysical properties of the interaction between TCRs and their cognate pMHC ligands. The binding affinity of a TCR is usually in the low micromolar range, which is comparable to the affinities of other molecular interactions at the lymphocyte cell surface. Yet, compared to the binding of other lymphocyte cell–cell recognition molecules, TCR–pMHC interactions usually have slower kinetics (van der Merwe and Davis, 2003). For instance, the association rate constant (k_{on}) of a TCR–pMHC interaction falls in the range of 10^3–10^5 $M^{-1}s^{-1}$, whereas other interactions have a k_{on}s of 10^5–10^6 $M^{-1}s^{-1}$ (van der Merwe and Davis, 2003). This may indicate that the TCR–pMHC interaction is a rate-control step for triggering a T cell signaling cascade. In addition, based on an average 20-fold longer half-life, the TCR–pMHC complex, once formed, is more stable than other most cellular interactions, which may be crucial for specifically amplifying signals during T cell activation (van der Merwe and Davis, 2003).

1.5.4 Altered binding topology of TCRs specific for self-antigens

Since negative selection prevents T cells with strong responses to self-antigens from entering the periphery, an autoimmune T cell may escape negative selection using certain strategies that compromise the overall stability of the signaling complex. Assuming the accessory molecules are invariant, this instability can be introduced by an unstable TCR–pMHC ternary complex. Recent biophysical and structural studies have shown that autoimmune TCRs adopt suboptimal binding modes for self-pMHC, resulting in reduced

affinities and altered binding topologies (Nicholson et al., 2005; Wucherpfennig et al., 2010).

The two human autoimmune complexes that currently have known structures are TCR Ob.1A12 bound to MBP 85-99–HLA-DR2b (Hahn et al., 2005) and TCR 3A6 bound to MBP 89-101–HLA-DR2a (Li et al., 2005). Both TCRs were isolated from MS patients and could induce EAE in humanized mice transgenic for the TCR and HLA-DR2b or HLA-DR2a. Because the previously known class I- and class II- TCR–pMHC complexes had presented similar structural features, the complex structures of these two autoimmune TCRs (Figure 1.8) have drawn considerable attention as they bind pMHC in ways that differ significantly from the classical mode of anti-foreign TCRs (Figure 1.7). The Ob.1A12 TCR engages pMHC with a crossing angle of 105 º, which is outside the diagonal-to-orthogonal range. Moreover, both Ob.1A12 and 3A6 bind to the N-terminal, instead of the central, portion of the MBP peptides. In addition, both TCRs are shifted toward the β1 helix, instead of being equally balanced between the two helices. These atypical topologies are also associated with low TCR affinities for self-pMHC ligands. Thus, Ob.1A12 binds to MBP–DR2b with K_D = 81 μM (Cole et al., 2007), whereas 3A6 binds to MBP–DR2a with even lower affinity (>200 μM) (Li et al., 2005). Studies of these two TCRs suggested that such suboptimal binding modes might be a common strategy used by autoimmune TCRs to escape negative selection.

Additionally, the aberrant docking angle of Ob.1A12 may represent a different mechanism for thymic escape. For T cell activation, the interaction between TCR and pMHC alone is not adequate for triggering activation. Assembly of the signaling complex

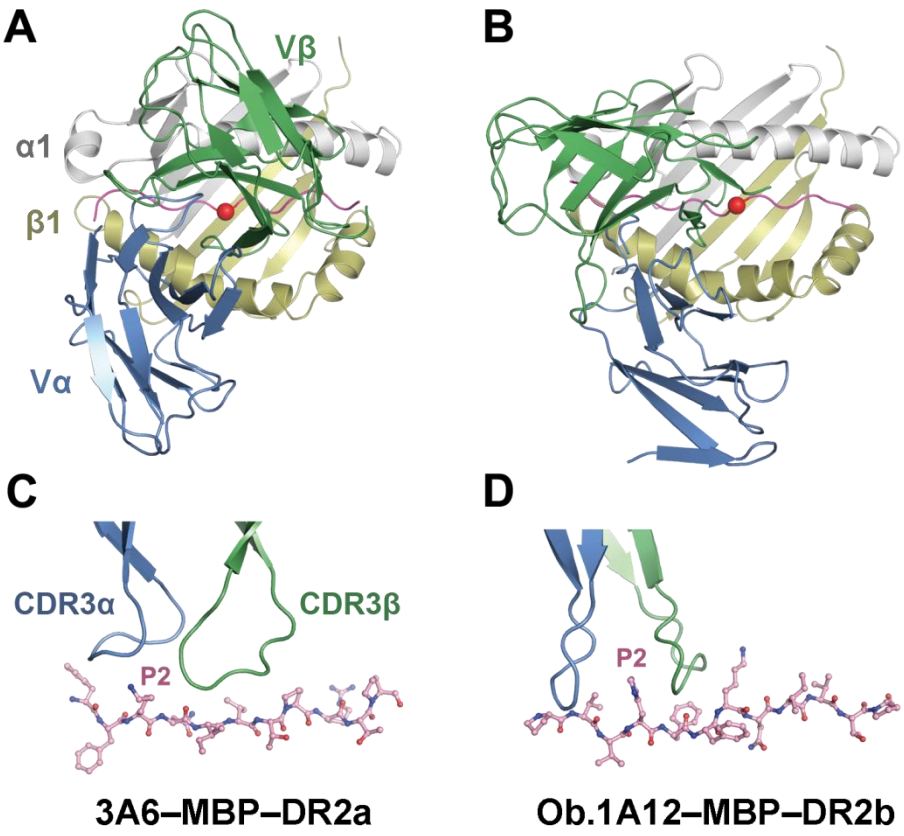

Figure 1.8 Altered binding topologies of autoimmune TCRs.

(A) Top view of the complex structure of TCR 3A6 bound to MBP 89-101–HLA-DR2a;

(B) Top view of the complex structure of Ob.1A12 bound to MBP 85-99–HLA-DR2b;

(C) Side view of the interaction between MBP and the CDR3 loops of TCR 3A6;

(D) Side view of the interaction between MBP and the CDR3 loops of TCR Ob.1A12.

Coloring and labeling are the same as in Figure 1.7.

involves co-receptors (CD4 or CD8) and other accessory molecules for recruitment of downstream signaling molecules such as the tyrosine kinase Lck. The engagement of accessory molecules should be optimal when TCR and pMHC are oriented in a conventional binding mode. The overall stability of this assembly should be able to exceed the activation threshold in order to elicit an immune response in the periphery. A similar threshold may apply to negative selection in the thymus, where stable assemblies with self-peptides induce programmed cell death to eliminate self-reactive T cells, whereas unstable assemblies permit survival. Although the affinity of Ob.1A12 is higher than that of 3A6, its 105^{o} crossing angle may affect ligation of the CD4 co-receptor, which is likely to allow the maturation of T cells bearing this TCR, since a sufficiently stable signaling complex may not form.

1.6 Autoimmune TCR MS2-3C8 recognizes MBP presented by HLA-DR4

1.6.1 MBP 111-129 is an immunodominant self-peptide in HLA-DRB1*0401 MS patients

Myelin basic protein (MBP) is the major protein component of the myelin sheath and a target for nerve tissue damage. Autoreactive T cells recognize various epitopes of MBP associated with different MHC molecules. In Caucasians, the MHC class II allele HLA-DRB1*1501 is the most common genetic risk factor for MS (Hillert and Olerup, 1993). MBP 81-99, recognized in the context of this allele in MS patients, has been the most investigated immunodominant epitope. However, therapies based on these studies may not apply to other ethnic groups with different genetic backgrounds. As mentioned above,

HLA-DR4 confers susceptibility to MS in Caucasians of Mediterranean origin. Examinations of MS patients carrying the HLA-DR4 (B1*0401) allele suggested a distinct immunodominant MBP epitope (Muraro et al., 1997). MBP exists as different isoforms resulting from alternative mRNA splicing. Among them, the classical form, 18.5 kDa MBP, is predominant in the nervous system, and is also expressed in immune organs, such as thymus (Pribyl et al., 1993). MBP 111–129, contained in this 18.5-kDa isoform, was found to be the immunodominant self-peptide in the context of HLA-DR4 (Muraro et al., 1997).

In one study, MBP-specific T cell lines (TCLs) were established from 12 subjects, all carrying the B1*0401 allele. A set of overlapping 19-mer peptides covering the full 18.5-kDa length of MBP was used for testing the fine peptide specificity of these TCLs. It was found that 65% of a total 275 TCLs responded to MBP 111–129, whereas the next most frequent peptide, MBP 81-99, only activated 6.6% of TCLs, indicating that MBP 111–129 dominates the MBP-specific T cell response in HLA-DR4-carrying subjects. Further investigations revealed a limited usage of TCR rearrangements in these MBP 111–129-specific T cells. Sequence analysis showed that the TCRA4.1 and TCRB2.1 or TCRB7.1 genes are overrepresented in the T cell pool. Characteristic amino acids found in the CDR3 sequences indicated that only TCLs with certain gene rearrangements could respond to MBP 111–129, further suggesting a restricted T cell repertoire for MBP 111–129/HLA-DR4 (Muraro et al., 1997).

Muraro et al. (1997) also performed peptide competition assay to measure the relative binding affinity of each MBP peptide for HLA-DR4. Surprisingly, the immunodominant MBP 111–129 epitope is such a weak binder that it binds DR4

approximately 75-fold less tightly than the influenza virus hemagglutinin epitope HA 307–319, a microbial peptide known to bind well to DR4. By contrast, MBP 81–99 binds efficiently to HLA-DR4 as well as HLA-DR2 alleles. Unlike MBP 111–129, MBP 81–99 elicits a diverse T cell repertoire. The affinity of the self-peptide for MHC determines the stability of the self-pMHC complex, as well as the overall stability of the TCR–pMHC complex, which may therefore affect the outcome of thymic selection. An inverse relationship between the diversity of a TCR repertoire and the affinity of the antigenic peptide for MHC has been further documented recently: Baumgartner et al. (2010) demonstrated in mice that peptides with high affinity for MHC class II recruit a more diversified $CD4^+$ T cell repertoire, whereas peptides with low affinity shape a more restricted TCR repertoire, but with higher functional TCR avidity. It is important to mention that the dose of administrated antigens also impacts TCR repertoire diversity, as low doses of high-affinty peptides also lead to limited usage of TCRs with higher avidities (Baumgartner et al., 2010).

1.6.2 MS2-3C8 is an MS-related TCR specific for MBP 111–129 in the context of HLA-DR4

MBP-specific TCLs were established from the peripheral blood of a DRB*0401-positive MS patient at two time points over two years apart. Of these TCLs, 80–90% responded to MBP 111–129 in the context of HLA-DR4. Sequence analysis showed that these MBP 111–129-specific TCLs resulted from clonal expansion of a single T cell clone (TCC), designated MS2-3C8. The repeated isolation and overrepresentation of MS2-3C8 in the patient's peripheral blood strongly suggested the involvement of this particular

TCC in MS disease pathogenesis. To assess the relevance of MS2-3C8 to disease incidence and progression, Quandt et al. (2004) generated humanized mice transgenic for MS2-3C8 and HLA-DR4. $CD4^+$ MS2-3C8 T cells were then isolated from the spleens of these mice. The pathogenic potential of TCR MS2-3C8 was demonstrated by the ability of these transgenic cells to induce EAE in HLA-DR4-transgenic mice, which displayed both clinical phenotypes of EAE and cellular inflammation in the CNS (Kawamura et al., 2008; Quandt et al., 2004).

In order to become pathogenic in the periphery, an autoimmune TCR must first escape the clonal deletion. MS2-3C8 recognizes MBP 111–129, which is a low-affinity epitope for HLA-DR4. It has been shown that the establishment of self-tolerance may be incomplete with a low-affinity epitope, whereas high-affinity epitopes (e.g. HLA-DR2-binding MBP 81–99) can efficiently induce T cell tolerance (Kawamura et al., 2008). However, the molecular basis for autoreactive TCR recognition of low-affinity epitopes is not clear. For MS2-3C8, we were interested in how this particular autoimmune TCR recognizes MBP 111-129 presented by HLA-DR4. Does this TCR indeed have a higher affinity than other autoreactive TCRs, as suggested by Baumgartner et al. (2010)? Structurally, does TCR MS2-3C8 follow the altered binding patterns seen in the other two autoimmune TCRs, 3A6 and Ob.1A12? If MS2-3C8 is a high-affinity TCR, it may not necessarily bind in the same way as 3A6 and Ob.1A12, the two low-affinity TCRs. Instead, it is more likely that MS2-3C8 engages its ligand as other high-affinity TCRs, namely anti-microbial TCRs. By characterizing the binding features of MS2-3C8, we hoped to gain insights into how this autoimmune TCR escaped negative selection.

Chapter 2

Protein expression and purification of MS2-3C8 and MBP–HLA-DR4

SUMMARY

There are different strategies available to acquire relatively large quantities of proteins for the purpose of crystallization. In order to obtain more homogeneous proteins, we chose to produce MS2-3C8 and MBP–HLA-DR4 using *in vitro* folding method. Since MBP 111–129 is a weak peptide for HLA-DR4, we covalently linked the peptide to the MHC to stabilize the pMHC complex. Initially, the yield of *in vitro* folding was not satisfactory. Efforts were then taken to optimize the folding conditions. The yields were significantly improved which made it possible for crystallization studies.

2.1 Background

Macromolecule crystallography requires high-purity protein samples for obtaining crystals suitable for X-ray diffraction analyses. Initial crystallization trials usually require at least a milligram of purified protein. Therefore, producing sufficient amounts of biologically active proteins is the first "bottleneck" for the determination of protein structures. For biophysical and structural studies of the interaction between autoimmune TCR MS2-3C8 and HLA-DR4 bearing the MBP 111–129 self-peptide, we produced these two proteins in soluble form.

The production of MHC molecules loaded with homogenous peptides has been much studied, as pMHC complexes are not only used for structural determination and biophysical characterization, but also in immunological assays, such as immunohistochemical staining or flow cytometric sorting of antigen-specific T cells. Compared to research on class I-oriented $CD8^+$ T cell responses, studies of $CD4^+$ T cells are more limited. One of the major reasons for this disparity is that class II molecules are technically more difficult to produce. Recombinant MHC class I molecules are typically folded *in vitro* from bacterial inclusion bodies with high yields. In some cases, MHC class II can be produced using similar methods (Arimilli et al., 1995; Frayser et al., 1999). However, yields are generally much lower than for MHC class I. Therefore, class II molecules are mostly produced using eukaryotic expression systems, including mammalian, yeast, and insect cells. Various approaches have been applied to increase the stability and expression level of MHC class II molecules. The two polypeptides of an MHC class II heterodimer are not covalently linked by disulfide bonds. To enhance their

association and therefore stabilize the heterodimer, Kalandadze et al. (1996) added a Fos/Jun leucine zipper pair to the C-termini of the α- and β-chains of HLA-DR2. The soluble protein was initially secreted by yeast strain *Pichia pastoris* at a relatively low level of 0.4 mg/L (Kalandadze et al., 1996). To prepare proteins for structural studies, Smith et al. (1998) switched to a baculovirus insect cell expression system for better expression. The leucine zipper was enzymatically cleaved before crystallization. In another case, HLA-DR4, when produced in a baculovirus system, gave better yields when co-expressed with a chaperone protein, calreticulin, to assist protein folding in the endoplasmic reticulum (Fourneau et al., 2004). Stably transfected *Drosophila* S2 cells are another popular source for MHC class II production for X-ray crystallographic studies (Amicosante et al., 2001; Hennecke et al., 2000).

The structure of HLA-DR4 was previously determined from proteins that were produced in either *Drosophila* S2 cells (Dessen et al., 1997; Hennecke and Wiley, 2002) or baculovirus-infected Hi5 cells (Bolin et al., 2000). The binding groove of MHC molecules expressed in insect cells is partially occupied by endogenous peptides (Hill et al., 1994; Scheirle et al., 1992). The unresolved side-chain conformation of the human collagen II (hCII) peptide in the DR4 structure (2SEB) is probably a result of heterogeneity in peptide binding (Dessen et al., 1997). Such heterogeneity would be problematic for co-crystallizing pMHC with TCR, since TCR only recognizes a specific peptide. Because MBP 111–129 binds weakly to HLA-DR4, it is difficult to achieve homogeneity by simply loading the peptide into the MHC molecule. To assure homogeneous association, the MBP peptide can be covalently attached to N-terminus of DR4 β-chain via a 16-amino acid linker (GGGGSLVPRGSGGGGS). This strategy, first

introduced by Kozono et al. (1994) (Figure 2.1), simplifies production by omitting the peptide loading step. More importantly, it effectively stabilized the peptide-bound MHC class II molecule, which was produced by baculovirus-infected Sf9 cells (Kozono et al., 1994).

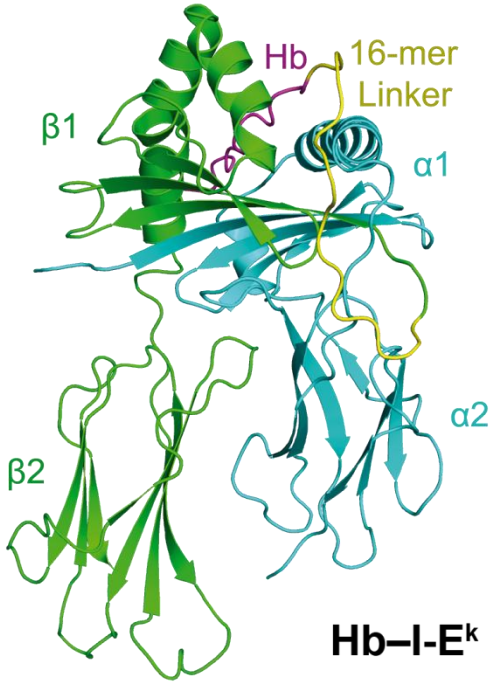

Figure 2.1 MHC class II I-E^k engineered with a covalently bound peptide.

Structure of I-E^k bound to hemoglobin peptide Hb 64–76 (magenta) covalently linked to the N-terminus of the β-chain (green) via a 16-mer peptide linker (yellow) (PDB code: 1IEA) (Fremont et al., 1996). The peptide linker is visible in the crystal structure because of its interaction with another I-E^k molecule in the asymmetric unit.

TCR molecules can be produced similarly to MHC molecules, either in insect cells or by *in vitro* folding from bacterial inclusion bodies. Several methods have been developed to engineer soluble and stable TCR proteins. First, a single-chain form of TCR (scTCR) was designed by connecting the two V domains with a 25-mer linker (Schodin

et al., 1996). However, because scTCRs lack C domains, they are not suitable for most biological assays. The low success rate of soluble scTCR expression is another reason that a more general method is needed for TCR production.

In another approach, the ectodomains of the TCR α- and β-chains are covalently linked by a disulfide bond formed by a pair of cysteine residues at the C-termini of the C domains. However, *in vitro* folding of TCRs with the C-terminal disulfide often gives satisfactory yields, while TCRs lacking this disulfide may be unstable. To overcome these problems, Boutler et al. (2003) introduced cysteine mutations in the middle of the C domains in order to create an artificial interchain disulfide link. In this way, soluble TCR proteins were obtained in relatively high yields; moreover, these engineered TCRs behave biochemically the same as native TCRs. A large number of TCR structures solved today include this artificial disulfide bond.

Thus, there are a number of options for producing recombinant TCR and MHC molecules. However, because each TCR or MHC is a unique protein, the best strategies to produce MS2-3C8 and MBP–HLA-DR4 had to be found empirically.

2.2 Results

2.2.1 Production of MBP-bound HLA-DR4

MBP 111–129 (LSRFSWGAEGQRPGFGYGG) is specifically recognized by the T cell clone MS2-3C8 in an HLA-DR4-restricted manner (Muraro et al., 1997; Quandt et al., 2004). These authors also determined that MBP 116–123 (WGAEGQRP) contains the minimal epitope for T cell stimulation, in which Trp116 serves as the P1 anchor residue.

Thus, we used residues 114–126 of MBP as a 13-mer core sequence for binding to HLA-DR4. Since this self-peptide is a low-affinity binder for HLA-DR4, it was possible that it would not stably associate with the MHC molecule. Therefore, we designed a peptide-linked construct to obtain MBP-bound HLA-DR4 proteins, in addition to a non-linked construct.

i. Non-peptide-linked HLA-DR4 is produced but is not stable

As a first attempt, chemically synthesized MBP 114–126 was added to an *in vitro* folding solution to incorporate the peptide into the binding groove of HLA-DR4 during the folding process. We achieved a reasonable yield of about 0.5 mg/L protein after purification. However, the purified MBP–HLA-DR4 did not maintain its integrity, probably due to dissociation of the heterodimer. In addition, non-linked MBP–HLA-DR4 failed to bind TCR MS2-3C8 in a surface plasmon resonance (SPR) assay, which indicated that the protein had lost its biological activity (data not shown). The behavior of this non-linked form of MBP–HLA-DR4 suggests that the affinity of the bound peptide is positively correlated with the overall stability of the MHC molecules (Dedier et al., 2000; Saito et al., 2004).

ii. Peptide-linked HLA-DR4 is stable but with low yield

To enhance the association of MBP 114–126 with HLA-DR4 and thereby stabilize the pMHC complex, we attached the peptide to the N-terminus of the β-chain via a 16-mer flexible linker (SGGGSLVPRGSGGGGS) (Figure 2.2). The engineered protein was

produced by *in vitro* folding similarly to non-linked form, but without the addition of synthetic MBP peptide. However, the yield of purified protein was too low for crystallographic studies. Nevertheless, this material was for testing binding to TCR MS2-3C8 by SPR, which revealed that the peptide-linked form of MBP–HLA-DR4 was biologically active (see Chapter 3).

```
-----> NdeI <-------------MBP(114-126)------------><--------
gatatacatatgtttagttggggtgcagaaggtcaacgtccaggttttggttctggtggt
          M  F  S  W  G  A  E  G  Q  R  P  G  F  G  S  G  G

-----------LINKER---------------------><------------HLA-DR4β
ggttctcttgttccacgtggttctggtggtggtggttctggggacacccgaccacgtttc
 G  S  L  V  P  R  G  S  G  G  G  G  S  G  D  T  R  P  R  F
```

Figure 2.2 Sequence of HLA-DRB1*0401 with MBP 114–126 covalently attached to its N-terminus via a 16-aa linker.

To improve the yield of *in vitro* folding, a folding matrix was designed based on our initial folding condition and available commercial folding kits (Table 2.1). Small scale foldings (1 ml) were set up for each condition of the folding matrix, which was sampled at two different time points, 3 and 7 days. Properly folded MBP–HLA-DR4 species was detected by ELISA using a mouse anti-HLA-DR monoclonal antibody (L243). The data showed that the folding yield was strongly affected by pH, that salt is a strong inhibitor of MBP–HLA-DR4 folding, and that varying the redox ratio did produce dramatic effects (Table 2.1, Figure 2.3). Moreover, longer folding time were necessary to achieve better yields. For large-scale production, the folding time was extended to a minimum of 2 weeks. This gave yields of 0.1-0.2 mg purified protein per liter of folding mixture, following gel filtration and ion exchange chromatography (Figure 2.4).

Table 2.1 Tested folding conditions for MBP–HLA-DR4.

Test No.	L-arginine (M)	Guanidine (M)	Glycerol (v/v%)	NaCl (mM)	GSH (mM)	GSSG (mM)	GSH/GSSG	pH
1.1	0	0	0	20	2	0.2	10	8.2
1.2	0.4	0	0	20	2	0.4	5	8.2
1.3	0.8	0	0	20	1	1	1	8.2
1.4	0	0.5	0	20	2	0.2	10	8.2
1.5	0	0.5	0	20	2	0.4	5	8.2
1.6	0	0.5	0	20	1	1	1	8.2
1.7	0	1	0	20	2	0.2	10	8.2
1.8	0	1	0	20	2	0.4	5	8.2
1.9	0	1	0	20	1	1	1	8.2
2.1	0	0	30	0	3	0.3	10	7.5
2.2	0	0	30	0	3	0.9	3.3	7.5
2.3	0	0	30	0	2	1.2	1.7	7.5
2.4	0	0	30	0	3	0.3	10	8
2.5	0	0	30	0	3	0.9	3.3	8
2.6	0	0	30	0	2	1.2	1.7	8
2.7	0	0	30	0	3	0.3	10	8.5
2.8	0	0	30	0	3	0.9	3.3	8.5
2.9	0	0	30	0	2	1.2	1.7	8.5
3.1	0	0	30	0	3	0.3	10	7.5
3.2	0	0	30	0	3	0.9	3.3	7.5
3.3	0	0	30	0	2	1.2	1.7	7.5
3.4	0	0	30	0	3	0.3	10	8
3.5	0	0	30	0	3	0.9	3.3	8
3.6	0	0	30	0	2	1.2	1.7	8
3.7	0	0	30	0	3	0.3	10	8.5
3.8	0	0	30	0	3	0.9	3.3	8.5
3.9	0	0	30	0	2	1.2	1.7	8.5

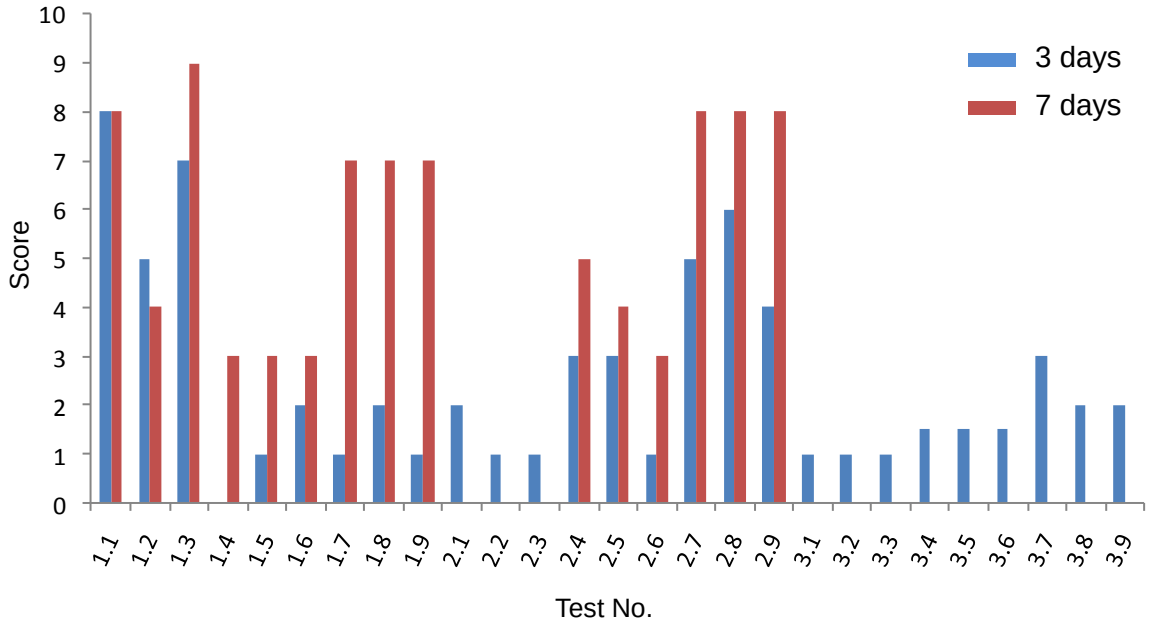

Figure 2.3 Folding conditions for MBP–HLA-DR4.

Folding yields of MBP–HLA-DR4 were analyzed for each condition by ELISA and scored with arbitrary numbers of 0 to 10 based on HLA-DR1 positive controls. 0 indicates blank, and 10 means saturation. All 27 conditions were tested on day 3, whereas only the first 18 conditions were tested on day 7.

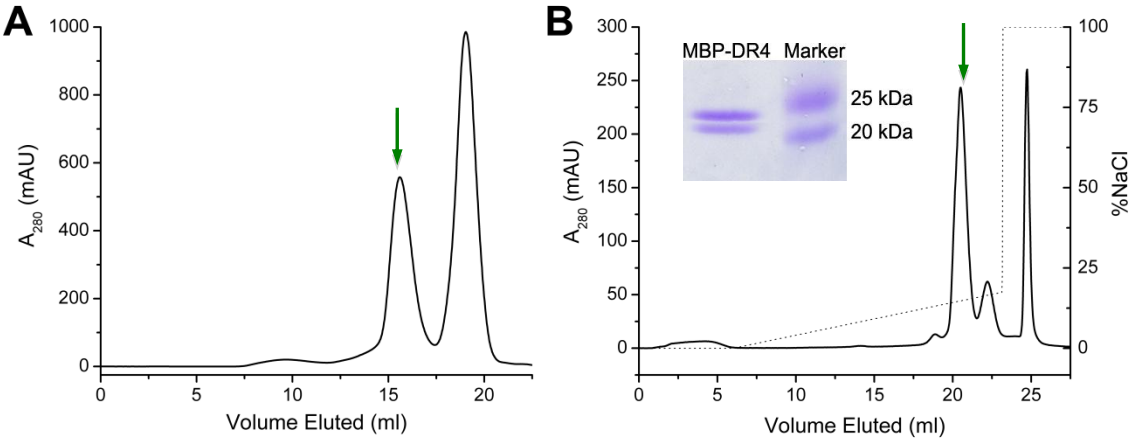

Figure 2.4 Purification profile of MBP–HLA-DR4.

(A) Size exclusion chromatography of MBP–HLA-DR4 using a Superdex-200 column. The green arrow indicates the fraction containing the folded protein.

(B) Anion exchange chromatography of MBP–HLA-DR4 using a MonoQ column.

2.2.2 Production of TCR MS2-3C8

The MBP-specific TCR, MS2-3C8, was also produced by *in vitro* folding with either the native or the artificial disulfide bridge. Although the construct contauining the artificial disulfide gave better yields than the native form, it was less stable and less amenable to crystallization. Thus, all subsequent work on MS2-3C8 used only the native form, which had a yield of about 1 mg per liter of folding mixture. Figure 2.5 shows typical chromatograms of MS2-3C8 by size exclusion column and anion exchange columns, from which this TCR was obtained at >95% purity. Analytical ultracentrifugation analysis of purified MS2-3C8 showed a peak with a sedimentation coefficient of 3.8 S, corresponding to the folded TCR heterodimer (Figure 2.6). Good binding activities of the folded molecules were demonstrated in SPR assays (see Chapter 3).

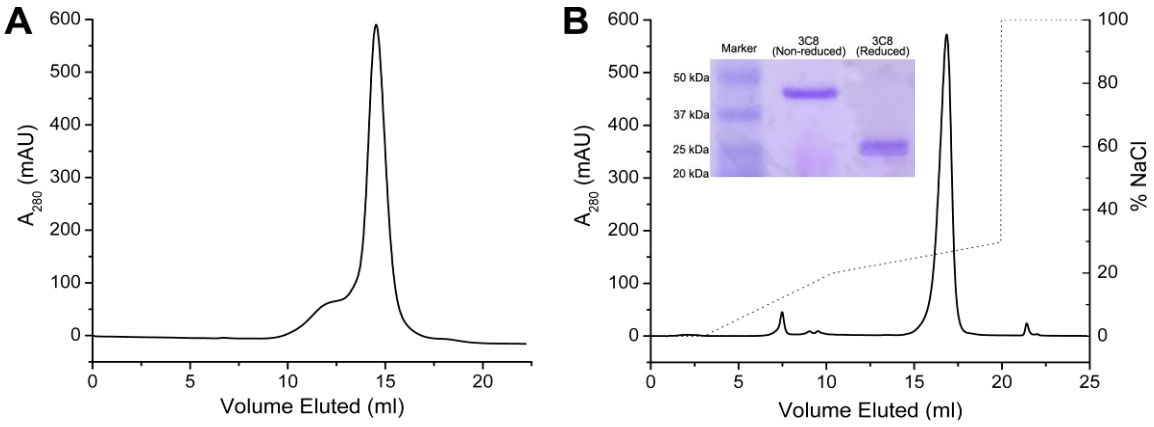

Figure 2.5 Protein purification profile of TCR MS2-3C8.

(A) Size exclusion chrmotagraphy of MS2-3C8 using a Superdex-200 column.

(B) Anion exchange chromatography of MS2-3C8 using a MonoQ column.

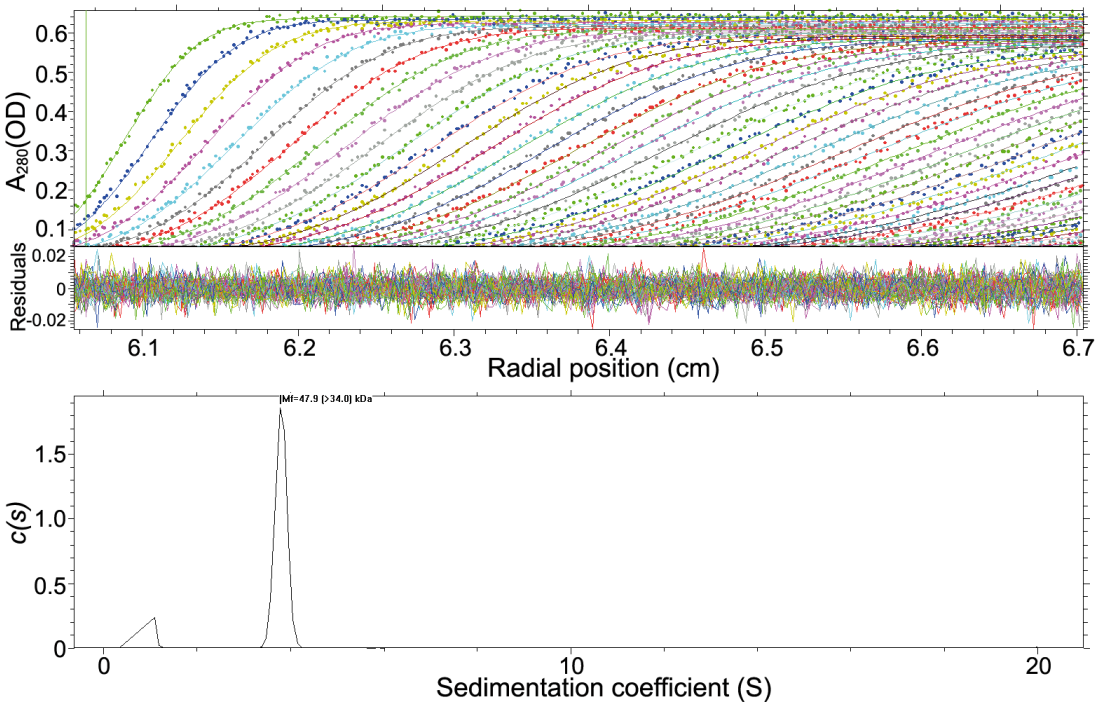

Figure 2.6 Analytical ultracentrifugation analysis of purified TCR MS2-3C8.

The top panel shows raw sedimentation velocity scans collected for purified MS2-3C8 at 0.4 mg/mL, overlayed with the best-fit curves obtained from data analysis. The residuals of the fit are shown below. The bottom panel shows the sedimentation coefficient distribution for TCR MS2-3C8. Apart from a small background peak, the single peak at 3.8 S confirms the homogeneity of the MS2-3C8 sample.

2.3 Discussion

Although there are numerous examples of successful production of MHC and TCR molecules by insect cell expression, we preferentially produced our proteins by *in vitro* folding from bacterial inclusion bodies. Basically, there are two non-economical reasons we prefer this approach. First, MHC and TCR are both glycoproteins. When expressed in insect cells, glycosylation will introduce heterogeneity, which can potentially interfere

with crystal packing during crystallization. Second, solubilized inclusion bodies used for *in vitro* folding, although denatured, are usually very pure. Therefore, *in vitro*-folded proteins are generally not fused with any purification tags. This effectively eliminates any risk to crystallization that might be caused by a tag.

One possible reason why *in vitro* folding of MBP–HLA-DR4 has such a low yield is the unusually weak binding of the MBP self-peptide. It has been reported that the affinity of the MHC molecule for the bound peptide correlates with the thermal stability of the pMHC complex (Saito et al., 2004). The non-linked MBP–HLA-DR4 quickly dissociated after purification, unless excess peptide was added, which is consistent with the peptide-dependent stability of MHC molecules. The MBP-linked HLA-DR4, albeit difficult to produce, is a stable molecule that can be employed for biophysical and structural analyses. However, the peptide-linking strategy may not guarantee pMHC stability in the case of a weaker peptide binder. Mouse MBP 1–11 is another low affinity peptide, which binds to the mouse MHC class II molecule, I-A^u, with an even lower affinity than MBP 111–129 binds HLA-DR4 (Fugger et al., 1996). To determine the crystal structure and binding kinetics of the MBP–I-A^u complex, a high-affinity variant (K4Y) of MBP 1–11 was used to connect with the β-chain because I-A^u was not sufficiently stabilized by attaching wild-type MBP 1–11 (He et al., 2002). It is fortunate in our case that linking wild-type MBP 114–126 was sufficient to stabilize the MBP–HLA-DR4 complex; otherwise, we would have faced the risk that high-affinity peptide analog may not retain the structural or biological properties of the wild type peptide.

During the process of *in vitro* folding, different factors modulate the balance between aggregation and refolding of a denatured protein. Identifying conditions that favor folding

over aggregation sometimes requires extensive trials; alternatively, one may simply switch to eukaryotic expression systems. Owing to our own preference for *in vitro* folding, we invested considerable efforts to optimizing the folding conditions. We concluded that time is an critical parameter for folding HLA-DR4, which indicates that the folding process is particularly slow and that it is difficult to reach equilibrium. The buffer pH seemed to be another parameter that impacted the rate and yield of HLA-DR4 refolding. On one hand, pH interacts with and controls the redox environment of folding (Khan et al., 2000); on the other hand, the stability of HLA-DR4 is also dependent on pH (Belmares et al., 2000). By characterizing the effects of each parameter, we were able to improve the folding yield of MBP–HLA-DR4, which enabled subsequent crystallographic studies.

MHC class II molecules present antigenic peptides to $CD4^+$ T cells and elicit helper T cell immune functions. The high demand for recombinant TCR and pMHC class II molecules for immunological studies contrasts with their low production yields, which hinders research in this area. For example, research on MHC class I-dependent cytotoxic T cell functions is far more advanced than that on MHC class II-dependent helper T cell functions. Moreover, the Protein Data Bank includes over 400 MHC class I structures, whereas less than 80 MHC class II structures have been determined. To date, only 7 human TCR–pMHC class II structures have been reported, 3 of which are very closely related (PDB code: 1ZGL, 1FYT and 1J8H, 1YMM and 2WBJ, 2IAM and 2IAN). To identify general mechanisms of $CD4^+$ T cell recognition of foreign or self-antigens, it is necessary to expand the structural database of TCR–pMHC class II complexes.

Chapter 3

MS2-3C8 is a high-affinity TCR for its MBP–HLA-DR4 self-ligand

SUMMARY

The low affinity of MBP for HLA-DR4 leads to unstable formation of the pMHC complex, which permits the escape of TCC MS2-3C8. In order to effectively cause autoimmune attacks in the periphery, MS2-3C8 is unlikely to bind to MBP–HLA-DR4 with a weak affinity. To characterize the binding interaction between MS2-3C8 and MBP–DR4, we performed both equilibrium and kinetics assays using SPR method. Directional immobilization of MBP-linked HLA-DR4 allows more reliable measurements. The affinity values obtained from equilibrium and kinetics assays agree with each other. MS2-3C8 binds to MBP–DR4 with a high affinity that represents the upper end of the affinity range for class II MHC recognition. Besides, the kinetic values indicate that the binding reaction is unusually slow.

3.1 Background

The initiation of T cell signaling, which is triggered by the binding of TCR to pMHC (Eq. 3.1), is remarkably specific and sensitive. Previous binding measurements indicated that the affinity, or the equilibrium constant (K_D), of a TCR for its pMHC ligand usually falls within a narrow window, ranging from 10^{-6} to 10^{-5} M (Cole et al., 2007; Rudolph et al., 2006). Additionally, both kinetic parameters, the dissociation rate constant (k_{off}) and the association rate constant (k_{on}) (Eq. 3.1), of a TCR binding reaction also fall within narrow ranges. The dissociation rate, or the derived half-life ($t_{½}$) (Eq. 3.3), reflects how long the TCR engages its pMHC ligand.

$$\mathrm{TCR} + \mathrm{pMHC} \underset{k_{off}}{\overset{k_{on}}{\rightleftharpoons}} \mathrm{TCR{\cdot}pMHC} \qquad \text{(Eq. 3.1)}$$

$$K_D = k_{off}/k_{on} \qquad \text{(Eq. 3.2)}$$

$$\text{Half-life } (t_{½}) = \ln 2 / k_{off} \qquad \text{(Eq. 3.3)}$$

It has been hotly debated whether the affinity or the half-life is better correlated to T cell activation. For example, Lyons et al. (1996) demonstrated that T cell stimulation is closely related to TCR affinity. Nevertheless, since differences in TCR affinities mainly derive from their k_{off} values (Eq. 3.2), these authors suggested that differential T cell responses largely depend on the half-life of the corresponding TCR–pMHC complex (Lyons et al., 1996). Kersh et al. (1998) obtained further evidence supporting this view by examining TCR–pMHC complexes having similar affinities but disparate half-lives (Kersh et al., 1998). However, the conclusion that T cell triggering is solely dependent on k_{off} may be pre-mature because no one has tested TCRs having similar off-rates but different affinities. The affinity of a TCR reflects the responsiveness of the TCR to a

certain concentration of its cognate pMHC ligand, which determines how many receptors on the T cell are bound to pMHC. The more TCRs bound, the easier it is to attain the triggering threshold. The differential activation status of an autoimmune TCR in different tissues, such as the thymus and the CNS, relies on its affinity and the variable availability of its self-pMHC ligand.

Surface plasmon resonance (SPR), usually performed using a Biacore instrument, is one of the standard techniques used for characterizing the binding interaction between TCR and pMHC. Compared to other biophysical methods, such as isothermal titration calorimetry (ITC), analytical ultracentrifugation (AUC), and fluorescence stopped-flow, SPR has several important advantages for analyzing TCR–pMHC interactions. First, SPR can measure both kinetic and thermodynamic parameters, whereas ITC or AUC cannot provide kinetic information. Second, SPR consumes much less protein sample. TCR–pMHC interactions have micromolar K_Ds. For instance, with an affinity of 10 μM, ITC requires at least 10 mg of each binding partner to perform a reliable measurement. By contrast, a Biacore experiment needs much less. One species, usually the pMHC ligand, is immobilized on a chip surface, which requires only microgram amounts of protein, while a total of about a half-milligram of TCR suffices for a binding measurement. This is especially important for our measurements of TCR MS2-3C8 binding to MBP–HLA-DR4, because both proteins, especially MBP–HLA-DR4, are difficult to produce. In addition, SPR delivers sensitive and accurate measurements, which is important for comparing TCRs displaying a narrow range of binding values.

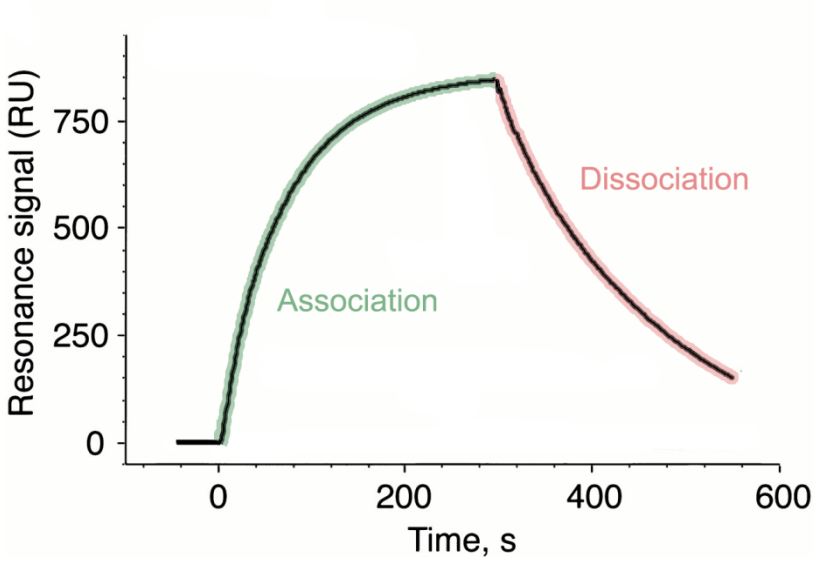

Figure 3.1 Example of an SPR sensorgram.

In this experiment, the injection of analyte was started at time 0. Association of the analyte to the ligand on the chip surface caused an increase in the resonance signal. Injection was stopped at 300 sec, which marked the start of the dissociation phase. The association curve is highlighted in green, and the dissociation curve is highlighted in red.

In a typical SPR experiment, one binding partner (e.g. pMHC) is immobilized on a biosensor chip surface, when the other binding partner (e.g. TCR) flows over the chip. During the association phase (Fig. 3.1), TCR molecules binding to immobilized pMHC will cause an increase in SPR signal, which is expressed as response units (RU). During the dissociation phase, when only buffer is flowed, the SPR signal decreases. For a simple 1:1 binding reaction like that between TCR and pMHC, the association and dissociation phases may be described by Eq. 3.4 and Eq. 3.6, respectively. Here, the concentration of TCR pMHC complex, [TCR pMHC], can be replaced by RU, and the total concentration of pMHC, equivalent to the maximal concentration of [TCR pMHC], can be replaced by RU_{max} (Eq. 3.5 and Eq. 3.7). These two equations are used,

respectively, for fitting the association and dissociation curves of a Biacore sensorgram, in which the concentration of TCR, [TCR], is inputted by the experimenter, RU and time t are two variables, and the two kinetic parameters, k_{off} and k_{on}, as well as RU_{max} are fitted. The affinity, K_D, is then calculated according to Eq. 3.2.

Association:

$$\frac{d[TCR\cdot\ pMHC]}{dt} = k_{on}[TCR][pMHC] - k_{off}[TCR\cdot\ pMHC] \quad \text{(Eq. 3.4)}$$

$$\frac{dRU}{dt} = k_{on}[TCR](RU_{max} - RU) - k_{off}RU \quad \text{(Eq. 3.5)}$$

Dissociation:

$$\frac{d[TCR\cdot\ pMHC]}{dt} = -k_{off}[TCR\cdot\ pMHC] \quad \text{(Eq. 3.6)}$$

$$\frac{dRU}{dt} = -k_{off}RU \quad \text{(Eq. 3.7)}$$

Table 3.1 Measurable values of rate constants for biological interactions by Biacore

	Biological interactions	**Measurable range**
k_{on} ($M^{-1}s^{-1}$)	10^3–10^9	10^3–10^8
k_{off} (s^{-1})	10^{-5}–1	10^{-5}–10^{-1}

Because of instrumental limitations, measurable kinetics of an interaction should not be too fast. For a Biacore biosensor, k_{off} should be smaller than 0.1 s^{-1} and k_{on} should be lower than 10^8 $M^{-1}s^{-1}$ (Table 3.1). Outside these ranges, kinetic values will not be

accurately fitted. However, it is still possible to obtain affinity values for fast interactions using equilibrium analysis. With a series of concentrations of TCR flowing over the sensor chip, SPR signals at the plateau of equilibrium are recorded. The equilibrium RU and TCR concentration are then used as two variables for fitting the affinity K_D using Eq. 3.8.

$$RU = \frac{[TCR]}{K_D + [TCR]} RU_{\max} \qquad \text{(Eq. 3.8)}$$

Our interest in measuring the binding of TCR MS2-3C8 MBP–HLA-DR4 was aroused primarily by the unusually weak binding of the MBP 111–129 self-peptide for HLA-DR4. The two MS-related TCRs of known complex structures, Ob.1A12 and 3A6, both displayed very low affinities for their pMHC class II ligands, which facilitated their escape from negative selection. In these two cases, the self-peptides bind strongly to MHC. In sharp contrast, for TCR MS2-3C8, it is the weak peptide–MHC association that may have destabilized the overall TCR–pMHC complex and thus enabled MS2-3C8 T cells to avoid thymic deletion. However, in order to become activated in the periphery, the T cell needs to form a TCR–pMHC complex that is sufficiently stable to initiate the signaling cascade. We hypothesized that triggering would be unlikely to occur if TCR MS2-3C8 had an affinity as low as Ob. 1A12 or 3A6. Instead, MS2-3C8 is more likely to have an affinity at the high end of the affinity range for TCRs recognizing pMHC class II. To test our hypothesis, we determined the affinity of MS2-3C8 as well as its binding kinetics for MBP–HLA-DR4.

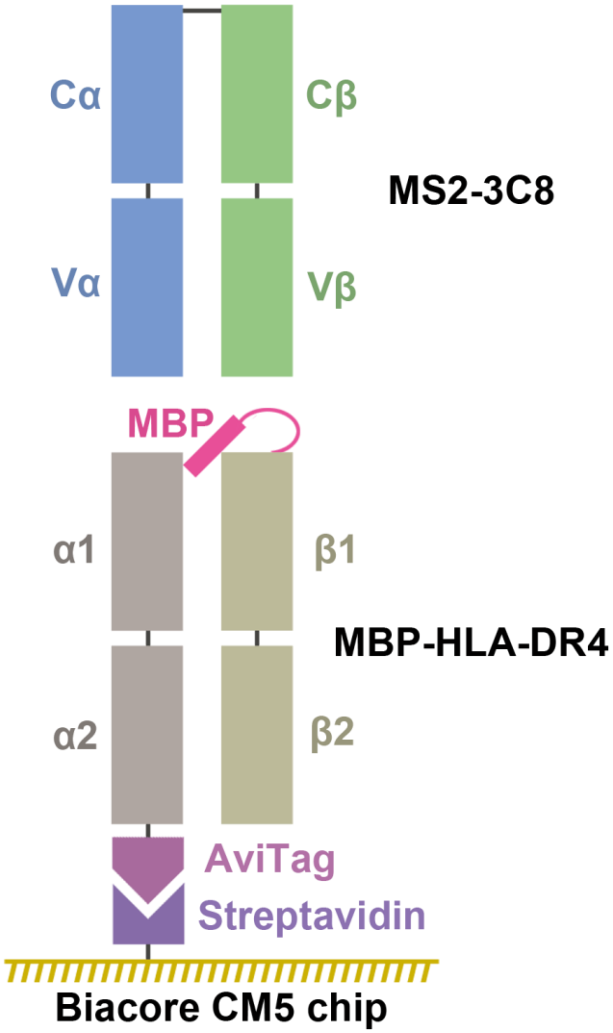

Figure 3.2 Experimental design for SPR analysis of the interaction between MS2-3C8 and MBP–HLA-DR4.

Instead of directly immobilizing MBP–DR4, a biotin acceptor peptide, AviTag, was added to the C-terminus of the α-chain for producing biotinylated MBP–DR4. Streptavidin is loaded to saturation onto the surface of a CM5 biosensor for capturing biotinylated MBP–DR4. In this way, MBP–DR4 molecules are directionally immobilized, which effectively reduces signal noise caused by heterogeneous immobilization.

3.2 Results

3.2.1 Immobilization of MBP–HLA-DR4 onto a biosensor chip

To obtain directional immobilization of MBP–HLA-DR4, we attached a biotin acceptor peptide sequence AviTag (Avidity, LLC) to the C-terminus of the α-chain of DR4. The fusion protein, MBP–HLA-DR4–AviTag, was produced the same way as MBP–HLA-DR4 (see Chapter 2). A CM5 biosensor chip was pre-immobilized with streptavidin by amine-coupling. MBP–HLA-DR4, which was biotinylated at the C-terminal AviTag by biotin protein ligase, was then captured by streptavidin on the chip surface (Figure 3.2). Streptavidin was loaded to saturation at over 3000 RU, whereas only 300 to 400 RU of MBP–DR4 was immobilized, in order to minimize steric hindrance that might interfere with the binding of MS2-3C8.

3.2.2 Kinetic and equilibrium measurements of MS2-3C8 binding to MBP-DR4

Different concentrations of MS2-3C8 were flowed over immobilized MBP–HLA-DR4 for kinetic or equilibrium SPR assays. Kinetic parameters (on- and off-rates) for the binding were: k_{on} = 1.7 × 103 $M^{-1}s^{-1}$ and k_{off} = 0.011 s^{-1}, corresponding to a dissociation constant (K_D) of 6.5 μM (Figure 3.3-A). Under equilibrium binding conditions, a K_D of 5.0 μM was obtained (Figure 3.3-B), in close agreement with the K_D from kinetic analysis. The affinity of MS2-3C8 for its self-antigen is therefore at the high end of the range for TCR interactions with peptide–MHC class I or peptide–MHC class II (1 to >100 μM)

(Cole et al., 2007; Rudolph et al., 2006; van der Merwe and Davis, 2003). Indeed, MS2-3C8 binds MBP–DR4 about as tightly as the most avid anti-microbial class I-restricted TCRs bind their respective ligands, and considerably more tightly than do anti-microbial class II-restricted TCRs (Cole et al., 2007). It also binds far more tightly than do human autoimmune TCRs 3A6 and Ob.1A12 (K_D > 100 μM) (Appel et al., 2000; Li et al., 2005), but similarly to mouse autoimmune TCR 172.10 (6 μM) (Garcia et al., 2001).

In addition to the usually high affinity, the binding of MS2-3C8 for MBP–DR4 also exhibits an unusually slow kinetics. The off-rate value of the interaction (0.011 s^{-1}, corresponding to a half-life of 69 s) is exceptionally small, compared to those of all other TCR–peptide–MHC interactions characterized to date (0.02 to >1 s^{-1}) (Cole et al., 2007). This slow off-rate is counterbalanced by a very slow on-rate (1.7 × 103 $M^{-1}s^{-1}$) relative to the on-rates of other TCRs (2 × 10^3 to >1 × 10^6 $M^{-1}s^{-1}$), which may imply conformational changes in MS2-3C8 and/or MBP–DR4 during complex formation. It is notable that the SPR measurements were conducted using an engineered version of the ligand designed to overcome the low affinity of MBP for HLA-DR4. Therefore, the results reveal the intrinsic high affinity of MS2-3C8 for MBP–DR4, whereas, in reality, the instability of the natural MBP–HLA-DR4 ligand would effectively decrease the half-life of the overall complex with TCR, which most likely allowed MS2-3C8 T cells to survive thymic deletion.

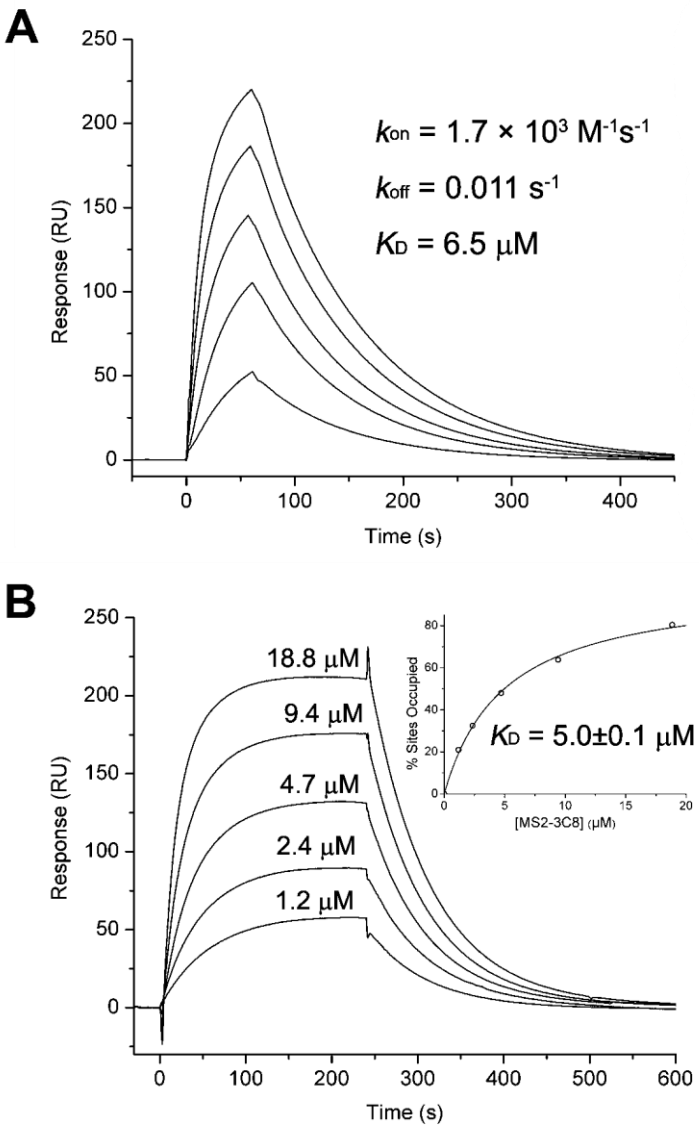

Figure 3.3. SPR analysis of the binding of TCR MS2-3C8 to MBP–DR4.

(A) For kinetic measurements, TCR MS2-3C8 at concentrations of 2.9 μM, 5.8 μM, 11.5 μM, 23 μM and 46 μM was injected over immobilized MBP–DR4 (320 RU). Sensograms were fitted to a 1:1 binding model to obtain on- and off- rates: $k_{on} = 1.7 \times 10^3 \pm 0.01$ $M^{-1}s^{-1}$ and $k_{off} = 0.011 \pm 0.0003$ s^{-1}. K_D was calculated as k_{off}/k_{on}. (B) For equilibrium measurements, TCR MS2-3C8 at concentrations of 1.2 μM, 2.4 μM, 4.7 μM, 9.4 μM and 18.8 μM was injected over immobilized MBP–DR4 (400 RU). Inset shows the fitting curve for equilibrium binding that resulted in a K_D of 5.0 ± 0.1 μM.

3.3 Discussion

Negative selection in the thymus is based on the functional avidity of T cells for self-antigens, which is comprehensively determined by: 1) the affinity of TCR for self-peptide–MHC, 2) the affinity of peptide for MHC, and 3) the availability of and need for co-receptors and signaling molecules (Anderton and Wraith, 2002). Assuming the co-receptor and other signaling molecules are invariable parameters, the notion of "functional avidity" includes all factors that affect the stability of the TCR–peptide–MHC complex, instead of only the affinity of TCR for pMHC. To be pathogenic, autoreactive T cells must meet two competing criteria: they must escape thymic deletion, but nevertheless signal with sufficient strength in the target organ to cause autoimmune disease. This means that, in the thymus, an autoimmune T cell must behave like an anti-foreign T cell, with no response to self-antigens, to escape the surveillance machinery of the negative selection, whereas, in the periphery, the interaction of the same autoreactive T cell with self-antigens must exceed a threshold to result in activation. It can then be deduced that the functional avidity of an autoimmune TCR lies between the avidities that lead to elimination or survival.

The relatively low stability of autoimmune complexes can be achieved by low affinity of the TCR for self-pMHC or low affinity of the self-peptide for MHC. For example, the affinity of autoimmune TCRs Ob.1A12 and 3A6 are lower than for all anti-foreign TCRs, which allowed the escape of these two T cell clones from the thymus. The MBP self-peptides in these two cases are both good binders. Alternatively, the weak affinity of a self-peptide for MHC can also facilitate the escape of an autoimmune T cell, such as TCR

MS2-3C8, studied here. The unusually high affinity as well as the extremely slow off-rate of MS2-3C8 suggests that, when the self-peptide is not stably associated with MHC, the autoimmune TCR must establish a strong interaction with pMHC in order to be successfully activated in the periphery. Notably, the affinity of MS2-3C8 for MBP–DR4 is at the high end of the affinity range for the peripheral TCR repertoire.

By examining T cells with high functional avidity for various myelin antigens (MBP, proteolipid protein, myelin oligodendrocyte glycoprotein), it was shown that immunodominant epitopes in MS patients are clearly biased toward epitopes, such as MBP 111–129, that bind HLA-DR molecules with low affinity (Bielekova et al., 2004). This negative correlation between immunodominance and strength of HLA-DR binding, which concurs with animal studies (Anderton et al., 2001; Goverman, 2009; Vanderlugt and Miller, 2002), supports the hypothesis that disease-associated MHC molecules permit escape of potentially deleterious high-avidity autoreactive T cells due to their poor peptide-binding properties (DiPaolo and Unanue, 2002; Stadinski et al., 2010; Starr et al., 2003). The system we have chosen exemplifies this concept of immunodominance: MBP 111–129 is an immunodominant epitope in MS patients that binds very weakly to HLA-DR4, whereas TCR MS2-3C8 binds MBP–DR4 with as high an affinity (K_D = 6.5 μM) as TCRs recognizing foreign ligands, and with an even slower off-rate (k_{off} = 0.011 s^{-1}). We propose that the tight binding of MS2-3C8 to MBP–DR4 overcomes the weak binding of MBP to HLA-DR4 to sufficiently stabilize the TCR–peptide–MHC ternary complex, thereby explaining the ability of this autoreactive TCR to induce CNS inflammation in MS2-3C8–DR4 transgenic mice (Quandt et al., 2004).

Chapter 4

Structural studies of autoimmune recognition of MBP–HLA-DR4 self-ligand by high-affinity TCR MS2-3C8

SUMMARY

The complex structure of MS2-3C8–MBP–HLA-DR4 was solved to the resolution of 2.8 Å by X-ray crystallography. The structure showed a loose accommodation of MBP in the HLA-DR4 binding groove, accounting for its low affinity. The distinctive conformation of the bound MBP peptide marks an altered anchor residue, P7 Arg. Instead of residing in the peptide-binding groove, the side chain of P7 Arg makes extensive contacts with the TCR. Topologically, MS2-3C8 engages MBP–DR4 via a docking mode that closely resembles the optimal topology of anti-microbial TCRs, but is distinct from that of two previously-characterized autoimmune TCRs. Conserved contacts were observed in the recognition of HLA-DR4 by MS2-3C8 and anti-microbial TCR HA1.7. Combined with a unique CDR3β conformation, this docking mode compensates for the weak binding of MBP to HLA-DR4 by maximizing interactions between MS2-3C8 and MBP–DR4.

4.1 Background

As discussed in previous chapters, thymic selection is primarily based on the stability of a TCR-self-pMHC complex. Any instability in the ternary complex, whether introduced by low TCR affinity for self-pMHC or by weak binding of self-peptide to MHC, facilitates escape from negative selection. In addition to studying the biophysical properties of autoimmune recognition, detailed investigation of the molecular assembly of the TCR–self-pMHC complexes may help us understand, at the atomic level, how such TCRs avoid thymic deletion, but still retain the ability to productively engage self-antigens in the periphery (Deng and Mariuzza, 2007; Wucherpfennig et al., 2009). In fact, structural studies of autoimmune TCRs bound to self-peptide–MHC ligands have begun to reveal some recognition pattern used by autoimmune TCRs. Five structures have been reported to date, involving two human TCRs from MS patients (Hahn et al., 2005; Li et al., 2005) and three mouse TCRs from the EAE model of MS (Feng et al., 2007; Maynard et al., 2005). The human TCRs are Ob.1A12, which recognizes myelin basic protein MBP 85–99 in the context of HLA-DR2b (Hahn et al., 2005), and 3A6, which recognizes MBP 89–101 presented by HLA-DR2a (Li et al., 2005). Both Ob.1A12 and 3A6 engage their MBP–HLA-DR ligands with docking topologies that differ substantially from the way TCRs specific for microbial or other foreign epitopes bind peptide–MHC. Whereas anti-microbial TCRs typically dock on peptide–MHC in a diagonal orientation over the center of the antigenic peptide, Ob.1A12 and 3A6 are displaced toward the N-terminus of MBP (Wucherpfennig et al., 2009). This suboptimal binding mode results in fewer specific interactions with the self-peptide, which is manifested by the much lower affinities of

Ob.1A12 and 3A6 compared to anti-microbial TCRs. The three mouse TCRs (172.10, 1934.4 and cl19) recognize acetylated MBP 1–11 (MBP Ac1–11) presented by I-A^u. The MBP–I-A^u ligand is structurally defective in that the peptide only partially fills the MHC binding groove (He et al., 2002). As a result, these mouse TCRs, like Ob.1A12 and 3A6, also exhibit suboptimal interactions with the MBP self-peptide, marked by a paucity of specific contacts. Together, these studies suggest that structural alterations, which destabilize the TCR–pMHC recognition unit, may enable certain self-reactive T cells to escape negative selection, without necessarily compromising their ability to cause autoimmune disease (Wucherpfennig et al., 2009). Indeed, mice transgenic for TCR Ob.1A12 and HLA-DR2b developed CNS inflammation (Madsen et al., 1999), and transfer into mice of T cell clones recognizing MBP–I-A^u induced EAE (Goverman, 2009).

Despite these advances, the database of autoimmune TCR–pMHC complexes is still too limited to describe the properties of autoreactive TCR recognition at the repertoire level, or to evaluate the extent to which autoreactive TCRs deviate from the rules followed by anti-foreign TCRs (Wucherpfennig et al., 2009). To expand our understanding of the structural mechanisms governing self-antigen recognition, we determined the structure of a human autoimmune TCR MS2-3C8 in complex with the weakly binding self-peptide MBP 114–126 and MS-associated MHC class II molecule HLA-DR4.

Notably, MBP 114–126 represents an immunodominant epitope of MBP in HLA-DR4-positive MS patients (Muraro et al., 1997; Sospedra and Martin, 2006). Unlike the MBP peptides recognized by TCRs Ob.1A12 and 3A6, which bind with high affinity to

HLA-DR2 and elicit a diverse TCR repertoire, MBP 111–129 binds weakly to HLA-DR4 and is recognized by a restricted TCR repertoire. The MBP 111–129-specific T cell clone MS2-3C8 was repeatedly isolated from the peripheral blood of a patient with relapsing-remitting MS over a two-year period (Muraro et al., 1997). In addition, the clonal overrepresentation and persistent expansion of MS2-3C8 T cells in this patient suggested an involvement in the disease process. The pathogenic potential of TCR MS2-3C8 was demonstrated using transgenic mice expressing this autoimmune TCR and HLA-DR4 (Quandt et al., 2004). These humanized mice readily developed EAE in adoptive transfer experiments without antigen administration.

Through detailed analyses of interfacial contacts between TCR MS2-3C8 and MBP-DR4, we expected to understand the basis for the weak binding of MBP to HLA-DR4, and to explain how this autoreactive TCR compensates for its unstable self-antigen to achieve sufficiently high avidity for T cell activation in the periphery and the induction of autoimmunity.

4.2 Results

4.2.1 Crystallization of TCR MS2-3C8 bound to MBP–HLA-DR4

The constructs used for crystallization studies are MBP 114–126-linked HLA-DR4 and MS2-3C8 with a natural interchain disulfide bridge (see Chapter 2). Both proteins were produced by *in vitro* folding from bacterially expressed inclusion bodies. Initial crystallization trials scored a hit using the Emerald Wizard I crystal screen kit (Emerald BioSystems, Inc.), which proved to be the MS2-3C8–MBP–HLA-DR4 complex (Figure

4.1-A). Small needle-like crystals were found in the drop containing 10% PEG-8000, 0.1 M imidazole, 0.2 M calcium acetate, pH8.0. After optimization of the crystallization conditions, the crystals changed form to small plates. Serial rounds of macro-seeding were performed, which increased the size of the plates (Figure 4.1-B). From a crystal of dimensions 0.5 × 0.2 × 0.05 mm^3, a 360˚ dataset to 2.8 Å resolution was collected at Brookhaven National Synchrotron Light Source (Upton, NY) (Figure 4.1-C).

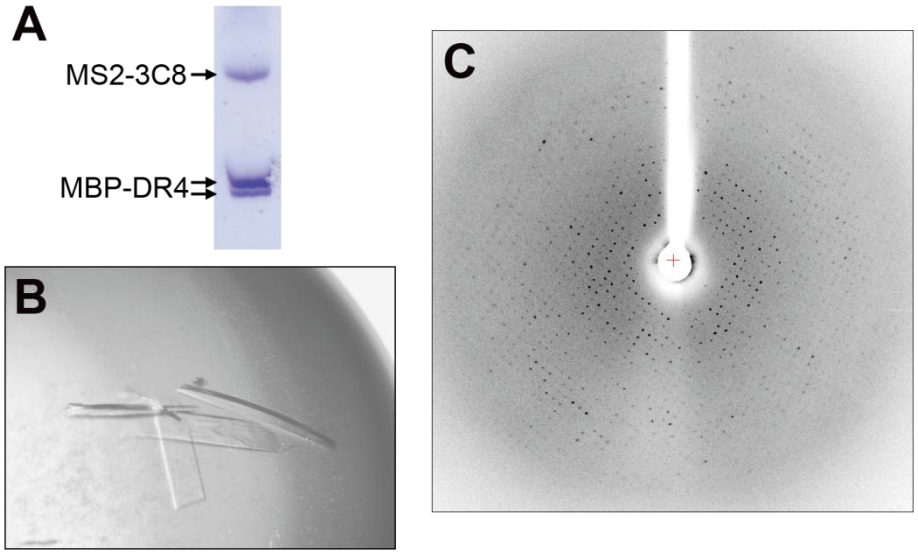

Figure 4.1 Crystallization of the complex between MS2-3C8 and MBP–HLA-DR4.

(A) SDS-PAGE of dissolved crystals showing that they contained both MS2-3C8 and MBP–DR4. Crystal was washed three times with crystallization solution before being dissolved in non-reducing SDS protein sample buffer.

(B) Microscopic image of optimized crystals of the MS2-3C8–MBP–DR4 complex. The right-most crystal has a length of about 0.5 mm.

(C) Diffraction pattern of a crystal of the complex.

4.2.2 Structure determination: Data process, molecular replacement and structure refinement

The space group of the crystal was determined as $P2_12_12$. Each asymmetric unit contains two MS2-3C8–MBP–HLA-DR4 complexes. The solvent content of the crystal was estimated as 62%. The complete dataset was processed to 2.8 Å, with an overall R_{merge} of 8.8% (Table 4.1). The completeness values of the dataset at the overall level and the last resolution shell are both 100%, which facilitated molecular replacement (MR).

Known MHC and TCR structures were used as MR search models. Two MBP–DR4 molecules were immediately found with the coordinates of HA–DR4 (PDB code 1J8H) (Hennecke and Wiley, 2002), but only one MS2-3C8 molecule was found using various TCRs (1YMM, 3DX9, 1KGC) (Archbold et al., 2009; Hahn et al., 2005; Kjer-Nielsen et al., 2002) as search models. A new search model consisting of a complex of MS2-3C8 and MBP–DR4 was then created by positioning a symmetry mate of the TCR opposite one of the found MBP–DR4 molecules. Two complete complexes were then readily located by Phaser (Adams et al., 2010).

Rigid-body and simulated-annealing refinements were conducted using CNS1.2 (Quandt et al., 2004). Manual model fitting was performed with the program Coot (van der Merwe and Davis, 2003). The 16-mer peptide connecting MBP to the HLA-DR4 β chain had visible electron density in one of the two complexes and was built accordingly. Subsequent refinements of positional and atomic displacement parameters were carried out using Phenix-1.5.2 (Adams et al., 2010). Water molecules were added with a distance cut-off of 3.4 Å. The interface between TCR and pMHC was unambiguous for each of the two molecules in the asymmetric unit of the crystal (Figure 4.2-B). Several loops in

Table 4.1 Data collection and refinement statistics

Data collection	
Space group	$P2_12_12$
Resolution (Å)	49.2–2.8
Unit cell (Å)	a = 102.5, b = 218.4, c = 98.4
Unique reflections	55,156
Multiplicity[a]	40.2 (5.0)
Completeness (%)[a]	100 (100)
Mean $I/\sigma(I)$[a]	29.7 (5.2)
R_{merge} (%)[a,b]	8.8 (35.5)
Refinement	
Resolution range (Å)	49.2–2.8
R_{work} (%)[c]	23.9
R_{free} (%)[c]	27.9
Protein atoms	12,876
Water molecules	27
R.m.s. deviations from ideality	
Bond lengths (Å)	0.010
Bond angles (°)	1.339
Ramachandran plot statistics	
Favored (%)	92.0
Allowed (%)	7.8
Outliers (%)	0.2

[a]Values in parentheses correspond to the highest resolution shell (2.80–2.90).

[b]$R_{merge}(I) = (\Sigma|I(i)-<I(h)>|/\Sigma I(i))$, where $I(i)$ is the ith observation of the intensity of the *hkl* reflection and $<I>$ is the mean intensity from multiple measurements of the *hkl* reflection.

[c]R_{work} (R_{free}) = $\Sigma||F_o| - |F_c||/\Sigma|F_o|$; 5% of data were used for R_{free}.

the MHC α2β2 and TCR CαCβ modules lacked electron density; however, these disordered regions are distant from the interface. Further refinement was conducted with non-crystallographic symmetry (NCS) restraints, interspersed with manual density map fitting. The final R_{work} and R_{free} values are 23.9% and 27.9%, respectively (Table 4.1).

4.2.3 Overview of the MS2-3C8–MBP–DR4 complex

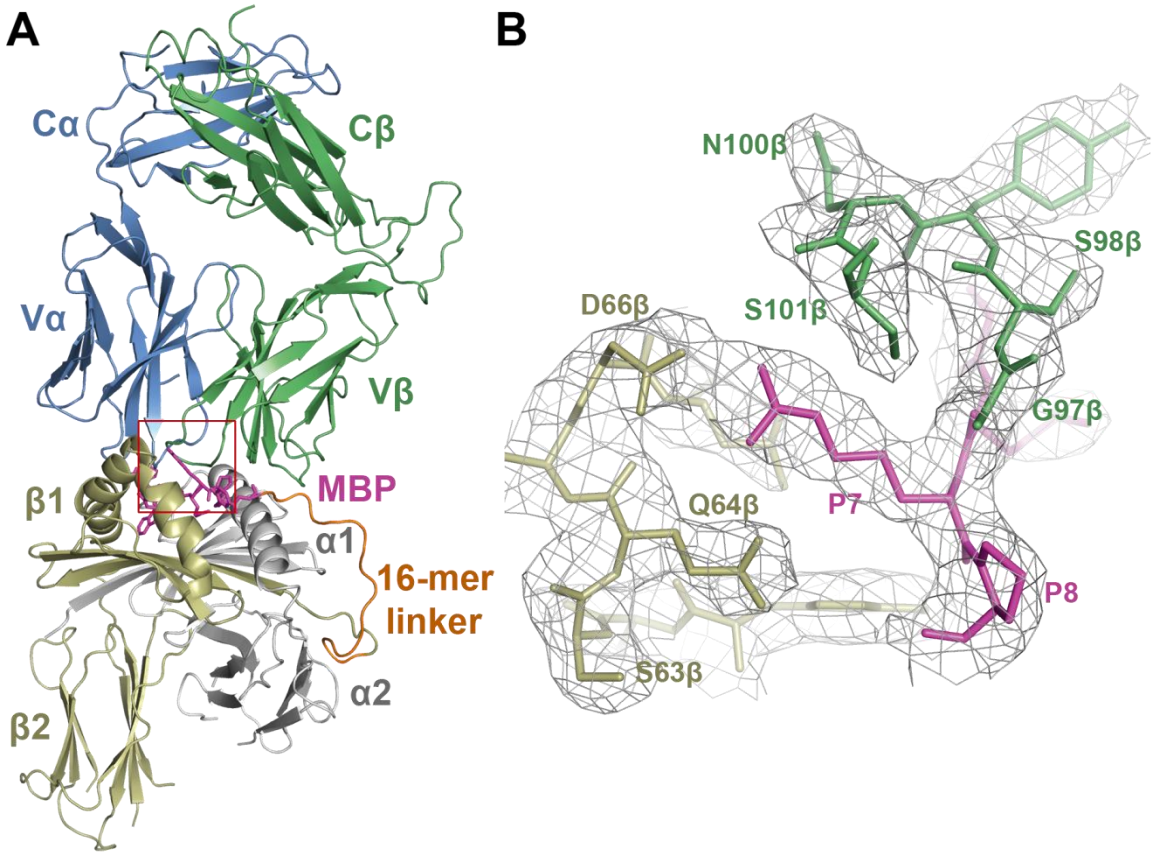

Figure 4.2 Structure of the MS2-3C8–MBP–HLA-DR4 complex.

(A) Side view of the MS2-3C8–MBP–DR4 complex (ribbon diagram), including the 16-mer peptide linking MBP to the HLA-DR4 β-chain. TCR α-chain, blue; TCR β-chain, green; MHC α-chain, gray; MHC β-chain, yellow; MBP peptide (stick representation), magenta; linker peptide, orange.

(B) Electron density in the interface of the MS2-3C8–MBP–DR4 complex. Density from the final $2F_o - F_c$ map at 2.8 Å resolution is contoured at 1σ.

The two complexes in the asymmetric unit are in close similarity, except that the 16-mer peptide linking MBP to the N-terminus of the HLA-DR4 β chain exhibited clear electron density in only one of the two complexes (Figure 4.2-A), probably due to crystal contacts with the Cβ domain of a neighboring complex molecule (Figure 4.3); no density could be detected for the linker peptide in the other complex, indicating flexibility. The root-mean-squared (r.m.s.) deviation in α-carbon positions for the TCR VαVβ and MHC α1β1 modules, including the MBP peptide, is 0.22 Å for the two complexes in the asymmetric unit. Because there is no significant difference, the following description of TCR–pMHC interactions applies to both complex molecules.

Compared to anti-microbial TCRs such as HA-specific TCR HA1.7 (Hennecke and Wiley, 2002), which typically dock over the central portion of the foreign peptide and interact symmetrically with the MHC α1 and β1 α-helices (Figure 4.4-A), the autoimmune TCRs Ob.1A12 and 3A6 (Hahn et al., 2005; Li et al., 2005) display substantially altered binding geometries, in which the TCR is shifted toward the N-terminus of the self-peptide and toward the MHC β1 α-helix (Figure 4.4-B, C). In sharp contrast to Ob.1A12 and 3A6, MS2-3C8 engages its self-ligand via a binding mode which closely resembles that of anti-foreign TCRs (Figure 4.4-D), as exemplified by the HA1.7–HA–DR4 complex (Figure 4.4-A). Thus, MS2-3C8 docks symmetrically over MBP–DR4 in a canonical diagonal orientation, with a crossing angle of TCR to peptide–MHC (Reinherz et al., 1999) of 65°, compared with 70° for the HA1.7–HA– DR4 complex. Moreover, MS2-3C8 is positioned directly over the central P5 residue of MBP, rather than being displaced toward the N-terminus of the self-peptide, as in the Ob.1A12–MBP–DR2b and 3A6–MBP–DR2a complexes (Figure 4.4, bottom panels).

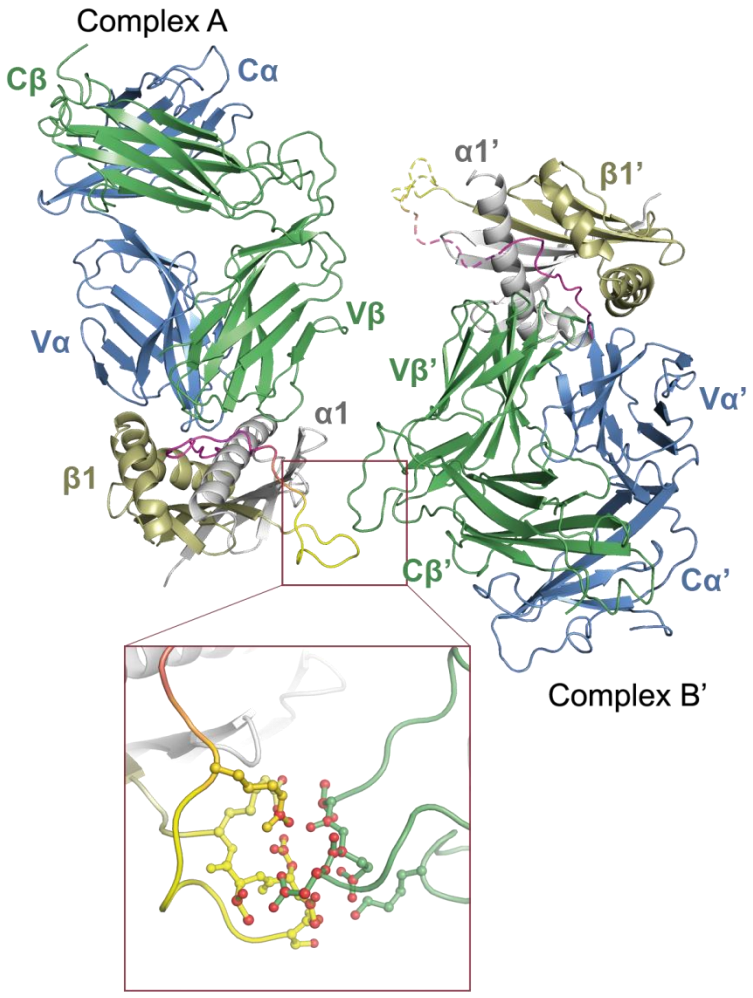

Figure 4.3 Crystal contacts between neighboring complexes.

Each asymmetric unit contains two MS2-3C8–MBP–DR4 complexes, A and B. Complex B' is a symmetry mate of complex B in a neighboring asymmetric unit. The peptide linker of complex A (yellow) makes contacts with the Cβ domain of complex B' (Cβ'). The bottom large square shows an enlarged view of the contact region. The contact residues are drawn in ball-and-stick format and the contact atoms as red spheres.

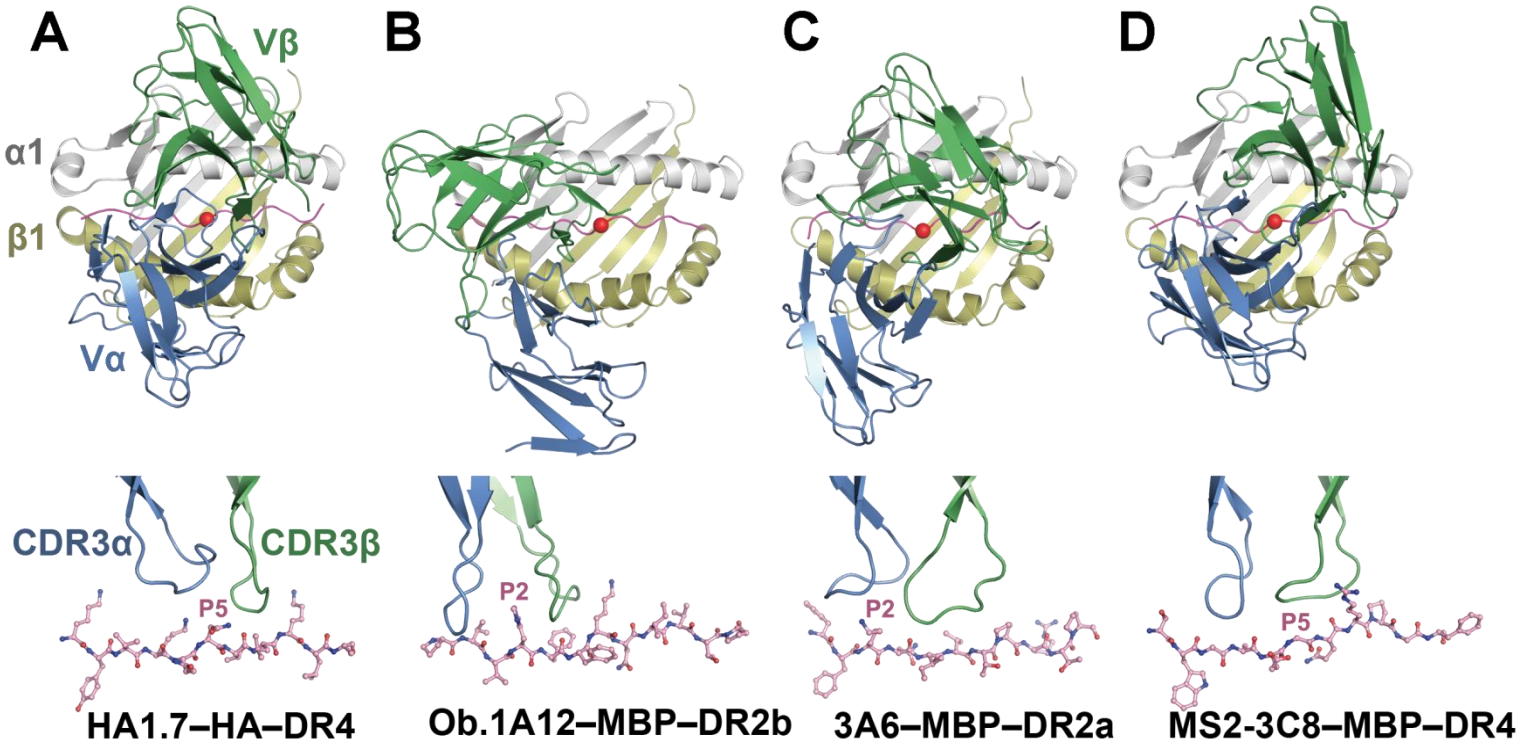
A
Vβ
α1
β1
Vα
B
C
D
CDR3α
CDR3β
P5
P2
P2
P5
HA1.7–HA–DR4
Ob.1A12–MBP–DR2b
3A6–MBP–DR2a
MS2-3C8–MBP–DR4

Figure 4.4 Comparison of human anti-microbial and autoimmune TCR–pMHC class II complexes.

(A) Upper panel: top view of the anti-microbial HA1.7–HA–DR4 complex (PDB code 1J8H) (Hennecke and Wiley, 2002). Colors of TCR, MHC and peptide are the same as in Figure 4.3. The central P5 residue of the peptide is shown as a red sphere. Bottom panel: position of the TCR CDR3 loops over the HA peptide. The peptide is drawn in ball-and-stick representation with carbon atoms in pink, oxygen atoms in red, and nitrogen atoms in blue. The CDR loops are positioned above the central P5 residue of the peptide.

(B) The autoimmune Ob1A12–MBP–DR2b complex (1YMM) (Hahn et al., 2005).

(C) The autoimmune 3A6–MBP–DR2a complex (1ZGL) (Li et al., 2005).

(D) The autoimmune MS2-3C8–MBP–DR4 complex.

The comparison shows that autoimmune TCR MS2-3C8, like anti-microbial TCR HA1.7, docks symmetrically over pMHC in a central diagonal orientation, whereas autoimmune TCRs Ob1A12 and 3A6 are displaced towards the peptide N-terminus and the HLA-DR β1 helix. The CDR3 loops of HA1.7 and MS2-3C8 are centered over peptide residue P5; those of Ob.1A12 and 3A6 are positioned over P2.

The classical docking mode of MS2-3C8 correlates with its high affinity for MBP–DR4, suggesting that it is an optimal binding mode that enables TCRs to achieve strong interactions with antigenic ligands. The MS2-3C8–MBP–DR4 complex also contradicted the previous notion that autoimmune TCRs only use altered or suboptimal binding modes for recognizing self-antigens.

The MS2-3C8–MBP–DR4 complex buries a total solvent-accessible surface of 2009 $Å^2$, comparable to that in other MHC class II complexes (Rudolph et al., 2006). The buried surface area on Vβ (673 $Å^2$, 66%) is nearly twice that on Vα (354 $Å^2$, 34%) (Figure 4.5-A). Such dominance by Vβ is unusual among TCR–pMHC complexes, in which Vα and Vβ typically contribute roughly equal buried surfaces, as in the HA1.7–HA–DR4 complex (Vα: 47%; Vβ: 53%) (Figure 4.5-B), or in which Vα dominates.

Indeed, only two other complexes displaying a similar degree of Vβ dominance as MS2-3C8–MBP–DR4 have been reported, one involving the HLA-A2-restricted TCR JM22 (67%) (Stewart-Jones et al., 2003) and the other the MBP-specific TCR 3A6 (61%) (Li et al., 2005).

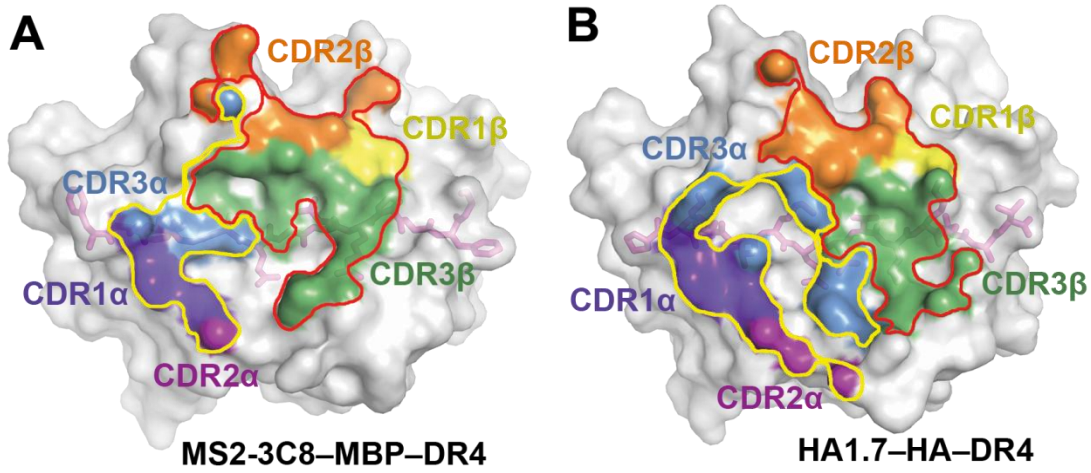

Figure 4.5 TCR footprints on the surface of peptide–DR4 ligands.

(A) Footprint of autoimmune TCR MS2-3C8 on MBP–DR4. The top of the MHC molecule is represented as a gray surface; the bound peptide (pink) is shown in stick format under the transparent surface. The areas contacted by individual CDR loops are color-coded: CDR1α, violet; CDR2α, purple; CDR3α, blue; CDR1β, yellow; CDR2β, orange; CDR3β, green. The contact areas of the V domains are contoured: Vα: yellow; Vβ: red.

(B) Footprint of anti-microbial TCR HA1.7 on HA–DR4.

4.2.4 Altered binding mode of low-affinty self-peptide MBP 114–126

Based on the complex structure, the primary anchor residues for MBP 114–126 bound to HLA-DR4 are Trp116 (P1) and Glu119 (P4), which constitute a conserved DR4-binding motif as seen in other DR4-binding peptides (Hammer et al., 1995; Hammer et al., 1993; Southwood et al., 1998). In the DR4-binding motif, P6 and P7 are two secondary anchor residues, both of which should be small nonpolar residues. However, in MBP 114–126, P6 and P7 are two large polar residues, Gln and Arg, which do not conform to the optimal binding motif for HLA-DR4. Whether these two non-optimal residues are the source of low-affinity binding of MBP 114–126 was examined based on the crystal structure of MBP–DR4.

The conformation of the MBP peptide was directly compared with those of three peptides known to bind HLA-DR4 with high affinity: HA 306–318 (PDB code 1J8H), human collagen II peptide 1168–1180 (CII) (PDB code 2SEB) and gp100 (internal laboratory communication, not published) (Dessen et al., 1997; Hammer et al., 1995; Hennecke and Wiley, 2002). Ignoring side chains, all three peptides display very similar main-chain conformations in their corresponding complexes with HLA-DR4, from residues P1 to P9 (Figure 4.6). However, MBP diverges from HA, CII and gp100 at residues P6 and P7, with an average displacement of 1.9 Å in the position of their α-carbons, up from the α1β1 platform of HLA-DR4. As a result, MBP sits less deeply in the peptide-binding groove, which reduces shape complementarity. The shape correlation statistic (*S*c) (Lawrence and Colman, 1993) of the MBP–DR4 interface is 0.75, whereas that of HA–DR4 is 0.83 (S_c = 1.0 for interfaces with perfect fits).

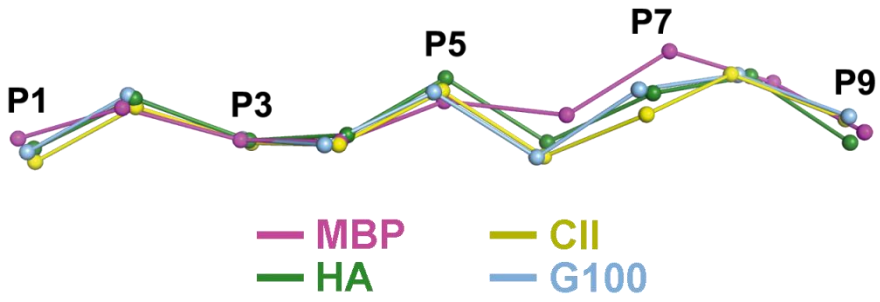

Figure 4.6 Structural alignment of HLA-DR4-binding peptides.

The α-carbon backbone of MBP (magenta) was compared with the α-carbon backbones of hemagglutinin peptide (HA) (green), collagen II peptide (CII) (yellow) and gp100 peptide (blue) by superposing the α1β1 domains of HLA-DR4 in the respective pMHC complexes. The peptides are viewed from the side of the β1 helix. MBP diverges from HA, CII and gp100 at residues P6 and P7.

In HA, CII and gp100, anchor residues P6 and P7 have short side chains (HA: Thr-Leu; CII: Ala-Ala; gp100: Thr-Glu), whereas in MBP these residues have long side chains (Gln-Arg). The shallower binding of MBP is mainly attributable to these longer side chains, but for different reasons. Thus, the side chain of P6 Gln pushes up the MBP main chain by pointing directly into the P6 pocket of HLA-DR4 (Figure 4.7), in the same direction as the shorter side chain of HA P6 Thr (Figure 4.7). By contrast, the long side chain of P7 Arg projects out toward the top of the DR4 β1 helix, rather than into the P7 pocket, in order to avoid colliding with the α1β1 platform if it pointed in the same direction as the side chain of HA P7 Leu (Figure 4.7). This side-chain orientation introduces a twist in the main chain of MBP, further elevating the self-peptide from the binding groove and weakening its interaction with HLA-DR4. Therefore, compared to

other peptide–MHC class II complexes, P7 Arg is not positioned as a typical anchor in MBP–DR4. Instead, this residue interacts extensively with TCR (see below).

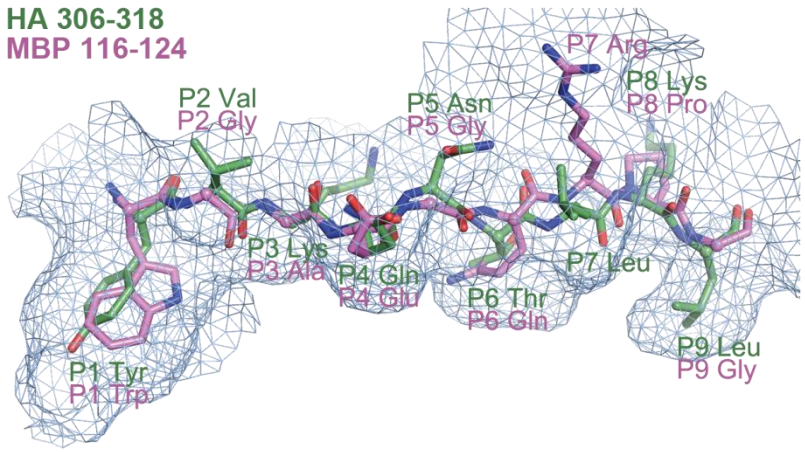

Figure 4.7 Altered topology of the MBP peptide in the DR4 peptide-binding groove.

The surface of HLA-DR4 is shown in blue mesh. Both the MBP (magenta) and HA (green) peptides are drawn as stick models. Residues P1 to P9 of both peptides are labeled in the same color as the peptide. The P6 and P7 residues of MBP do not fit into the HLA-DR4 anchor pockets as well as residues P6 and P7 of the HA peptide.

In the HA–HLA-DR4 structure, the HA peptide forms four hydrogen bonds with β-sheet residues on the floor of the peptide-binding groove (Figure 4.8-B). However, the elevation of MBP results in loss of the hydrogen bond between the main-chain nitrogen of P7 and the Oη atom of Tyr30β (Figure 4.8-A). In addition, the twist in MBP eliminates a hydrogen bond between the main-chain oxygen of P7 and the Nδ2 atom of Asn69α on the DR4 α1 helix found in the HA–DR4 complex (Figure 4.8-C,D). The MBP–HLA-DR4 complex also lacks two side-chain–side-chain hydrogen bonds to Glu55α and Asn62α, due to the absence of suitable hydrogen bond donors at P-1 and P3. This net loss of four

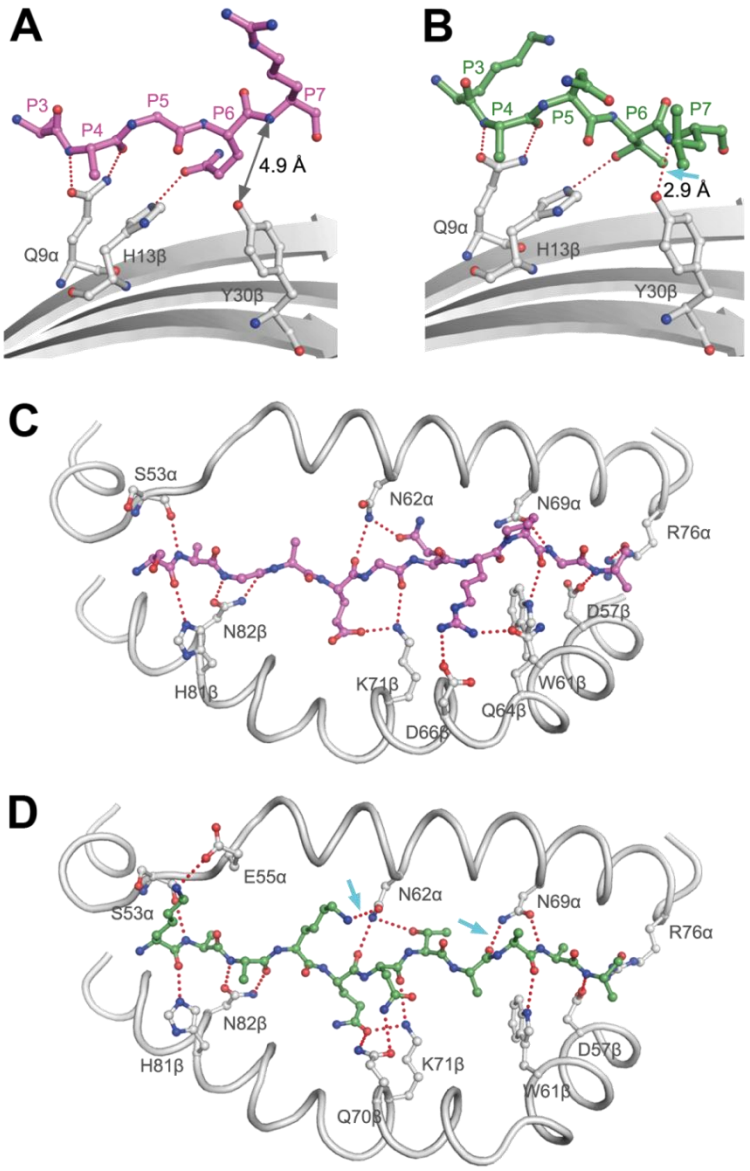

Figure 4.8 Structural basis for low-affinity binding of MBP 114–126 to HLA-DR4.

(A, B) Interactions between MBP (A) or HA (B) and the β-sheet floor of the HLA-DR4 binding groove (gray). The peptides are oriented the same as in Figure 4.7. Hydrogen bonds are shown as dotted red lines. The arrow in (B) indicates the hydrogen bond between P7 and Tyr30β in the HA–DR4 complex that is absent in the MBP–DR4 complex, where the corresponding atoms are too distant (4.9 Å) for hydrogen bond formation (A).

(C, D) Interactions between MBP (C) or HA (D) and the α1 and β1 helices of HLA-DR4. The arrows in (D) indicate three additional hydrogen bonds in the HA–DR4 complex not present in the MBP–DR4 complex (C).

hydrogen bonds, along with 35 fewer van der Waals contacts between peptide and MHC, likely explains the much weaker affinity of MBP than HA for HLA-DR4 (Muraro et al., 1997).

4.2.5 Conserved interactions between TCR MS2-3C8 and HLA-DR4

Overall, Vβ makes 57 van der Waals contacts with HLA-DR4, compared to only 19 by Vα. These contacts are mediated by 11 Vβ and 6 Vα residues and involve 15 MHC residues (Table 4.2), of which 12 are contacted by HA1.7 and 10 by 3A6 (Table 4.3). All six CDR loops of MS2-3C8 participate in binding HLA-DR4. Although the germline-encoded CDR1 and CDR2 loops of MS2-3C8 (Vα4.1, Vβ2.1) and HA1.7 (Vα1.2, Vβ3.1) differ in both sequence and conformation, they contact similar sites on HLA-DR4, which explains the conserved docking orientation. In both the MS2-3C8–MBP–DR4 and HA1.7–HA–DR4 complexes, CDR1α and CDR2α interact extensively with DR4 α-helical residues Thr77β and His81β (Figure 4.9-A,B). These two residues are conserved across all HLA-DR molecules. Besides multiple van der Waals contacts involving structurally equivalent TCR residues, these interactions include two hydrogen bonds linking CDR1α Ser27 and Thr29 of MS2-3C8 to His81β and Thr77β of HLA-DR4, respectively, which are absent in the HA1.7– HA–DR4 complex (Table 4.3). Regarding CDR1β and CDR2β, these loops contact Lys39α, Ala64α and Lys67α in both the MS2-3C8–MBP–DR4 and HA1.7–HA–DR4 structures (Figure 4.9-C,D). Of particular note is a conserved salt bridge between CDR2β Glu50 (Asp51 in HA1.7) and Lys67α, which may play an important role in anchoring MS2-3C8 and HA1.7 to the MHC α1 helix. By

contrast, the overall shift by autoimmune TCR 3A6 toward the N-terminus of the MBP self-peptide relative to the central position of MS2-3C8 results in engagement of different MHC residues by structurally equivalent CDR1 and CDR2 residues (Table 4.3). This is also the case for TCR Ob.1A12, which uses the same Vβ segment (Vβ2.1) as MS2-3C8.

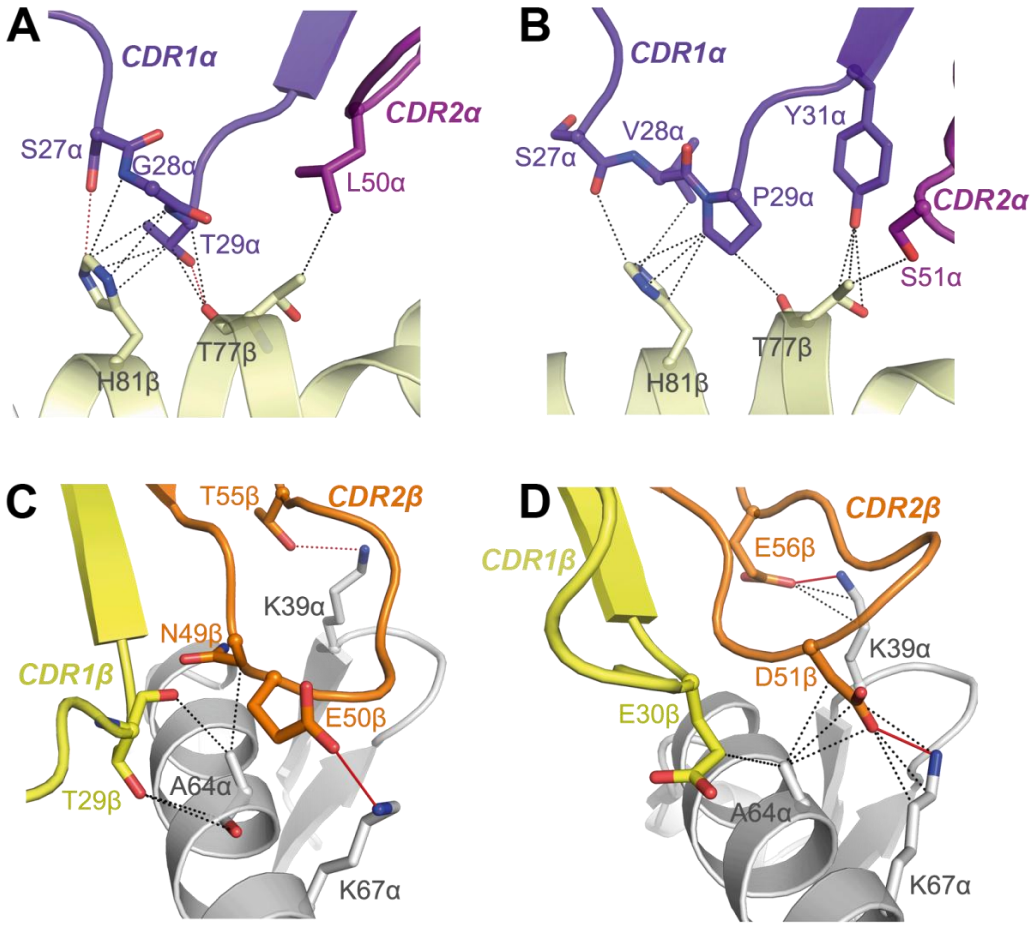

Figure 4.9 Conserved contacts between germline-encoded CDR loops and HLA-DR4.

(A, B) Conserved interactions between the DR4 β1 helix and the CDR1α/2α loops of MS2-3C8 (A) or HA1.7 (B). CDR1α, violet; CDR2β, purple; DR4 β chain, yellow.

(C, D) Conserved interactions between the DR4 α1 helix and the CDR1β/2β loops of MS2-3C8 (C) or HA1.7 (D). CDR1β, yellow; CDR2β, orange; DR4 α chain, gray. Van der Waals contacts are shown as dotted black lines, hydrogen bonds as dotted red lines, and salt bridges as solid red lines.

Table 4.2 Interactions between TCR MS2-3C8 and MBP-DR4

	TCR		Hydrogen bonds		Number of van der Waals contacts
TCR-DR4 contacts					
CDR1α	Ser 27α	Oγ	His 81β	Nε	1
	Gly 28α		His 81β		3
	Thr 29α	O	Thr 77β	Oγ	3
			His 81β		6
CDR2α	Leu 50α		Thr 77β		1
CDR3α	Asn 95α		Gly 58α		1
			Ala 61α		1
	Lys 96α	Nη	Gln 57α	Oε	3
CDR1β	Thr 29β		Ala 61α		1
			Ala 64α		3
			Val 65α		6
	Thr 30β		Ala 61α		1
CDR2β	Asn 49β		Leu 60α		2
			Ala 61α		6
			Ala 64α		1
	Glu 50β	Oε	Lys 67α	Nη	1
	Thr 55β	Oγ	Lys 39α	Nη	
			Gln 57α		1
CDR3β	Arg 95β		Ala 61α		1
	Gly 97β		Val 65α		2
	Ser 98β		Gly 58α		1
			Ala 61α		5
		Oγ	Asn 62α	Oδ	4
			Val 65α		1
	Tyr 99β		Phe 54α		2
			Gly 58α		9
			Ala 59α		1
			Asn 62α		2
	Asn 100β	O	Gln 70β	Nε	6
	Pro 102β		Asp 66β		1
TCR-MBP contacts					
CDR1α	Ser 27α		Ser P-1		3
CDR3α	Gly 92α		Trp P1		1
			Gly P2		3
		O	Ala P3	N	6
	Ala 93α		Ser P-1		1
CDR3β	Gly 96β		Arg P7		4
			Pro P8		2
	Gly 97β		Gln P6		2
	Ser 98β	N	Gln P6	O	
	Tyr 99β		Ala P3		7
			Gly P5		1
	Asn 100β		Arg P7		1
	Ser 101 β	Oγ	Arg P7	Nε	6
	Pro 102β		Arg P7		1

Hydrogen bonds were calculated using a cut-off distance of 3.4 Å. The cut-off distance for van der Waals contacts was 4.0 Å.

Table 4.3 Interactions between TCR and MHC molecules in the MS2-3C8–MBP–DR4, HA1.7–HA–DR4 and 3A6–MBP–DR2 complexe

HLA-DR4	MS2-3C8		HA1.7		HLA-DR2	3A6	
	Hydrogen bonds and salt bridges (bold)	Van der Waals contacts	Hydrogen bonds and salt bridges (bold)	Van der Waals contacts		Hydrogen bonds and salt bridges (bold)	Van der Waals contacts
K39α	K39α (Nζ) - T55β (Oγ)		K39α (Nη) - K55β (O) **K39α (Nη) - E56β (Oε2)**	E56β	K39α		
F54α		Y99β			F54α		
E55α				E94α	E55α	E55α (Oε2) - S101α (N) E55α (Oε2) - S101α (Oγ)	S101α, Y102α, N56β
Q57α	Q57α (Oε) - K96α (Nη)	K96α, T55β		Y50β, E56β	Q57α	Q57α (Nε) - Q54β (Nε)	Q54β, R55β
G58α		N95α, S98β, Y99β			G58α		G102α, R55β
A59α		Y99β			A59α		
L60α		N49β		M54β	L60α		T53β
A61α		N95α, T29β, T30β, N49β, R95β, S98β		E102α, Y50β, T97β	A61α		T53β
N62α	N62α (Oδ) - S98β (Oγ)	S98β, Y99β		T97β	N62α		
A64α		T29β, N49β		E30β, D51β	A64α		N51β
V65α		T29β, G97β, S98β		G98β	V65α		F50β, S51β
K67α	**K67α (Nη) - E50β (Oε1)**	E50β	**K67α (Nη) - D51β (Oδ1)**	D51β	K67α		
A68α				E30β	A68α		
Y60β					Y60β	Y60β (Oη) - R30β (Nη2)	R30β
W61β					W61β		R30β
Q64β				P100β	Q64β		
D66β		P102β		F97α	D66β	D66β (O) - R99β (Nη2) **D66β (Oδ2) - R99β (Nη2)**	R99β
L67β				P100β	F67β		D98β
E69β			E69β (Oε2) - T50α (Oγ)	A52α	E69β		
Q70β	Q70β (Nε) - N100β (O)	N100β		P96α, F97α	D70β	D70β (Oδ1) - V100β (N)	R99β, V100β
D76β					D76β		Y29α
T77β	T77β (O) - T29α (Oγ)	T29α, L50α		P29α, Y31α, S51α	T77β		Y29α, V100β, N101β
R80β					R80β		Y29α
H81β	H81β (Nε) - S27α (Oγ)	S27α, G28α, T29α		S27α, V28α, P29α	H81β		G28α, Y29α, G94α

4.2.6 The dominant role of CDR3β in self-ligand recognition

i. Interactions between CDR3 loops and HLA-DR4

Whereas the CDR3α loop of MS2-3C8 forms only a few contacts with the α1 helix of HLA-DR4 (Figure 4.10-A), the CDR3β loop straddles the peptide-binding groove and interacts extensively with both the α1 and β1 helices (Figure 4.10-B). These interactions, which are mediated by CDR3β residues 95–102, include 35 van der Waals contacts (46% of the total to HLADR4) to α1 residues Phe54α, Gly58α, Ala59α, Ala61α, Asn62α and Val65α, and to β1 residues Asp66β and Gln70β, in addition to two hydrogen bonds (CDR3β Ser98 Oγ–Oδ1 DR4 Asn62α; CDR3β Asn100 O–Nε2 DR4 Gln70β) (Table 4.2). Of particular note are CDR3β Gly97 and Ser98, which contact the α1 helix (Figure 4.10-B). These junctional residues were found to be highly conserved among 23 TCRs recognizing MBP–DR4 (Muraro et al., 1997), even for TCRs using different Vβ segments; this suggests similar interactions between CDR3β and the DR4 helices to those observed for MS2-3C8. Of the total buried surface on HLA-DR4, excluding MBP, CDR1α, CDR2α and CDR3α contribute 19%, 4%, and 12%, respectively, compared with 10%, 23%, and 32%, respectively, for CDR1β, CDR2β and CDR3β. Hence, CDR3β of MS2-3C8 accounts for more of the binding interface with MHC than any other CDR. The dominance of CDR3β in the MS2-3C8–MBP–DR4 complex is further emphasized by comparing the number of contacts made by this loop in all known TCR–pMHC class II structures (Table 4.4).

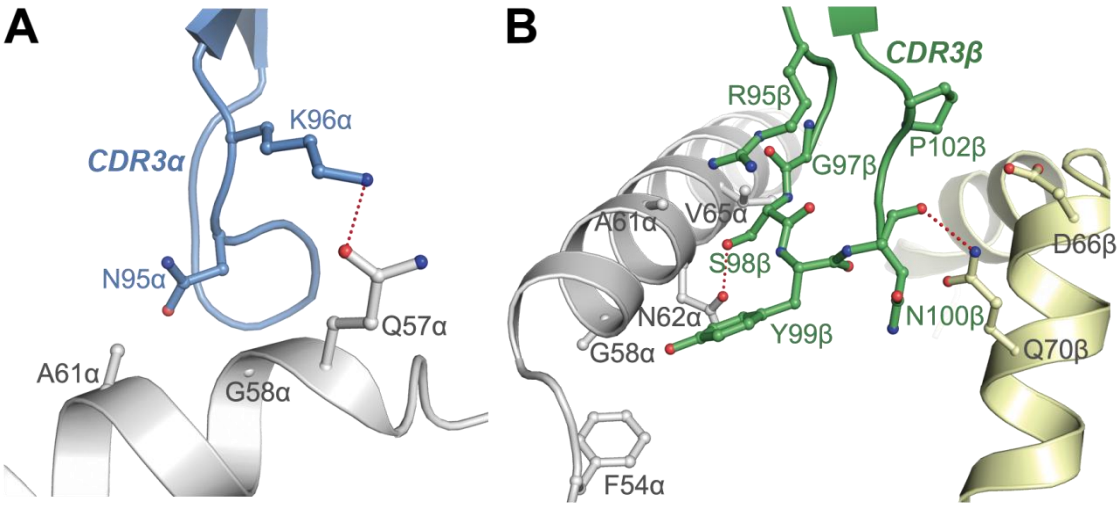

Figure 4.10 Interactions between CDR3 loops and HLA-DR4.

(A) Interactions between CDR3α and the α1 helix of HLA-DR4. (B) Interactions between CDR3β and the α1 and β1 helices of HLA-DR4. CDR3α, blue; CDR3β, orange; DR4 α chain, gray; DR4 β chain, yellow. Van der Waals contacts are shown as dotted black lines and hydrogen bonds as dotted red lines.

ii. Interactions between CDR loops and MBP 114–126

TCRs specific for foreign peptides presented by MHC class I or class II molecules typically utilize four of six CDR loops for peptide recognition: CDR1α, CDR3α, CDR1β and CDR3β (Rudolph et al., 2006). By contrast, most autoimmune TCRs contact peptide using only CDR3α and CDR3β, due to altered binding topology or to partial occupancy of the peptide-binding groove (Wucherpfennig et al., 2009). In this respect, MS2-3C8 is clearly more akin to autoimmune than to anti-foreign TCRs, despite its canonical docking mode and full occupancy of the peptide-binding groove of HLA-DR4 by MBP. Except for some minor contacts between CDR1α Ser27 and P-1 Ser, all interactions between MS2-3C8 and MBP are mediated by the CDR3 loops, primarily CDR3β (Table 4.4).

Table 4.4 Number of contacts between CDR3 loops and peptide-MHC class II ligands

Human class II	MS2-3C8		HA1.7 (1J8H)		Ob.1A12 (1YMM)		3A6 (1ZGL)		E8 (2IAM)	
	CDR3α	CDR3β	CDR3α	CDR3β	CDR3α	CDR3β	CDR3α	CDR3β	CDR3α	CDR3β
MHC	1/0/5	2/0/35	0/0/12	0/0/9	2/0/16	2/0/13	2/0/11	1/1/26	1/0/23	3/0/31
α1	1/0/5	1/0/28	0/0/3	0/0/3	None	0/0/10	2/0/11	None	0/0/12	None
β1	None	1/0/7	0/0/9	0/0/6	2/0/16	2/0/3	None	1/1/26	1/0/11	3/0/31
Peptide	1/0/11	2/0/24	1/2/13	1/0/12	1/0/16	1/0/26	2/0/13	0/0/6	0/0/8	2/0/21
Total	2/0/16	4/0/59	1/2/25	1/0/21	3/0/32	3/0/39	4/0/24	1/1/32	1/0/31	5/0/52

Mouse class II	D10 (1D9K)		172.10 (1U3H)		cl19 (2Z31)		1934.4 (2PXY)		B3K506 (3C5Z)		2W20 (3C6L)		YAe62 (3C60)		21.30 (3MBE)	
	CDR3α	CDR3β	CDR3α	CDR3β	CDR3α	CDR3β	CDR3α	CDR3β	CDR3α	CDR3β	CDR3α	CDR3β	CDR3α	CDR3β	CDR3α	CDR3β
MHC	1/0/6	5/0/18	0/0/9	3/0/17	1/0/19	3/0/11	1/0/20	4/0/10	2/0/15	1/0/27	1/0/8	4/0/36	0/0/4	0/0/28	2/2/17	2/0/16
α1	0/0/4	None	0/0/4	1/0/11	0/0/16	0/0/1	0/0/14	0/0/5	2/0/15	None	1/0/8	0/0/18	0/0/4	0/0/28	2/0/12	2/0/8
β1	1/0/2	5/0/18	0/0/5	2/0/16	1/0/3	3/0/10	1/0/6	4/0/5	None	1/0/27	None	4/0/18	None	None	0/2/5	0/0/8
Peptide	0/0/21	0/0/7	4/0/18	1/0/6	1/0/10	0/0/10	1/0/12	0/0/14	4/1/11	1/0/13	1/0/4	1/0/22	0/0/4	0/0/16	0/0/8	1/2/26
Total	1/0/27	5/0/25	4/0/33	4/0/23	2/0/36	3/0/21	2/0/43	4/0/24	6/1/26	2/0/40	2/0/12	5/0/58	0/0/4	0/0/44	2/2/25	3/2/42

Hydrogen bonds/salt bridges/van der Waals contacts were calculated using the program CONTACT in the CCP4 suite with cut-off distances of 3.4/3.4/4.0 Å. For CDR3β, interactions with the first and second highest number of contacts are marked in red.

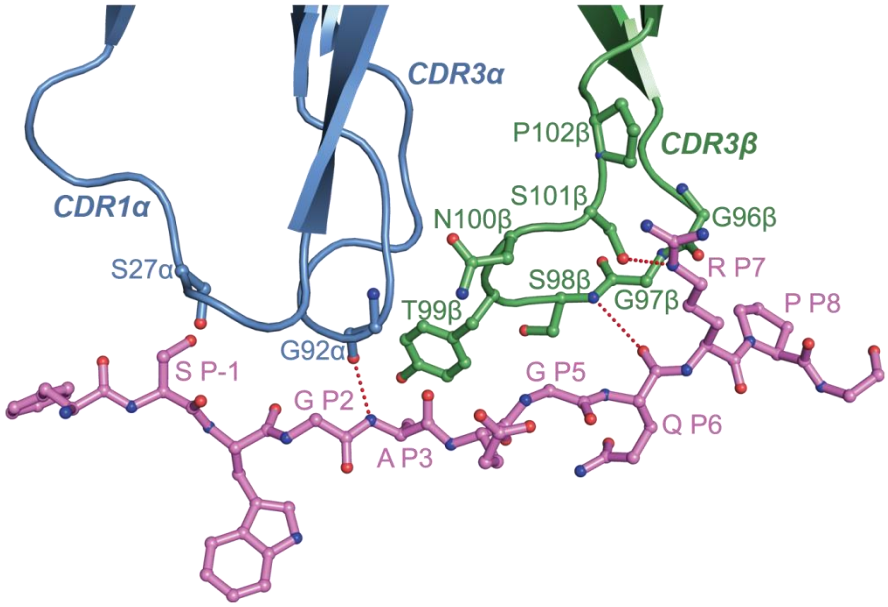

Figure 4.11 Interactions between CDR loops and MBP 114-126.

Contact residues are drawn and labeled. TCR α-chain, blue; TCR β-chain, green; MBP peptide (ball-and-stick representation), magenta. Hydrogen bonds are indicated by dotted red lines.

As shown in Figure 4.11, CDR3α contacts MBP residues P1 to P3, while CDR3β contacts residues P3 to P8. In agreement with the crystal structure, these residues comprise the minimal epitope recognized by MS2-3C8, as defined by T cell proliferation assays (Muraro et al., 1997). The CDR3β loop resembles a horseshoe stepping on the C-terminal three-quarters of the MBP peptide (Figure 4.11). As a result, the contact interface between CDR3β and MBP is large (253 $Å^2$) and flat, with good shape complementarity. Thus, the shape correlation statistic (S_c) (Lawrence and Colman, 1993) for the interface between CDR3β and MBP–DR4 is 0.78, which is significantly higher than the S_c for the whole interface (0.65). By comparison, the corresponding S_c values for the HA1.7–HA–DR4 complex, which has 6-fold lower affinity than the MS2-3C8–MBP–

DR4 complex (Cole et al., 2007), are both 0.56. Because the tip of CDR3β is directed toward CDR3α rather than the peptide, MS2-3C8 lacks the open pocket between CDR3 loops found in other TCRs that typically accommodates the side chain of residue P5. In MBP, P5 is glycine, whose lack of a side chain nonetheless permits this residue to pack against the CDR3β flap sealing off the CDR3 pocket of MS2-3C8 (Figure 4.11). Indeed, the interaction of CDR3β with MBP is distinguished by the multiple close contacts made by this loop to the main chain of the self-peptide (Figure 4.11). These factors, combined with the engagement of both DR4 helices by CDR3β, are probably key to the unexpectedly high affinity of MS2-C38 for its self-antigen.

4.2.7 Contribution of P7 Arg to complex stability

As described above, secondary anchor residue P7 Arg is not situated in the P7 pocket of HLA-DR4. Rather, it is sandwiched between the DR4 β1 helix and the CDR3β loop so as to interact substantially with both molecules (Figure 4.2-B). The long side chain of P7 Arg projects over the residues Gln64β, Asp65β and Leu67β of HLA-DR4, thus making 16 van der Waals contacts and 3 hydrogen bonds. On the other side, P7 Arg alone accounts for half (12 of 24) the van der Waals contacts made between CDR3β and MBP, as well as a side-chain–side-chain hydrogen bond linking the guanidinium group of P7 Arg to the Oγ atom of CDR3β Ser101 (Table 4.4; Figure 4.11). Collectively, these interactions underscore the importance of P7 Arg to securing complex formation. The long side chain of P7 Arg compensates for destabilizing the MBP–DR4 self-ligand, which likely enabled MS2-3C8 T cells to escape thymic deletion, by reinforcing the

interaction between MBP and TCR, which permitted activation of these autoreactive cells in the periphery. We therefore conclude that P7 Arg plays a key role in the autoimmune function of MS2-3C8 by playing the dual role of weakening the interaction of MBP with HLA-DR4 while strengthening that between MBP and MS2-3C8.

4.3 Discussion

4.3.1 Correlation between binding affinities and topologies

Since the structures of the two autoimmune complexes were published in 2005 (Hahn et al., 2005; Li et al., 2005), both displaying strikingly distinct binding features comparing to anti-foreign TCRs, it has been widely assumed that all autoimmune TCRs adopt suboptimal binding modes in order to escape negative selection (Deng and Mariuzza, 2007; Nicholson et al., 2005; Wucherpfennig et al., 2009). Having now solved the structure of the autoimmune MS2-3C8–MBP–HLA-DR4 complex, we have shown that not every autoimmune TCR uses an altered binding mode to engage self-pMHC. MS2-3C8 docks onto MBP–DR4 in a way that closely resembles anti-microbial TCRs, which sit on the center of the pMHC surface with a diagonal docking angle. The classical docking mode of autoimmune TCR MS2-3C8, inconsistent with those of Ob.1A12 and 3A6, dispels the notion that the altered docking mode is a necessary feature of autoimmune TCRs.

On the other hand, the structure of MS2-3C8 demonstrates that the docking mode is correlated with TCR binding affinity. The classical binding mode, as broadly defined by anti-microbial TCRs, can be viewed as an optimal strategy for TCRs to engage pMHC,

which leads to higher binding affinities. By contrast, the altered binding mode used by TCRs Ob.1A12 and 3A6 can be viewed as a suboptimal binding strategy, as manifested by their low affinities. Although studies have shown that the TCR repertoire before positive selection is biased against pMHC (Blackman et al., 1986; Merkenschlager et al., 1997; Zerrahn et al., 1997), it is still possible that positive selection may further exclude a very small percentage of functionally inactive TCRs that recognize irregular epitopes. Considering the structural constraints provided either intrinsically or by positive selection, a TCR might achieve high affinity only with a canonical binding mode, which maximizes the interaction between TCR and pMHC. Therefore, the binding topology of a particular TCR is not directly linked with autoimmunity, but correlates with its binding affinity.

4.3.2 Altered docking mode of TCR vs. altered sitting mode of peptide

The structure of the MS2-3C8–MBP–DR4 complex revealed why the self-peptide binds weakly to HLA-DR4. Compared with peptides that bind HLA-DR4 with high affinity, MBP 114-129 resides less deeply in the binding groove, due to suboptimal anchor resides at positions P6 and P7. This elevation results in the net loss of several hydrogen bonds and numerous van der Waals contacts relative to high-affinity peptide–DR4 complexes.

MHC molecules, albeit highly homologous, are basically different proteins with respect to peptide binding. Their polymorphic peptide-binding grooves are constructed with structural or chemical differences that determine the conformations of bound peptides; that is, the peptide conformation is MHC-specific. Therefore, it is not possible

to propose a universal peptide-binding mode for all MHCs. The structural alterations we observed in the MBP–DR4 complex may only be correlated with the low affinity of MBP for DR4, rather being characteristic of other pMHC complexes associated with autoimmunity. The structural database of human MHC class II molecules bound to self-peptides is so far too small for us to draw general conclusions on this issue.

4.3.3 Comparison between two autoimmune TCR MS2-3C8 and 172.10

172.10 is a mouse MHC class II I-A^u-restricted TCR that is specific for an acetylated N-terminal peptide of mouse MBP, Ac1-11 (Maynard et al., 2005). It was selected from a T cell line established from I-A^u-positive mice immunized with MBP (Urban et al., 1988). Thus, TCR 172.10 is autoreactive and responsible for the autoimmune inflammation in the central nervous system of mice with EAE. The existence of 172.10 in the periphery indicates that this TCR also escaped from negative selection. When encountering the burst of administrated MBP, it became activated and started to attack myelin self-tissues (Urban et al., 1988). In this regard, 172.10 is a mouse autoimmune TCR.

There are several features that are shared by TCR MS2-3C8 and 172.10. First, the antigenic self-peptide MBP Ac1-11 also has very low affinity for MHC, and is therefore unable to form a stable complex with I-A^u (Fairchild et al., 1993; Fugger et al., 1996; Mason et al., 1995). Second, the TCR repertoire selected against MBP Ac1-11 in the background of I-A^u showed limited sequence diversity. Similarly, restricted usage of TCR V genes was observed in MS patients with HLA-DR4 background. Both systems agree with the proposition that low-affinity antigenic peptides are linked with a more restricted

TCR repertoire (Baumgartner et al., 2010). The structure of the 172.10–MBP–I-A^u ternary complex (Maynard et al., 2005) showed that 172.10 also used a central docking mode for MBP–I-A^u and achieved a binding affinity close to that of MS2-3C8 (Garcia et al., 2001).

In spite of the shared features, TCR 172.10 also presents major differences compared to MS2-3C8. The MBP–I-A^u ligand is unusual in that the N-terminal one-third of the binding groove is empty (He et al., 2002). The groove contains only the first seven residues of the MBP Ac1–11 peptide, leaving the P1 and P2 pockets of I-A^u unoccupied. By contrast, the binding groove of HLA-DR4 is completely filled by MBP 114–126, although portions of the peptide are loosely accommodated. Thus, TCR 172.10 only recognizes six peptide residues (P3 to P8), compared with nine (P-1 to P8) in the case of MS2-3C8. Moreover, the interaction of TCR 172.10 with MBP Ac1–11 is characterized by a paucity of specific contacts between TCR and peptide (Maynard et al., 2005). However, such structural degeneracy is not evident in the interface of MS2-3C8 with MBP 114–126, which possesses high shape and chemical complementarity. In addition, whereas MS2-3C8 and 172.10 have similar binding affinities, the binding kinetics of 172.10 is completely opposite to that of MS2-3C8. In contrast to the slow kinetics of MS2-3C8 (k_{on} = 1.7 × 10^3 M^{-1} s^{-1}; k_{off} = 0.011 s^{-1}), 172.10 binding to MBP–I-A^u has about 20-fold faster on- and off-rates (k_{on} = 3.7 × 10^4 M^{-1} s^{-1}; k_{off} = 0.22 s^{-1}). Differential kinetics may mediate different signaling processes and result in different cell fate decisions. Indeed, the activation process of 172.10 upon MBP administration is probably different from that of MS2-3C8, which was repeatedly isolated from an MS patient. It is not very likely that a large amount of MBP is suddenly released into blood at the early

stage of MS development. However, how the slow kinetics may contribute to the signaling decision of MS2-3C8 T cells in the thymus, and how they may relate to disease onset and development are not clear.

Collectively, in terms of TCR recognition, MS2-3C8 does share a few features with TCR 172.10, e.g. low-affinity self-peptide, high affinity TCR binding and canonical docking modes. These common features may represent a type of autoimmune TCR complementary to the previously characterized autoimmune TCRs Ob.1A12 and 3A6, the type represented by low TCR affinity and aberrant docking modes. The MS2-3C8–MBP–DR4 structure therefore provides a framework for understanding how autoreactive T cells can successfully target pathogenic self-epitopes with unfavorable MHC-binding properties that may nevertheless be dominant in autoimmune disease.

Chapter 5

Conclusions and future perspectives

T cell-mediated autoimmune diseases, e.g. MS, T1D, etc., are initiated by the activation of autoreactive T cells. T cell responses to self-antigens lead to tissue damage. Activated $CD4^+$ autoreactive T cells can assist cytotoxic T cells and macrophages and direct them to target self-tissues. Autoimmune T cells isolated from the periphery blood of MS patients specifically recognized the self-antigen MBP and mediated myelin destruction in the CNS. Since self-reactive T cell clones are normally deleted during thymic development via the mechanism of negative selection, these autoimmune cells are not allowed to enter the periphery. However, negative selection is not perfect, insofar as some autoimmune T cells escape surveillance. Structural and biophysical studies of the antigen receptors on these T cells may provide information on the molecular mechanisms underlying escape from thymic deletion.

Our structure of the MS2-3C8–MBP–HLA-DR4 complex displayed striking contrasts to the two known human autoimmune TCR–pMHC complexes. Based on the high affinity of TCR MS2-3C8, we propose an alternative mechanism for evading negative selection. In the previous model, the TCR binds weakly to self-pMHC, preventing formation of a stable self-complex that triggers programmed cell death of the T cell. Therefore, the low-affinity T cell survives. In our model, it is weak binding of the self-peptide to MHC that compromises the stability of the TCR–pMHC complex and allowed escape of MS2-3C8. On the other hand, despite the instability of the TCR–

pMHC complex, an autoimmune T cell must still be activated under certain conditions in the periphery in order to cause disease. This means that the TCR–pMHC complex must still possess a certain level of stability. In our case, MS2-3C8 shows high-affinity binding to MBP–HLA-DR4, which also has an unusually long half-life.

Our results dispel the notion that all autoimmune TCRs bind their self-ligands with altered binding topologies. Since MS2-3C8 adopts a classical binding mode, the binding topology is no longer the sole parameter for assessing autoimmune recognition. Instead, binding topology must be assessed in the context of binding affinity. The classical binding mode correlates with high-affinity binding, whereas altered binding modes correlate with low-affinity binding. Nevertheless, compared to the classical binding mode, altered binding topologies may cause more distruption to the effectiveness of negative selection. Since T cell activation also depends on the function of co-receptors (CD4 or CD8), it is possible that altered co-receptor binding to the TCR–pMHC complex may contribute as well to thymic escape of autoimmune T cells. In this scenario, the altered binding topology of an autoimmune TCR may affect the ligation state of CD4 or CD8, thereby compromising the overall stability of the signaling assembly. To assess this, we expect that there exists an autoreactive TCR that uses altered binding topology, but maintains an average binding affinity. We expect that our understanding of the mechanisms governing self-recognition and escape from negative selection will expand as additional structures of autoimmune TCR–pMHC complexes are determined.

Appendices

Materials, Methods and Protocols

Contents

1. List of constructs and *E. coli* stocks

Name	DR2α
Description	Ectodomain of HLA-DRA*0101
Plasmid	pLM1
Expression strain	BL21(DE3)pLysS
Antibiotics	$Amp^{+}Chl^{+}$
Protein sequence	MIKEEHVIIQAEFYLNPDQSGEFMFDFDGDEIFHVDMAKKETVWRL EEFGRFASFEAQGALANIAVDKANLEIMTKRSNYTPITNVPPEVTVLT NSPVELREPNVLICFIDKFTPPVVNVTWLRNGKPVTTGVSETVFLPRE DHLFRKFHYLPFLPSTEDVYDCRVEHWGLDEPLLKHWEFDA
Protein MW (kDa)	21.3
Protein pI	4.8
1 OD_{280} (mg/mL)	0.76

Name	DR2α-AviTag
Description	DR2α with an AviTag attached to its C-terminus
Plasmid	pLM1
Expression strain	BL21(DE3)pLysS
Antibiotics	$Amp^{+}Chl^{+}$
Protein sequence	MIKEEHVIIQAEFYLNPDQSGEFMFDFDGDEIFHVDMAKKETVWRL EEFGRFASFEAQGALANIAVDKANLEIMTKRSNYTPITNVPPEVTVLT NSPVELREPNVLICFIDKFTPPVVNVTWLRNGKPVTTGVSETVFLPRE DHLFRKFHYLPFLPSTEDVYDCRVEHWGLDEPLLKHWEFDAGGGLN DIFEAQKIEWHE
Protein MW (kDa)	23.2
Protein pI	4.7
1 OD_{280} (mg/mL)	0.69

Name	DR4β
Description	Ectodomain of HLA-DRB1*0401
Plasmid	pET-26b (+)
Expression strain	BL21(DE3)
Antibiotics	Kan^{+}
Protein sequence	MGDTRPRFLEQVKHECHFFNGTERVRFLDRYFYHQEEYVRFDSDVG EYRAVTELGRPDAEYWNSQKDLLEQKRAAVDTYCRHNYGVGESFT VQRRVYPEVTVYPAKTQPLQHHNLLVCSVNGFYPGSIEVRWFRNGQ EEKTGVVSTGLIQNGDWTFQTLVMLETVPRSGEVYTCQVEHPSLTSP LTVEWRARS
Protein MW (kDa)	22.6
Protein pI	6.0
1 OD_{280} (mg/mL)	0.61

Name	MBP–DR4β
Description	DR4β fused with MBP 114-126 and a 16-mer linker to its N-terminus
Plasmid	pET-26b (+)
Expression strain	BL21(DE3)
Antibiotics	Kan^+
Protein sequence	MFSWGAEGQRPGFGSGGGSLVPRGSGGGGSGDTRPRFLEQVKHECH FFNGTERVRFLDRYFYHQEEYVRFDSDVGEYRAVTELGRPDAEYWN SQKDLLEQKRAAVDTYCRHNYGVGESFTVQRRVYPEVTVYPAKTQP LQHHNLLVCSVNGFYPGSIEVRWFRNGQEEKTGVVSTGLIQNGDWT FQTLVMLETVPRSGEVYTCQVEHPSLTSPLTVEWRARS
Protein MW (kDa)	25.3
Protein pI	6.2
1 OD_{280} (mg/mL)	0.59

Name	3C8α
Description	Ectodomain of the α chain of TCR MS2-3C8
Plasmid	pET-22b (+)
Expression strain	BL21(DE3)pLysS
Antibiotics	Amp^+Chl^+
Protein sequence	MGDAKTTQPNSMESNEEEPVHLPCNHSTISGTDYIHWYRQLPSQGPE YVIHGLTSNVNNRMASLAIAEDRKSSTLILHRATLRDAAVYYCTVYG GATNKLIFGTGTLLAVQPNIQNPDPAVYQLRDSKSSDKSVCLFTDFDS QTNVSQSKDSDVYITDKTVLDMRSMDFKSNSAVAWSNKSDFACANA FNNSIIPEDTFFPSPESSC
Protein MW (kDa)	22.9
Protein pI	5.0
1 OD_{280} (mg/mL)	1.0

Name	3C8β
Description	Ectodomain of the β chain of TCR MS2-3C8
Plasmid	pET-22b (+)
Expression strain	BL21(DE3)pLysS
Antibiotics	Amp^+Chl^+
Protein sequence	MVVSQHPSWVIAKSGTSVKIECRSLDFQATTMFWYRQFPKQSLMLM ATSNEGSKATYEQGVEKDKFLINHASLTLSTLTVTSAHPEDSSFYICSA RGGSYNSPLHFGNGTRLTVTEDLKNVFPPEVAVFEPSEAEISHTQKAT LVCLATGFYPDHVELSWWVNGKEVHSGVSTDPQPLKEQPALNDSRY SLSSRLRVSATFWQNPRNHFRCQVQFYGLSENDEWTQDRAKPVTQI VSAEAWGRADC
Protein MW (kDa)	27.6
Protein pI	6.1
1 OD_{280} (mg/mL)	0.56

Name	3C8α-intC
Description	3C8α engineered for replacing C-terminal disulfide bond of MS2-3C8 with an artificial disulfide bond between the constant domains
Plasmid	pET-26b (+)
Expression strain	BL21(DE3)pLysS
Antibiotics	$Kan^{+}Chl^{+}$
Protein sequence	MGDAKTTQPNSMESNEEEPVHLPCNHSTISGTDYIHWYRQLPSQGPE YVIHGLTSNVNNRMASLAIAEDRKSSTLILHRATLRDAAVYYCTVYG GATNKLIFGTGTLLAVQPNIQNPDPAVYQLRDSKSSDKSVCLFTDFDS QTNVSQSKDSDVYITDKCVLDMRSMDFKSNSAVAWSNKSDFACAN AFNNSIIPEDTFFPSPESS
Protein MW (kDa)	22.9
Protein pI	5.0
1 OD_{280} (mg/mL)	1.0

Name	3C8β-intC
Description	3C8β engineered for replacing C-terminal disulfide bond of MS2-3C8 with an artificial disulfide bond between the constant domains
Plasmid	pET-26b (+)
Expression strain	BL21(DE3)pLysS
Antibiotics	$Kan^{+}Chl^{+}$
Protein sequence	MVVSQHPSWVIAKSGTSVKIECRSLDFQATTMFWYRQFPKQSLMLM ATSNEGSKATYEQGVEKDKFLINHASLTLSTLTVTSAHPEDSSFYICSA RGGSYNSPLHFGNGTRLTVTEDLKNVFPPEVAVFEPSEAEISHTQKAT LVCLATGFYPDHVELSWWVNGKEVHSGVCTDPQPLKEQPALNDSRY ALSSRLRVSATFWQNPRNHFRCQVQFYGLSENDEWTQDRAKPVTQI VSAEAWGRAD
Protein MW (kDa)	27.6
Protein pI	6.1
1 OD_{280} (mg/mL)	0.56

2. Molecular cloning

PCR and subcloning were performed according to *Molecular Cloning*[1] or product manuals. The gene encoding extracellular residues Ile1–Ala182 of the HLA-DR4 a chain (HLA-DRA*0101) was inserted into the expression vector pLM1. The construct for the HLA-DR4 b chain (HLA-DRB1*0401), which residues Gly1–Ser192 of the b chain, was cloned into the vector pET-26b(+) (Novagen). MBP-linked DR4 b chain (MBP-DR4b),

[1] Sambrook, J., and D.W. Russell. 2001. Molecular cloning : a laboratory manual. Cold Spring Harbor Laboratory Press, Cold Spring Harbor, N.Y.

which encoded a fusion protein comprising MBP 114–126 (FSWGAEGQRPGFG) connected by a 16-mer peptide linker (SGGGSLVPRGSGGGGS) to the b chain (Figure 2.2), was cloned into the same vector. For the production of biotinylated HLA-DR proteins, a 15-amino acid AviTag (GLNDIFEAQKIEWHE) was added to the C-terminus of the a chain with two glycine residues inserted as a spacer. The a and b chains of TCR MS2-3C8 (residues 1–206 and 1–245, respectively) were also cloned into pET-26b(+). To construct 3C8α-intC and 3C8β-intC, the constant domains of the two chains were respectively switched with those of TCR G4α-intC and E8β-intC, two TCR polypeptides pre-constructed with the artificial disulfide bond in our lab. The two modified chains were cloned into pET-26b(+). All constructs were verified by DNA sequencing before being transformed into expression strains BL21(DE3) or BL21(DE3)pLysS (see Appendix 1).

3. Freezing bacteria

A single colony of DH5α or BL21(DE3) strain containing the correct construct was inoculated in LB medium containing the correct antibiotics (see Appendix 1). The grown bacterial culture was supplemented with 1/4 to 1/5 volume of 50% glycerol (1:1 mixture of LB and 100% glycerol) before being stored in -80℃ freezer. Overgrowth of the bacterial culture should be avoided due to the risk of losing plasmids.

4. Growth of *E. coli* cultures for expression of inclusion bodies

1) Grow overnight pre-culture by inoculating 20 μL frozen BL21(DE3) bacteria stock into 120 mL LB medium containing the correct antibiotics (see Appendix 1). Shake at 30℃ for 12-14 hrs.
2) Dilute the pre-culture into 6 bottles of 1L antibiotics-supplemented LB-medium at a 1:20 ratio. Shake at 300 rpm at 37℃.
3) Monitor the cell density until OD600 reaches 0.6.
4) Add 1mM IPTG to the cultures at OD600 of 0.6-0.8 to induce protein expression.

5) Harvest the cells after 3 hrs by centrifuging at 6,500 rpm for 15 min in a Backman Coulter JLA-8.1000 rotor.
6) Discard supernatant and transfer the cell pellets into 250-ml centrifuge bottles.
7) Cell pellets can be processed immediately for extraction of inclusion bodies, or be stored at -20 ℃ for a few weeks.

5. Preparation of inclusion bodies

Solutions:

Wash buffer I

5% (v/v) Glycerol
2% (v/v) Triton X-100
50 mM Tris Cl, pH 8.0
150 mM NaCl
1 mM EDTA

Wash buffer II

50 mM Tris Cl, pH 8.0
150 mM NaCl
1 mM EDTA

Urea solution

50 mM Tris Cl, pH 8.5
8 M Urea
1 mM EDTA
10 mM DTT

Guanidine solution

50 mM Tris Cl, pH 8.5
6 M Guanidine-HCl
1 mM EDTA
10 mM DTT

Procedure (for pellet from less than 6 L culture):

1) Add 100 mL pre-chilled Wash buffer I into the bottle that contains the cell pellet. Break the pellet using a small spoon.
2) Sonicate the mixture for 4 minutes with the bottle in ice bath.
   Sonicator setting (Branson Sonifier 450):

   Duty cycle – 50%

   Output level – 7

3) Spin down at 8,000 rpm for 10 min in a JA-14 rotor and discard supernatant carefully.
4) Resuspend the pellet in 100 mL cold Wash buffer I.

5) Repeat steps 2), 3) and 4).
6) Repeat step 2) and 3).
7) Resuspend the pellet in 100 mL Wash buffer II and sonicate briefly for 2 min.
8) Spin down at 8,000 rpm and discard supernatant.
9) Repeat step 7).
10) Split the 100-ml homogenized mixture into two 50-ml corning tubes.
11) Spin down at 4,500 rpm for 30 min in a tabletop centrifuge and discard supernatant.
12) For solubilizing MHC inclusion bodies, add 20 mL freshly made Urea solution into each inclusion body pellet. For solubilizing TCR, add 20 mL freshly made Guanidine solution into each pellet. Use 1 mL pipette tips to break the pellets for more efficient solubilization.
13) Rotate the corning tubes at 4 ℃ overnight.
14) Clean the solubilized inclusion bodies by ultracentrifugation at 45,000 rpm for 45 min.
15) Store the supernatant at -80 ℃ until ready to use.

6. Purification of HLA-DR4 inclusion bodies using HQ50 column

Solutions (freshly made and filtered):

Buffer A: 20 mM Tris Cl, pH 8.5, 8 M Urea, 1 mM DTT;

Buffer B: 20 mM Tris Cl, pH 8.5, 8 M Urea, 1 mM DTT, 1 M NaCl.

Procedure:

1) Pack 20 mL Poros HQ50 resin (Perspective Biosystems) in a XK16/20 column.
2) Install the column onto a Biocad HPLC machine.
3) Dilute the inclusion bodies 1:2 in buffer A.
4) Inject 5 mL inclusion body at 2 mL/min into the HQ column each cycle.
5) Change the flow rate to 6 mL/min and run a gradient of 0-30% buffer B over 100 mL.

6) Collect all peaks with OD280 over 1.5 except the peak of flow through until the end of the gradient.
7) Pool all collected fractions and concentrate to 1/3 of the volume at room temperature using an Amicon stirred cell.

7. *In vitro* folding of proteins from solubilized inclusion bodies (large scale)

1) Make refolding buffer without the glutathione redox pair and chill it overnight in a cold room.
2) Mix the inclusion bodies of α and β chains of HLA-DR4 or MS2-3C8.
3) Dissolve glutathione pair into the refolding buffer and stir rapidly.
4) Add the inclusion body mixture into the refolding buffer slowly drop by drop.
5) Keep the refolding mixture stirring in a cold room for several days (see below).

7.1 Refolding of HLA-DR4 proteins including MBP/HLA-DR4, MBP–HLA-DR4 and MBP–HLA-DR4–AviTag

Refolding buffer

50 mM Tris Cl, pH 8.5
30% (v/v) Glycerol
0.5 mM EDTA
3 mM glutathione reduced (GSH)
0.9 mM glutathione oxidized (GSSG)

1) Add 5 mM MBP peptide before adding inclusion bodies if refolding MBP non-linked HLA-DR4.
2) Mix 20 mg/L inclusion bodies for each chain before diluting into the refolding buffer.
3) Stir at 4℃ for at least 2 weeks

7.2 Refolding of MS2-3C8

Refolding buffer

50 mM Tris Cl, pH 9.0
0.4 M Arginine-HCl
0.5 mM EDTA
3 mM glutathione reduced (GSH)
0.9 mM glutathione oxidized (GSSG)

1) Mix 25 mg/L inclusion bodies for each chain before rapid dilution.
2) Stir at 4 ℃ for 3 days.

8. Quantification of small-scale refolding efficiency of MBP–HLA-DR4 by ELISA

For setting up small scale refolding tests, make 1 mL buffer for each condition in a 1.5-ml microtube (Table 2.1). Add a total 40 μg of 1:1 mix of α and β inclusion bodies into each tube and vortex immediately. Rotate the tubes at 4 ℃.

ELISA steps:

1) Coat the capture antibody: Dilute mouse anti-DR monoclonal antibody L243 to 1 μg/mL with PBS. Add 100 μL of diluted L243 antibody into each well of a Nunc MaxiSorp plate and incubate overnight at 4 ℃.
2) Wash once: aspirate wells and wash once with PBS.
3) Blocking: Add 100 μL of 2% BSA in PBS to each well and incubate at room temperature for 1 hour.
4) Wash three times with PBS.
5) Transfer 100 μL of refolding mixture 1:5 diluted with PBS from each condition to the wells. Incubate at room temperature for 2 hours.
6) Wash five times with PBS plus 0.5% Tween-20.

7) Add 100 μL of 1:200 diluted pre-absorbed[2] rabbit anti-DR sera CHAMP. Incubate at room temperature for 1 hour.
8) Wash five times with PBS plus 0.5% Tween-20.
9) Add 100 μL of 1:10,000 diluted goat anti-rabbit IgG-HRP conjugate (Sigma) into each well.
10) Wash three times with PBS plus 0.5% Tween-20.
11) Wash three times with PBS.
12) Add 100 μL of TMB substrate (Pierce). Keep the plate in dark and incubate at room temperature for 15 min.
13) Stop reaction with 100 μL 2 M sulfuric acid.
14) Measure OD450 for each well.

Negative control:

1) Replace test sample with 100 μL PBS.
2) Replace both test sample and CHAMP with 100 μL PBS.

Standard/positive controls:

Replace test sample with 8 wells of 1:2 serially diluted HLA-DR1 at 1 μg/mL.

9. Purification of *in vitro* folded proteins

** The samples need to be kept cold during process.*

1) Filter the refolding mixture through filter paper.
2) Concentrate the refolding mixture 50 times using a Sartorius concentrator with a 10-kDa cutoff.
3) Dialyze at least 12 hrs against 2 L 50 mM MES pH6.0 at 4 ℃.

[2] CHAMP anti-DR sera is cross-reactive to L243 mAb. To absorb the cross-reactivity, 400 μl CHAMP was rotated overnight at 4°C with 200 μl L243-coupled agarose beads. The next morning spin down the beads at 3,000 rpm for 5 min. Transfer the supernatant of absorbed CHAMP into a new tube and supplement with 0.02% NaN3.

4) Remove aggregation by ultracentrifuging for 30 min at 20,000 rpm using a JA-25.5 rotor.
5) Concentrate to 4 mL using Amicon centrifugal filter units (Millipore).
6) Clear the solution by spinning for 10 min at 14,000 rpm followed by filtering through 0.22 μM membranes.
7) Run gel filtration with Superdex 200 column on a FPLC system. Inject 0.5-1 mL of sample each time. Run with PBS at a flow rate of 0.5 mL/min. Collect the peak around 14- to 17-ml elution volume.
8) Pool all collected fractions and dilute 1:2 with 50 mM Tris Cl, pH 8.0.
9) Run anion exchange with MonoQ column. Inject 5 mL each time. Run with 50 mM Tris Cl, pH 8.0 at a flow rate of 1 mL/min. Use a NaCl gradient of 1%-per-ml increase to elute the proteins. Collect peaks according to Figure 2.4-B and Figure 2.5-B.
10) Concentrate the purified proteins to at least 1 mg/mL. Aliquot and flash-freeze using liquid nitrogen. Store at -80 ℃.

10. Biotinylation and purification of MBP–HLA-DR4–AviTag

Reagents:

Biotin protein ligase at 1 mg/mL purchased from Avidity, LLC

Supplied solutions:

10x Biomix A
10x Biomix B
0.5 mM Biotin

1) Dialyze the purified MBP–HLA-DR4–AviTag overnight against 20 mM Tris Cl, pH 8.0 at 4 ℃.
2) Adjust the concentration to 40 μM, i.e. about 2 mg/mL and measure the volume of the protein solution.
3) Add 1/7 volume of Biomix A, 1/7 volume of Biomix B and 1/7 volume of biotin (0.5 mM).

4) For every mg of MBP–HLA-DR4–AviTag, add 5 μL of BirA biotin ligase (1 mg/mL).
5) Incubate 45 min at 30 ℃.
6) Remove the enzyme and excess biotin by running the reaction mix through a Superdex 200 column.
7) Collect the fraction. Store in -80 ℃ freezer.

11. Sedimentation velocity analysis of MS2-3C8

The analytical ultracentrifuge used is Beckman Optima XL-A, which monitors the absorbance change of analyzed samples. To correlate the absorbance and the distribution of molecules in the solution, we prepared three concentrations of MS2-3C8: 0.2 mg/mL, 0.4 mg/mL and 0.7 mg/mL. All samples were analyzed by their OD_{280}.

1) Dialyze 0.5 mL MS2-3C8 at 2 mg/mL against 1 L PBS for 24 hours.
2) Filter the dialysis buffer after washing the filter membrane with the buffer three times. Use the filtered dialysis buffer as test blank and for diluting the protein samples to the three tested concentrations.
3) Assemble three analytical cells with double-sector centerpieces as instructed. The cells are numbered 1 to 3, which fits into the correspondently numbered spaces on the rotor.
4) Fill the reference sectors of the three cells (left with the screw-ring end facing toward you) with 420 μL PBS using 200 μL long micropipette tips.
5) Fill the right sample sectors respectively with 400 μL three concentrations of MS2-3C8 samples.
6) Place a new red plug gasket on each filling hole and seal the holes by screwing the housing plugs in. Do not tighten them too much. Otherwise, you may risk distorting the analytical cells and break the housing plugs that are made of metal a bit soft.
7) Weigh the assembled cells. The sample cells should be within 0.5 gram of each other. Otherwise, check the volumes in the sectors. Weigh the counterbalance that is

going to be placed opposite to cell #2. Use the weights to adjust the counterbalance so that its weight is equal to or within 0.5 gram less than cell #2.

8) Load the counterbalance in cell hole 4 of an An-55 rotor and the other three assembled cells to position 1 to 3. Match the scribe lines on the cells with those on the rotor.
9) Power on the machine and open the program.
10) Insert the rotor into the ultracentrifuge and mount the optical arm. Close the chamber door.
11) Switch on the vacuum and set temperature to 20 ℃. Watch the pressure drop until it is below 100 microns. Let the temperature equilibrate for at least an hour.
12) Start running at 50,000 rpm at 20 ℃. Collect OD280 scan data from 6.0 to 7.2 cm of radial distance. Only 1 replicate will be recorded. Set the acceleration speed to maximum.
13) Stop the run after 4 hours because the boundary has completely moved to the bottom of the cells.
14) A total of 68 scans were collected for each concentration of MS2-3C8.
15) Data process was performed using SEDFIT[3]. Figure 2.6 shows the fitting of cell #2 which contains 0.4 mg/mL MS2-3C8. Global fitting of all three data sets gave the sedimentation coefficient of 3.8 S and 48.4 kDa, which are obtained with parameter settings for solvent density (ρ = 1.005 mg/mL), viscosity (η = 0.0102 Poise) and partial specific volume of the protein (ν = 0.73 mL/mg).

12. SPR analysis of MS2-3C8 binding to MBP–HLA-DR4 using Biacore T100 instrument

Running buffer:

1x HBSP

50 mM HEPES, pH7.4

[3] Lebowitz, J., M.S. Lewis, and P. Schuck. 2002. Modern analytical ultracentrifugation in protein science: a tutorial review. *Protein Sci*. 11:2067-2079.

150 mM NaCl
0.05% Surfactant P-20

1) Insert a CM5 Biacore sensor chip into the chip cassette.
2) Prime the system with the running buffer HBSP.
3) Set system temperature to 25 ℃.
4) Immobilization of Streptavidin: Dilute 1 mg/mL Streptavidin to 0.1 mg/mL using 10 mM NaAc, pH4.5. Open the pre-programmed amine coupling method in Biacore T100 control software for immobilization of streptavidin. Use a contact time of 360 s to have over 3,000-RU incorporation. This step was applied to flow cell 1 and 2. Flow cell 1would serve as blank control, whereas flow cell 2 is the experimental one.
5) Capture of MBP–HLA-DR4: Inject 2 μg/mL biotinylated MBP–HLA-DR4–AviTag for 15 s in flow cell 2. This will result in 400 to 500 RU of MBP–HLA-DR4 being captured onto the chip surface.
6) Block the chip surface by injecting 20 μM biotin for 30 s for both flow cell 1 and flow cell 2.
7) Inject of analyte MS2-3C8: Set flow rate at 10 μL/min. For a binding cycle of kinetics measurement, inject a concentration of MS2-3c8 for 60 s; for equilibrium measurement, inject for 240 s. Dissociation length is set to 600 s. The highest concentration should be about 10 times of the estimated K_D. For a precise equilibrium measurement, use 8 times of the K_D value as the highest concentration. Do 1:2 serial dilutions with HBSP for 6 more concentrations. The overall range for tested concentrations is within one-eighth to 8 times of K_D .
8) Global fitting of the kinetics data was performed using the software BiaEvaluation 4.0 using a 1:1 binding model. The equilibrium RU was read directly from sensorgrams. Data fitting of the equilibrium data was done with the software Origins 7.0 using Eq. 3.8. All plots were prepared using Origins 7.0.

13. Protein analysis

13.1 Mass spectrometry to confirm size of the purified protein

Matrix solution:

20 mg/mL sinapinic acid
50% Acetonitrile
0.1% Trifluoroacetic acid

Mix well and store in aliquots at -20 ℃

1) Mix 1 μL protein sample and 1 μL matrix solution on a 100-well sample plate. The protein solution should be at 1 mg/mL and have very low ionic concentration.
2) Put the sample plate at 37 ℃ to allow the drop dry faster.
3) Insert the plate into the mass spectrometer and acquire data.
4) Compare the mass spec peak position with the theoretical molecular weight of the tested protein.

13.2 SDS-PAGE using PhastSystem to check the purity of protein samples

1) Prepare non-reduced samples by mixing 2 μL protein and 2 μL 2× Laemmli sample buffer. For preparing reduced samples, add an extra 0.5 μL 1 M DTT.
2) Heat samples at 100 ℃ for 5 min.
3) Carefully load 4 μL sample into each well of the sample applicator.
4) Set up a 20% homogeneous PhastGel on the PhastSystem unit. Insert the buffer strips. Slide in the sample applicator.
5) Close the lid and run the preset program for 20% PhastGel.

Ethanol-based fast coomassie staining:

Coomassie blue stain

50% Ethanol	50 mL	
0.25% Coomassie R250	0.31 g	
40% H_2O	40 mL	Total
10% Acetic acid	10 mL	100 mL

Mix everything else before adding acetic acid. Filter to remove non-dissolved chemicals.

Fix solution

50% Ethanol	250 mL	
7% Acetic acid	35 mL	Total
43% H2O	215 mL	500 mL

Stain/Destain solution

5% Ethanol	25 mL	
7.5% Acetic acid	37.5 mL	Total
87.5% H2O	447.5 mL	500 mL

Preserving solution

5% Glycerol	50 mL	
10% Acetate acid	100 mL	Total
85% H2O	850 mL	1 L

1) Make the staining solution by adding 1 mL Coomassie blue stain into 100 mL Stain/Destain solution.
2) Add 100 mL fix solution to cover gel.
3) Microwave both for 1 min.
4) Transfer the gel into the staining solution and put on a rocking shelf.
5) Bands can be seen after 10 min and will become darker if continuing staining.
6) Destain if needed with the Stain/Destain solution. Or directly transfer into preserving solution for destaining and preserving.

13.3 UV spectrometry to determine protein concentration

1) Use the buffer of the protein solution as blank.
2) Dilute protein samples X times with the same buffer until the measured A280 is in the range of 0.1 to 1.

3) Check the value of absorbance parameters for each protein (see Appendix.1) and calculate the concentration of the protein in mg/mL or μM using the following two equations:

$$[protein]\ (mg/mL) = A280 \times X \times (mg/mL\ per\ OD280)$$

$$[protein]\ (\mu M) = A280 \times X \times 106 \div Extinction\ Coefficient$$

UV spectrometry is not ideal for precise determination of the absolute concentration of a protein sample. But it is probably the most convenient method. If done carefully, the reproducibility, one of the most important issues for crystallization, should be acceptable.

14. Co-crystallization of MS2-3C8 and MBP–HLA-DR4

1) Dialyze overnight both MS2-3C8 and MBP–HLA-DR4 against 10 mM Tris Cl, pH 8.0, 5 mM NaCl at 4 ℃.
2) Concentrate both proteins to 10 mg/mL.
3) Mix 50 μL MS2-3C8 and 46 μL MBP–HLA-DR4 for 1:1 molar ratio. The ratio can be roughly checked by SDS-PAGE.
4) Set up hanging-drop crystallization using the available commercial crystal screening kits, including Crystal Screen I (Hampton Research), II and Lite, Wizard I and II (Emerald Biosystems), etc. Briefly, add 480 μL of each crystallization solution into a well of a crystallization plate. Pipette 0.5 μL of the crystallization solution to the cover slip. Add 0.5 μL protein mixture into the drop.
5) Seal the wells using the cover slips with the crystallization drop facing downwards.
6) Put the crystal plates at room temperature in a dark and disturbance-free place.
7) Look for crystals in each crystallization drop under a microscope after 2 days.

15. Optimization of crystallization conditions and seeding

Initial crystal screen gave three hits with PEG as precipitants: Crystal screen I #14,

Crystal screen lite #17and Wizard I #46. The crystals are all in the form of small needles. Trying to optimize the crystals, a 3x4-well matrix was made for each condition, which included either modified PEG concentration or modified pH. The volume used for optimization was doubled as 1 μL crystallization solution plus 1μL protein. One condition modified from Wizard I #46 grew small plates, whereas other conditions did not support crystal formation or still grew crystal needles. The new condition was 1 mL protein solution and 1 mL 10% (w/v) polyethylene glycol 8000, 0.2 M calcium acetate, and 0.1 M imidazole (pH 8.5) (solution M). This condition was repeated, but not every drop could yield crystals. This may indicate that the nucleation step of crystal growth could have some difficulty.

Therefore, crystal seeding was used to deliver pre-formed crystal nuclei that may help grow bigger crystals. In addition, to control the evaporation rate during crystal growth, the well solutions were replaced by crystal screen #6 (we have a bulk stock.) plus different amount of water. Briefly, there are several steps to perform a seeding experiment.

1) Mix crystal screen #6 with 0, 50, 100, 150, 200, 250, 300, 350, 400 μL ddH_2O to make a total 500 μL well solution.
2) Set up crystallization drop by mixing 1 μL MS2-3C8/MBP–DR4 protein mixture and 1 μL solution M.
3) Equilibrate for 6 hours before start of seeding.
4) Make the wash solution by mixing 2 parts of water and 3 parts of solution M.
5) Pipette 2 drops of 1 μL wash solution on a single cover slip.
6) Transfer a crystal plate from the crystallization drop to one of the wash drops using a 0.05-mm crystal loop.
7) Shake the crystal in the drop a few times and transfer the crystal plate to the other drop.
8) Break the crystal into tiny pieces with the loop.
9) Pick up a loop of solution containing the crystal seeds (you may not see it, but it is there) and transfer it to each equilibrated crystallization drop.
10) Check for crystals the next morning.

The well solution with 150 μL gave the biggest crystals. The same seeding conditions were repeated for 12 more drops, which yielded crystals of good diffraction qualities.

16. Flash freezing and storage of protein crystals

1) Make 500 μL of cryoprotectant solution that contains all the ingredients of solution M plus 20% glycerol.
2) Fill a cylindrical dewar (Pope scientific, height: 337 mm) with liquid nitrogen (LN). Slowly immerse a CryoCane (Hampton research) in LN.
3) Place a cryo vial in the vial clamp and set aside.
4) Select a CrystalCap mounted with a CryoLoop that fits the size of the crystal to be frozen.
5) Put the CrystalCap on a CrystalWand.
6) Pipette 2 drops of 1 μL cryo-solution on a clean cover slip.
7) Manipulate the CrystalWand to pick up a single crystal and wash quickly through two cryo drops.
8) Immerse the crystal in LN.
9) Use the other hand to handle the clamp and immerse the cryo vial.
10) Slowly slide the crystal into the vial until the CrystalCap locks in the vial.
11) Transfer the vial from the clamp onto the CryoCane. Always put from the bottom of the cane.
12) Fill all the spaces on a CryoCane except the top one. Immerse a CryoSleeve in LN. Insert the cane in the sleeve.
13) Transfer the sleeved cane into a big LN tank for storage.

17. X-ray data collection and process

X-ray diffraction can be done with an in-house X-ray source or by sending the frozen

crystals to a synchrotron. To send the crystals for remote collection, make sure that the nitrogen dry shipper works well before putting in the crystals.

For in-house collection, there is no need to pre-freeze the crystals. Simply mount the crystal on the goniometer after two washes. Adjust the position of the crystal so that it is centered at the X-ray beam. Set the goniometer to 0 degree and lock.

For initial screening, set the crystal-to-detector distance to 200 mm. Collect 5 or 10 min exposure data for both 0 and 90 degrees. In-house diffraction of MS2-3C8 complex crystals can reach about 3.2 Å. Index gave the space group of P43212 and cell parameters.

For an in-house data collection, each image was collected from 30-min exposure. A total180 °dataset was collected with 0.5 °steps.

Frozen crystals were also sent to National Synchrotron Light Sourse in Brookhave National Laboraotry, the best of which diffracted to 2.8 Å with a 1.075 Å X-ray beam. The diffraction quality of synchrotron light was much better than in-house collection, since both the wavelength and intensity of X-ray was more advanced. At NSLS, a complete 360 °data set was collected with 1 °steps.

Data process was performed with HKL-20004 programs and scaled to 2.8 Å with ScalePack[4].

18. Molecular replacement

Data truncation was performed using old truncation program in CCP4 suite. Molecular replacement (MR) was done with reflections lower than 3.5 Å using the program Phaser[5]. Details of the searching steps were described in chapter 4.2. A correct solution should lead to an R_{free} of less than 50%.

[4] Otwinowski, Z., and W. Minor. 1997. Processing of X-ray Diffraction Data Collected in Oscillation Mode. *Methods in Enzymology*. 276:307-326.

[5] Storoni, L.C., A.J. McCoy, and R.J. Read. 2004. Likelihood-enhanced fast rotation functions. Acta Crystallogr D Biol Crystallogr. 60:432-438.

19. Structure refinement and manual model fitting

After two MS2-3C8 complexes were correctly placed in the asymmetric unit, rigid body refinement was completed with the program CNS[6]. 5% of the reflections were assigned to the test set. The first $2F_o$-F_c and F_o-F_c electron density maps were also generated by CNS. The two maps were loaded into the model-building program Coot[7]. It was shown that the CDR loops were not fit well into the densities due to the difference from the MR model. In addition, clear electron density was shown at the linker region in one of the MS2-3C8 complexes. The model was manually adjusted to fit the electron densities. Later structure refinement and map calculation was performed with the program Phenix[8]. Model fitting was constantly monitored by R_{work} and R_{free} values. Water molecules were added using a cutoff distance of 3.4 Å and only added at the positions with unambiguous electron densities. Some loops that are distant from the binding interface did not show densities. The amino acid residues for those regions were omitted from the model. To validate the structure model, deviated atom positions were corrected as far as they agreed with the electron densities. The final step of refinement gave the R_{work} of 23.9% and R_{free} of 27.9%. An optional TLS[9] refinement was also performed using Phenix, which resulted a further drop for both R_{work} (22.2%) and R_{free} (26.3%) values.

---

[6] Brunger, A.T., P.D. Adams, G.M. Clore, W.L. DeLano, P. Gros, R.W. Grosse-Kunstleve, J.S. Jiang, J. Kuszewski, M. Nilges, N.S. Pannu, R.J. Read, L.M. Rice, T. Simonson, and G.L. Warren. 1998. Crystallography & NMR system: A new software suite for macromolecular structure determination. Ibid. 54:905-921.

[7] Emsley, P., B. Lohkamp, W.G. Scott, and K. Cowtan. 2010. Features and development of Coot. Ibid. 66:486-501.

[8] Adams, P.D., P.V. Afonine, G. Bunkoczi, V.B. Chen, I.W. Davis, N. Echols, J.J. Headd, L.W. Hung, G.J. Kapral, R.W. Grosse-Kunstleve, A.J. McCoy, N.W. Moriarty, R. Oeffner, R.J. Read, D.C. Richardson, J.S. Richardson, T.C. Terwilliger, and P.H. Zwart. Ibid.PHENIX: a comprehensive Python-based system for macromolecular structure solution.213-221.

[9] Winn, M.D., M.N. Isupov, and G.N. Murshudov. 2001. Use of TLS parameters to model anisotropic displacements in macromolecular refinement. Ibid. 57:122-133.

20. Structure analysis and figure preparation

Solvent-accessible surface areas were calculated using the program AREAIMOL (Collaborative Computational Project No. 4, 1994) with a probe radius of 1.4 Å. Contacts were identified by CONTACT using a cut-off distance of 4.0 Å. All structure figures were prepared using PyMOL[10], a feasible whereas powerful and versatile molecular graphics program that was contributed by late Dr. Warren L. DeLano.

[10] http://pymol.org

Bibliography

Adams, P.D., P.V. Afonine, G. Bunkoczi, V.B. Chen, I.W. Davis, N. Echols, J.J. Headd, L.W. Hung, G.J. Kapral, R.W. Grosse-Kunstleve, A.J. McCoy, N.W. Moriarty, R. Oeffner, R.J. Read, D.C. Richardson, J.S. Richardson, T.C. Terwilliger, and P.H. Zwart. 2010. PHENIX: a comprehensive Python-based system for macromolecular structure solution. *Acta Crystallogr D Biol Crystallogr*. 66:213-221.

Amicosante, M., N. Sanarico, F. Berretta, J. Arroyo, G. Lombardi, R. Lechler, V. Colizzi, and C. Saltini. 2001. Beryllium binding to HLA-DP molecule carrying the marker of susceptibility to berylliosis glutamate beta 69. *Hum Immunol*. 62:686-693.

Anderson, G., and E.J. Jenkinson. 2001. Lymphostromal interactions in thymic development and function. *Nat Rev Immunol*. 1:31-40.

Anderton, S.M., C.G. Radu, P.A. Lowrey, E.S. Ward, and D.C. Wraith. 2001. Negative selection during the peripheral immune response to antigen. *J Exp Med*. 193:1-11.

Appel, H., L. Gauthier, J. Pyrdol, and K.W. Wucherpfennig. 2000. Kinetics of T-cell receptor binding by bivalent HLA-DR.Peptide complexes that activate antigen-specific human T-cells. *J Biol Chem*. 275:312-321.

Appella, E., E.A. Padlan, and D.F. Hunt. 1995. Analysis of the structure of naturally processed peptides bound by class I and class II major histocompatibility complex molecules. *EXS*. 73:105-119.

Archbold, J.K., W.A. Macdonald, S. Gras, L.K. Ely, J.J. Miles, M.J. Bell, R.M. Brennan, T. Beddoe, M.C. Wilce, C.S. Clements, A.W. Purcell, J. McCluskey, S.R. Burrows, and J. Rossjohn. 2009. Natural micropolymorphism in human leukocyte antigens provides a basis for genetic control of antigen recognition. *J Exp Med*. 206:209-219.

Arimilli, S., C. Cardoso, P. Mukku, V. Baichwal, and B. Nag. 1995. Refolding and reconstitution of functionally active complexes of human leukocyte antigen DR2 and myelin basic protein peptide from recombinant alpha and beta polypeptide chains. *J Biol Chem*. 270:971-977.

Banchereau, J., V. Pascual, and A.K. Palucka. 2004. Autoimmunity through cytokine-induced dendritic cell activation. *Immunity*. 20:539-550.

Barcellos, L.F., J.R. Oksenberg, A.B. Begovich, E.R. Martin, S. Schmidt, E. Vittinghoff, D.S. Goodin, D. Pelletier, R.R. Lincoln, P. Bucher, A. Swerdlin, M.A. Pericak-

Vance, J.L. Haines, and S.L. Hauser. 2003. HLA-DR2 dose effect on susceptibility to multiple sclerosis and influence on disease course. *Am J Hum Genet*. 72:710-716.

Baumgartner, C.K., A. Ferrante, M. Nagaoka, J. Gorski, and L.P. Malherbe. 2010. Peptide-MHC Class II Complex Stability Governs CD4 T Cell Clonal Selection. *J Immunol*. 184:573-581.

Belmares, M.P., J.D. Rabinowitz, W. Liu, E.D. Mellins, and H.M. McConnell. 2000. pH stability of HLA-DR4 complexes with antigenic peptides. *Biochemistry*. 39:14558-14566.

Bielekova, B., M.H. Sung, N. Kadom, R. Simon, H. McFarland, and R. Martin. 2004. Expansion and functional relevance of high-avidity myelin-specific CD4+ T cells in multiple sclerosis. *J Immunol*. 172:3893-3904.

Bjorkman, P.J., M.A. Saper, B. Samraoui, W.S. Bennett, J.L. Strominger, and D.C. Wiley. 1987. Structure of the human class I histocompatibility antigen, HLA-A2. *Nature*. 329:506-512.

Blackman, M., J. Yague, R. Kubo, D. Gay, C. Coleclough, E. Palmer, J. Kappler, and P. Marrack. 1986. The T cell repertoire may be biased in favor of MHC recognition. *Cell*. 47:349-357.

Bolin, D.R., A.L. Swain, R. Sarabu, S.J. Berthel, P. Gillespie, N.J. Huby, R. Makofske, L. Orzechowski, A. Perrotta, K. Toth, J.P. Cooper, N. Jiang, F. Falcioni, R. Campbell, D. Cox, D. Gaizband, C.J. Belunis, D. Vidovic, K. Ito, R. Crowther, U. Kammlott, X. Zhang, R. Palermo, D. Weber, J. Guenot, Z. Nagy, and G.L. Olson. 2000. Peptide and peptide mimetic inhibitors of antigen presentation by HLA-DR class II MHC molecules. Design, structure-activity relationships, and X-ray crystal structures. *J Med Chem*. 43:2135-2148.

Brunger, A.T., P.D. Adams, G.M. Clore, W.L. DeLano, P. Gros, R.W. Grosse-Kunstleve, J.S. Jiang, J. Kuszewski, M. Nilges, N.S. Pannu, R.J. Read, L.M. Rice, T. Simonson, and G.L. Warren. 1998. Crystallography & NMR system: A new software suite for macromolecular structure determination. *Acta Crystallogr D Biol Crystallogr*. 54:905-921.

Bruno, R., L. Sabater, M. Sospedra, X. Ferrer-Francesch, D. Escudero, E. Martinez-Caceres, and R. Pujol-Borrell. 2002. Multiple sclerosis candidate autoantigens except myelin oligodendrocyte glycoprotein are transcribed in human thymus. *Eur J Immunol*. 32:2737-2747.

Chelvanayagam, G. 1997. A roadmap for HLA-DR peptide binding specificities. *Hum Immunol*. 58:61-69.

Cole, D.K., N.J. Pumphrey, J.M. Boulter, M. Sami, J.I. Bell, E. Gostick, D.A. Price, G.F. Gao, A.K. Sewell, and B.K. Jakobsen. 2007. Human TCR-binding affinity is governed by MHC class restriction. *J Immunol*. 178:5727-5734.

Collins, E.J., and D.S. Riddle. 2008. TCR-MHC docking orientation: natural selection, or thymic selection? *Immunol Res*. 41:267-294.

Constantinescu, C.S., B. Hilliard, T. Fujioka, M.K. Bhopale, D. Calida, and A.M. Rostami. 1998. Pathogenesis of neuroimmunologic diseases. Experimental models. *Immunol Res*. 17:217-227.

Dedier, S., S. Reinelt, T. Reitinger, G. Folkers, and D. Rognan. 2000. Thermodynamic stability of HLA-B*2705. Peptide complexes. Effect of peptide and major histocompatibility complex protein mutations. *J Biol Chem*. 275:27055-27061.

Deighton, C.M., D.J. Walker, I.D. Griffiths, and D.F. Roberts. 1989. The contribution of HLA to rheumatoid arthritis. *Clin Genet*. 36:178-182.

Deng, L., and R.A. Mariuzza. 2007. Recognition of self-peptide-MHC complexes by autoimmune T-cell receptors. *Trends Biochem Sci*. 32:500-508.

Dessen, A., C.M. Lawrence, S. Cupo, D.M. Zaller, and D.C. Wiley. 1997. X-Ray Crystal Structure of HLA-DR4 (DRA*0101, DRB1*0401) Complexed with a Peptide from Human Collagen II. *Immunity*. 7:473-481.

DiPaolo, R.J., and E.R. Unanue. 2002. Cutting edge: the relative distribution of T cells responding to chemically dominant or minor epitopes of lysozyme is not affected by CD40-CD40 ligand and B7-CD28-CTLA-4 costimulatory pathways. *J Immunol*. 169:2832-2836.

Doherty, P.C., and R.M. Zinkernagel. 1975. Enhanced immunological surveillance in mice heterozygous at the H-2 gene complex. *Nature*. 256:50-52.

Emsley, P., B. Lohkamp, W.G. Scott, and K. Cowtan. 2010. Features and development of Coot. *Acta Crystallogr D Biol Crystallogr*. 66:486-501.

Fairchild, P.J., R. Wildgoose, E. Atherton, S. Webb, and D.C. Wraith. 1993. An autoantigenic T cell epitope forms unstable complexes with class II MHC: a novel route for escape from tolerance induction. *Int Immunol*. 5:1151-1158.

Feng, D., C.J. Bond, L.K. Ely, J. Maynard, and K.C. Garcia. 2007. Structural evidence for a germline-encoded T cell receptor-major histocompatibility complex

interaction 'codon'. *Nat Immunol*. 8:975-983.

Fernandez, M.M., M.C. De Marzi, P. Berguer, D. Burzyn, R.J. Langley, I. Piazzon, R.A. Mariuzza, and E.L. Malchiodi. 2006. Binding of natural variants of staphylococcal superantigens SEG and SEI to TCR and MHC class II molecule. *Mol Immunol*. 43:927-938.

Fourneau, J.M., H. Cohen, and P.M. van Endert. 2004. A chaperone-assisted high yield system for the production of HLA-DR4 tetramers in insect cells. *J Immunol Methods*. 285:253-264.

Frayser, M., A.K. Sato, L. Xu, and L.J. Stern. 1999. Empty and peptide-loaded class II major histocompatibility complex proteins produced by expression in Escherichia coli and folding in vitro. *Protein Expr Purif*. 15:105-114.

Fremont, D.H., W.A. Hendrickson, P. Marrack, and J. Kappler. 1996. Structures of an MHC Class II Molecule with Covalently Bound Single Peptides. *Science*. 272:1001-1004.

Fugger, L., J. Liang, A. Gautam, J.B. Rothbard, and H.O. McDevitt. 1996. Quantitative analysis of peptides from myelin basic protein binding to the MHC class II protein, I-Au, which confers susceptibility to experimental allergic encephalomyelitis. *Mol Med*. 2:181-188.

Garboczi, D.N., P. Ghosh, U. Utz, Q.R. Fan, W.E. Biddison, and D.C. Wiley. 1996. Structure of the complex between human T-cell receptor, viral peptide and HLA-A2. *Nature*. 384:134-141.

Garcia, K.C., J.J. Adams, D. Feng, and L.K. Ely. 2009. The molecular basis of TCR germline bias for MHC is surprisingly simple. *Nat Immunol*. 10:143-147.

Garcia, K.C., M. Degano, R.L. Stanfield, A. Brunmark, M.R. Jackson, P.A. Peterson, L. Teyton, and I.A. Wilson. 1996. Anab T Cell Receptor Structure at 2.5 A and Its Orientation in the TCR-MHC Complex. *Science*. 274:209-219.

Garcia, K.C., C.G. Radu, J. Ho, R.J. Ober, and E.S. Ward. 2001. Kinetics and thermodynamics of T cell receptor- autoantigen interactions in murine experimental autoimmune encephalomyelitis. *Proc Natl Acad Sci U S A*. 98:6818-6823.

Gold, R., C. Linington, and H. Lassmann. 2006. Understanding pathogenesis and therapy of multiple sclerosis via animal models: 70 years of merits and culprits in experimental autoimmune encephalomyelitis research. *Brain*. 129:1953-1971.

Goverman, J. 2009. Autoimmune T cell responses in the central nervous system. *Nat Rev*

Immunol. 9:393-407.

Hafler, D.A., M.G. Saadeh, V.K. Kuchroo, E. Milford, and L. Steinman. 1996. TCR usage in human and experimental demyelinating disease. *Immunol Today*. 17:152-159.

Hahn, M., M.J. Nicholson, J. Pyrdol, and K.W. Wucherpfennig. 2005. Unconventional topology of self peptide-major histocompatibility complex binding by a human autoimmune T cell receptor. *Nat Immunol*. 6:490-496.

Hammer, J., C. Belunis, D. Bolin, J. Papadopoulos, R. Walsky, J. Higelin, W. Danho, F. Sinigaglia, and Z.A. Nagy. 1994. High-Affinity Binding of Short Peptides to Major Histocompatibility Complex Class II Molecules by Anchor Combinations. *PNAS*. 91:4456-4460.

Hammer, J., F. Gallazzi, E. Bono, R.W. Karr, J. Guenot, P. Valsasnini, Z.A. Nagy, and F. Sinigaglia. 1995. Peptide binding specificity of HLA-DR4 molecules: correlation with rheumatoid arthritis association. *J. Exp. Med.* 181:1847-1855.

Hammer, J., P. Valsasnini, K. Tolba, D. Bolin, J. Higelin, B. Takacs, and F. Sinigaglia. 1993. Promiscuous and allele-specific anchors in HLA-DR-binding peptides. *Cell*. 74:197-203.

Harkiolaki, M., S.L. Holmes, P. Svendsen, J.W. Gregersen, L.T. Jensen, R. McMahon, M.A. Friese, G. van Boxel, R. Etzensperger, J.S. Tzartos, K. Kranc, S. Sainsbury, K. Harlos, E.D. Mellins, J. Palace, M.M. Esiri, P.A. van der Merwe, E.Y. Jones, and L. Fugger. 2009. T cell-mediated autoimmune disease due to low-affinity crossreactivity to common microbial peptides. *Immunity*. 30:348-357.

He, X.-l., C. Radu, J. Sidney, A. Sette, E.S. Ward, and K.C. Garcia. 2002. Structural Snapshot of Aberrant Antigen Presentation Linked to Autoimmunity: The Immunodominant Epitope of MBP Complexed with I-Au. *Immunity*. 17:83-94.

Henderson, K.N., J.A. Tye-Din, H.H. Reid, Z. Chen, N.A. Borg, T. Beissbarth, A. Tatham, S.I. Mannering, A.W. Purcell, N.L. Dudek, D.A. van Heel, J. McCluskey, J. Rossjohn, and R.P. Anderson. 2007. A structural and immunological basis for the role of human leukocyte antigen DQ8 in celiac disease. *Immunity*. 27:23-34.

Hennecke, J., A. Carfi, and D.C. Wiley. 2000. Structure of a covalently stabilized complex of a human alphabeta T-cell receptor, influenza HA peptide and MHC class II molecule, HLA-DR1. *Embo J*. 19:5611-5624.

Hennecke, J., and D.C. Wiley. 2002. Structure of a complex of the human alpha/beta T cell receptor (TCR) HA1.7, influenza hemagglutinin peptide, and major

histocompatibility complex class II molecule, HLA-DR4 (DRA*0101 and DRB1*0401): insight into TCR cross-restriction and alloreactivity. *J Exp Med*. 195:571-581.

Hickey, W.F. 1999. Leukocyte traffic in the central nervous system: the participants and their roles. *Semin Immunol*. 11:125-137.

Hill, C.M., A. Liu, K.W. Marshall, J. Mayer, B. Jorgensen, B. Yuan, R.M. Cubbon, E.A. Nichols, L.S. Wicker, and J.B. Rothbard. 1994. Exploration of requirements for peptide binding to HLA DRB1*0101 and DRB1*0401. *J Immunol*. 152:2890-2898.

Hillert, J., and O. Olerup. 1993. HLA and MS. *Neurology*. 43:2426-2427.

Huseby, E.S., J.W. Kappler, and P. Marrack. 2008. Thymic selection stifles TCR reactivity with the main chain structure of MHC and forces interactions with the peptide side chains. *Mol Immunol*. 45:599-606.

Huseby, E.S., J. White, F. Crawford, T. Vass, D. Becker, C. Pinilla, P. Marrack, and J.W. Kappler. 2005. How the T cell repertoire becomes peptide and MHC specific. *Cell*. 122:247-260.

Janeway, C.A., Jr., and J.M. Jason. 1980. How T lymphocytes recognize antigen. *Crit Rev Immunol*. 1:133-164.

Kalandadze, A., M. Galleno, L. Foncerrada, J.L. Strominger, and K.W. Wucherpfennig. 1996. Expression of Recombinant HLA-DR2 Molecules. REPLACEMENT OF THE HYDROPHOBIC TRANSMEMBRANE REGION BY A LEUCINE ZIPPER DIMERIZATION MOTIF ALLOWS THE ASSEMBLY AND SECRETION OF SOLUBLE DR alpha beta HETERODIMERS. *J. biol. Chem.* 271:20156-20162.

Kawamura, K., K.A. McLaughlin, R. Weissert, and T.G. Forsthuber. 2008. Myelin-reactive type B T cells and T cells specific for low-affinity MHC-binding myelin peptides escape tolerance in HLA-DR transgenic mice. *J Immunol*. 181:3202-3211.

Kermode, A.G., A.J. Thompson, P. Tofts, D.G. MacManus, B.E. Kendall, D.P. Kingsley, I.F. Moseley, P. Rudge, and W.I. McDonald. 1990. Breakdown of the blood-brain barrier precedes symptoms and other MRI signs of new lesions in multiple sclerosis. Pathogenetic and clinical implications. *Brain*. 113 (Pt 5):1477-1489.

Kersh, G.J., E.N. Kersh, D.H. Fremont, and P.M. Allen. 1998. High- and low-potency ligands with similar affinities for the TCR: the importance of kinetics in TCR

signaling. *Immunity*. 9:817-826.

Khan, A.R., B.M. Baker, P. Ghosh, W.E. Biddison, and D.C. Wiley. 2000. The structure and stability of an HLA-A*0201/octameric tax peptide complex with an empty conserved peptide-N-terminal binding site. *J Immunol*. 164:6398-6405.

Kjer-Nielsen, L., C.S. Clements, A.G. Brooks, A.W. Purcell, J. McCluskey, and J. Rossjohn. 2002. The 1.5 A crystal structure of a highly selected antiviral T cell receptor provides evidence for a structural basis of immunodominance. *Structure*. 10:1521-1532.

Kozono, H., J. White, J. Clements, P. Marrack, and J. Kappler. 1994. Production of soluble MHC class II proteins with covalently bound single peptides. *Nature*. 369:151-154.

Krangel, M.S. 2009. Mechanics of T cell receptor gene rearrangement. *Curr Opin Immunol*. 21:133-139.

Lawrence, M.C., and P.M. Colman. 1993. Shape complementarity at protein/protein interfaces. *J Mol Biol*. 234:946-950.

Lebowitz, J., M.S. Lewis, and P. Schuck. 2002. Modern analytical ultracentrifugation in protein science: a tutorial review. *Protein Sci*. 11:2067-2079.

Lefranc, M.-P., V. Giudicelli, C. Ginestoux, J. Jabado-Michaloud, G. Folch, F. Bellahcene, Y. Wu, E. Gemrot, X. Brochet, J. Lane, L. Regnier, F. Ehrenmann, G. Lefranc, and P. Duroux. 2009. IMGT®, the international ImMunoGeneTics information system®. *Nucleic Acids Research*. 37:D1006-D1012.

Li, Y., Y. Huang, J. Lue, J.A. Quandt, R. Martin, and R.A. Mariuzza. 2005. Structure of a human autoimmune TCR bound to a myelin basic protein self-peptide and a multiple sclerosis-associated MHC class II molecule. *Embo J*. 24:2968-2979.

Lucchinetti, C.F., W. Bruck, M. Rodriguez, and H. Lassmann. 1996. Distinct patterns of multiple sclerosis pathology indicates heterogeneity on pathogenesis. *Brain Pathol*. 6:259-274.

Lyons, D.S., S.A. Lieberman, J. Hampl, J.J. Boniface, Y. Chien, L.J. Berg, and M.M. Davis. 1996. A TCR binds to antagonist ligands with lower affinities and faster dissociation rates than to agonists. *Immunity*. 5:53-61.

Madsen, L.S., E.C. Andersson, L. Jansson, M. krogsgaard, C.B. Andersen, J. Engberg, J.L. Strominger, A. Svejgaard, J.P. Hjorth, R. Holmdahl, K.W. Wucherpfennig, and L. Fugger. 1999. A humanized model for multiple sclerosis using HLA-DR2 and a human T-cell receptor. *Nat Genet*. 23:343-347.

Marrack, P., and J. Kappler. 1988. The T-cell repertoire for antigen and MHC. *Immunol Today*. 9:308-315.

Marrack, P., J.P. Scott-Browne, S. Dai, L. Gapin, and J.W. Kappler. 2008. Evolutionarily conserved amino acids that control TCR-MHC interaction. *Annu Rev Immunol*. 26:171-203.

Marrosu, M.G., F. Muntoni, M.R. Murru, G. Spinicci, M.P. Pischedda, F. Goddi, P. Cossu, and M. Pirastu. 1988. Sardinian multiple sclerosis is associated with HLA-DR4: a serologic and molecular analysis. *Neurology*. 38:1749-1753.

Mason, K., D.W. Denney, Jr., and H.M. McConnell. 1995. Myelin basic protein peptide complexes with the class II MHC molecules I-Au and I-Ak form and dissociate rapidly at neutral pH. *J Immunol*. 154:5216-5227.

Matthews, A.G., and M.A. Oettinger. 2009. RAG: a recombinase diversified. *Nat Immunol*. 10:817-821.

Maynard, J., K. Petersson, D.H. Wilson, E.J. Adams, S.E. Blondelle, M.J. Boulanger, D.B. Wilson, and K.C. Garcia. 2005. Structure of an autoimmune T cell receptor complexed with class II peptide-MHC: insights into MHC bias and antigen specificity. *Immunity*. 22:81-92.

Merkenschlager, M., D. Graf, M. Lovatt, U. Bommhardt, R. Zamoyska, and A.G. Fisher. 1997. How many thymocytes audition for selection? *J Exp Med*. 186:1149-1158.

Messaoudi, I., J.A. Guevara Patino, R. Dyall, J. LeMaoult, and J. Nikolich-Zugich. 2002. Direct link between mhc polymorphism, T cell avidity, and diversity in immune defense. *Science*. 298:1797-1800.

Muraro, P.A., M. Vergelli, M. Kalbus, D.E. Banks, J.W. Nagle, L.R. Tranquill, G.T. Nepom, W.E. Biddison, H.F. McFarland, and R. Martin. 1997. Immunodominance of a low-affinity major histocompatibility complex-binding myelin basic protein epitope (residues 111-129) in HLA-DR4 (B1*0401) subjects is associated with a restricted T cell receptor repertoire. *J Clin Invest*. 100:339-349.

Nicholson, M.J., M. Hahn, and K.W. Wucherpfennig. 2005. Unusual features of self-peptide/MHC binding by autoimmune T cell receptors. *Immunity*. 23:351-360.

NMSS, N.M.S.S. 2010. How many people have MS? *http://www.nationalmssociety.org/about-multiple-sclerosis/what-we-know-about-ms/faqs-about-ms/index.aspx*.

Otwinowski, Z., and W. Minor. 1997. Processing of X-ray Diffraction Data Collected in Oscillation Mode. *Methods in Enzymology*. 276:307-326.

Pribyl, T.M., C.W. Campagnoni, K. Kampf, T. Kashima, V.W. Handley, J. McMahon, and A.T. Campagnoni. 1993. The human myelin basic protein gene is included within a 179-kilobase transcription unit: expression in the immune and central nervous systems. *Proc Natl Acad Sci U S A*. 90:10695-10699.

Quandt, J.A., M. Baig, K. Yao, K. Kawamura, J. Huh, S.K. Ludwin, H.J. Bian, M. Bryant, L. Quigley, Z.A. Nagy, H.F. McFarland, P.A. Muraro, R. Martin, and K. Ito. 2004. Unique clinical and pathological features in HLA-DRB1*0401-restricted MBP 111-129-specific humanized TCR transgenic mice. *J Exp Med*. 200:223-234.

Raddrizzani, L., T. Sturniolo, J. Guenot, E. Bono, F. Gallazzi, Z.A. Nagy, F. Sinigaglia, and J. Hammer. 1997. Different modes of peptide interaction enable HLA-DQ and HLA-DR molecules to bind diverse peptide repertoires. *J Immunol*. 159:703-711.

Reinherz, E.L., K. Tan, L. Tang, P. Kern, J. Liu, Y. Xiong, R.E. Hussey, A. Smolyar, B. Hare, R. Zhang, A. Joachimiak, H.C. Chang, G. Wagner, and J. Wang. 1999. The crystal structure of a T cell receptor in complex with peptide and MHC class II. *Science*. 286:1913-1921.

Reizis, B., M. Eisenstein, F. Mor, and I.R. Cohen. 1998. The peptide-binding strategy of the MHC class II I-A molecules. *Immunology Today*. 19:212-216.

Rudolph, M.G., J.G. Luz, and I.A. Wilson. 2002. STRUCTURAL AND THERMODYNAMIC CORRELATES OF T CELL SIGNALING. *Annual Review of Biophysics and Biomolecular Structure*. 31:121-149.

Rudolph, M.G., R.L. Stanfield, and I.A. Wilson. 2006. HOW TCRS BIND MHCS, PEPTIDES, AND CORECEPTORS. *Annual Review of Immunology*. 24:419-466.

Saito, K., M. Oda, A. Sarai, T. Azuma, and H. Kozono. 2004. Bound peptide-dependent thermal stability of major histocompatibility complex class II molecule I-Ek. *Biochemistry*. 43:10186-10191.

Scheirle, A., B. Takacs, L. Kremer, F. Marin, and F. Sinigaglia. 1992. Peptide binding to soluble HLA-DR4 molecules produced by insect cells. *J Immunol*. 149:1994-1999.

Schodin, B.A., C.J. Schlueter, and D.M. Kranz. 1996. Binding properties and solubility of single-chain T cell receptors expressed in E. coli. *Mol Immunol*. 33:819-829.

Seamons, A., A. Perchellet, and J. Goverman. 2003. Immune tolerance to myelin proteins. *Immunol Res*. 28:201-221.

She, J.X. 1996. Susceptibility to type I diabetes: HLA-DQ and DR revisited. *Immunol Today*. 17:323-329.

Sinigaglia, F., and J. Hammer. 1994. Defining rules for the peptide-MHC class II interaction. *Curr Opin Immunol*. 6:52-56.

Sospedra, M., and R. Martin. 2005. Immunology of multiple sclerosis. *Annu Rev Immunol*. 23:683-747.

Sospedra, M., and R. Martin. 2006. Molecular mimicry in multiple sclerosis. *Autoimmunity*. 39:3-8.

Southwood, S., J. Sidney, A. Kondo, M.F. del Guercio, E. Appella, S. Hoffman, R.T. Kubo, R.W. Chesnut, H.M. Grey, and A. Sette. 1998. Several common HLA-DR types share largely overlapping peptide binding repertoires. *J Immunol*. 160:3363-3373.

Stadinski, B.D., L. Zhang, F. Crawford, P. Marrack, G.S. Eisenbarth, and J.W. Kappler. 2010. Diabetogenic T cells recognize insulin bound to IAg7 in an unexpected, weakly binding register. *Proc Natl Acad Sci U S A*. 107:10978-10983.

Starr, T.K., S.C. Jameson, and K.A. Hogquist. 2003. Positive and negative selection of T cells. *Annu Rev Immunol*. 21:139-176.

Steinman, L. 1996a. A few autoreactive cells in an autoimmune infiltrate control a vast population of nonspecific cells: a tale of smart bombs and the infantry. *Proc Natl Acad Sci U S A*. 93:2253-2256.

Steinman, L. 1996b. Multiple sclerosis: a coordinated immunological attack against myelin in the central nervous system. *Cell*. 85:299-302.

Stern, L.J., and D.C. Wiley. 1994. Antigenic peptide binding by class I and class II histocompatibility proteins. *Structure*. 2:245-251.

Stewart-Jones, G.B., A.J. McMichael, J.I. Bell, D.I. Stuart, and E.Y. Jones. 2003. A structural basis for immunodominant human T cell receptor recognition. *Nat Immunol*. 4:657-663.

Stone, J.D., A.S. Chervin, and D.M. Kranz. 2009. T-cell receptor binding affinities and kinetics: impact on T-cell activity and specificity. *Immunology*. 126:165-176.

Storoni, L.C., A.J. McCoy, and R.J. Read. 2004. Likelihood-enhanced fast rotation functions. *Acta Crystallogr D Biol Crystallogr*. 60:432-438.

Swanson, P.C. 2004. The bounty of RAGs: recombination signal complexes and reaction outcomes. *Immunol Rev*. 200:90-114.

Tillman, R.E., A.L. Wooley, M.M. Hughes, B. Khor, and B.P. Sleckman. 2004. Regulation of T-cell receptor beta-chain gene assembly by recombination signals:

the beyond 12/23 restriction. *Immunol Rev*. 200:36-43.

Urban, J.L., V. Kumar, D.H. Kono, C. Gomez, S.J. Horvath, J. Clayton, D.G. Ando, E.E. Sercarz, and L. Hood. 1988. Restricted use of T cell receptor V genes in murine autoimmune encephalomyelitis raises possibilities for antibody therapy. *Cell*. 54:577-592.

van der Merwe, P.A., and S.J. Davis. 2003. Molecular interactions mediating T cell antigen recognition. *Annu Rev Immunol*. 21:659-684.

Vanderlugt, C.L., and S.D. Miller. 2002. Epitope spreading in immune-mediated diseases: implications for immunotherapy. *Nat Rev Immunol*. 2:85-95.

Williams, K.C., and W.F. Hickey. 1995. Traffic of hematogenous cells through the central nervous system. *Curr Top Microbiol Immunol*. 202:221-245.

Winn, M.D., M.N. Isupov, and G.N. Murshudov. 2001. Use of TLS parameters to model anisotropic displacements in macromolecular refinement. *Acta Crystallogr D Biol Crystallogr*. 57:122-133.

Wucherpfennig, K.W., M.J. Call, L. Deng, and R. Mariuzza. 2009. Structural alterations in peptide-MHC recognition by self-reactive T cell receptors. *Curr Opin Immunol*.

Wucherpfennig, K.W., E. Gagnon, M.J. Call, E.S. Huseby, and M.E. Call. 2010. Structural biology of the T-cell receptor: insights into receptor assembly, ligand recognition, and initiation of signaling. *Cold Spring Harb Perspect Biol*. 2:a005140.

Zavala-Ruiz, Z., E.J. Sundberg, J.D. Stone, D.B. DeOliveira, I.C. Chan, J. Svendsen, R.A. Mariuzza, and L.J. Stern. 2003. Exploration of the P6/P7 region of the peptide-binding site of the human class II major histocompatability complex protein HLA-DR1. *J Biol Chem*. 278:44904-44912.

Zerrahn, J., W. Held, and D.H. Raulet. 1997. The MHC reactivity of the T cell repertoire prior to positive and negative selection. *Cell*. 88:627-636.

Zhou, T., L. Xu, B. Dey, A.J. Hessell, D. Van Ryk, S.H. Xiang, X. Yang, M.Y. Zhang, M.B. Zwick, J. Arthos, D.R. Burton, D.S. Dimitrov, J. Sodroski, R. Wyatt, G.J. Nabel, and P.D. Kwong. 2007. Structural definition of a conserved neutralization epitope on HIV-1 gp120. *Nature*. 445:732-737.